

Conversion of a Scroll Compressor to an Expander for Organic Rankine Cycle: Modeling and Analysis

By
Emre Oralli

A Thesis Submitted in Partial Fulfillment
of the Requirements for the Degree of

Master of Applied Science in Mechanical Engineering

Faculty of Engineering and Applied Science
University of Ontario Institute of Technology

December 2010

© Emre Oralli, 2010

Abstract

In this thesis, a refrigeration scroll compressor as expander for power generation applications with Rankine cycle is analyzed through a comprehensive mathematical model. The methodology adopted has three phases. In the first phase, a scroll compressor is selected from a refrigeration manufacturer catalog namely Copeland ZF06K4E. Based on catalog data and thermodynamic model the specific parameters of the compressor such as built-in volume ratio and leakage coefficient are determined through mathematical regression as 7.3 and 1.36×10^{-6} , respectively. In the second phase, the parameters and the efficiency of the Rankine cycle are determined, which use the selected scroll machine in reverse, namely as expander, without any geometrical modifications and keeping the range of temperatures and pressures constant as the same as that characterizing the compressor operation. An expander model is used to predict the efficiency of the prime mover and of the Rankine cycle for the working fluids such as R404a, Toulene, R123, R141b, R134a and NH_3 . The highest efficiency is obtained with R404a as 18% by applying supercritical conditions for the working fluid and it is observed that the expander does not operate optimally when converted from a compressor without any modifications. In the third phase, the geometry of the expander is modified with respect to rolling angle in order to obtain the appropriate built-in volume ratio which assures better efficiency of the Rankine heat engine. R404a clearly gave the best results for the modified geometry and the energy efficiency is increased to 25% from 19% while the exergy efficiency is increased to 61% from 50%. The results showed that it is possible to improve the efficiency of the cycle by adjusting the scroll geometry for the fluids used.

Keywords: Scroll compressor, expander, Rankine cycle, heat recovery, heat engines

Acknowledgements

I would like to sincerely express my appreciation to my supervisors Dr. Ibrahim Dincer for his support and guidance. He gave me the courage and self confidence to explore and experiment. His confidence in me was a great source of motivation during the time I have worked with them.

I would like to acknowledge the financial support provided by the Ontario Center of Excellence (OCE) and Cleanfield Energy Inc.

A great deal of this research is inspired and made possible through the teamwork of Dr. Dincer's research group, in particular Calin Zamfirescu and Md. Ali Tarique. I would like to thank all of them.

Also, I would like to thank my friends Halil Sadi Hamut, Kevork Hacatoglu, Mehmet Gezgin, Mahmut Utku Bak, Mehmet Fatih Orhan, Ahmet Ozbilen, Kursad Cohce. I have greatly benefited from their support and experience.

Last but the most I want to thank my family; Mehtap, Tuncay, Ozge Oralli. If there is any honor in this degree it belongs to them.

Table of Contents

Abstract	i
Acknowledgements	ii
Table of Contents	iii
List of Table Captions	x
Nomenclature	xi
Greek Letters	xiii
1 INTRODUCTION	1
1.1 Energy and Environmental Impact.....	1
1.2 Low Temperature Power Generation	3
2 MOTIVATION AND OBJECTIVES.....	6
3 BACKGROUND	8
3.1 Low Temperature Heat Recovery	8
3.1.1 Carnot Cycle	8
3.1.2 Kalina Cycle	9
3.1.3 Transcritical CO ₂ Cycle	12
3.1.4 Stirling Engine	14
3.1.5 Thermoelectric Generators	17
3.1.6 Organic Rankine Cycle.....	18
3.1.6.1 Cycle Configuration.....	18
3.1.6.2 Working Fluids	19
3.1.6.3 Irreversibilities	22
3.1.1.4 Cycle Improvements	22
3.1.7 Comparison of Cycles	24
3.2 Classification of Expanders.....	25
3.2.1 Turbines	25
3.2.2 Reciprocating Piston Engines.....	28
3.3.3 Rotary Vane Expander.....	30
3.3.4 Rolling Piston Expander	32
3.3.5 Gerator	33
3.3.6 Scroll Expander	35

3.3.7 Comparison of Expansion Devices.....	39
4 LITERATURE REVIEW	43
4.1 Scroll Geometry	43
4.2 Dynamic Analysis	43
4.3 Compressor Process	44
4.3.1 Suction Process.....	44
4.3.2 Compression Process.....	45
4.3.3 Discharge Process.....	46
4.4 Evaluation of Losses	46
4.4.1 Leakage.....	46
4.4.2 Heat Transfer	47
4.4.3 Frictional Losses.....	48
4.5 Noise and Vibration	49
4.6 Comprehensive Modeling of Scroll Compressors	49
4.7 Experimental Investigations.....	50
4.8 Design Variations.....	51
4.9 Scroll Expander Modeling	51
5 ANALYSIS AND MODELLING	53
5.1 Geometric Analysis.....	53
5.2 Thermodynamic Analysis	61
5.2.1 Differential Equations Governing the Expansion Process	61
5.2.2 Heat Transfer	63
5.2.3 Expander Model	64
5.2.4 Cycle Analysis.....	67
5.2.4.1 Pump.....	69
5.2.4.2 Boiler.....	70
5.2.4.3 Expander	71
5.2.4.4 Condenser	72
5.2.4.5 Cycle Energy Efficiency.....	73
5.2.4.6 Total Cycle Exergy Destruction.....	73
5.2.4.7 Cycle Exergy Efficiency.....	73
5.3 Thermo-economic Optimization	73

5.3.1 Economic Model.....	74
5.3.1.1 Cost Estimation.....	74
5.3.1.2 Fixed Charges	74
5.3.1.3 Comparison with Alternative and Selection of Overall Optimum Cost ...	76
5.3.2 Multi-objective Optimization	77
5.3.2.1 Objective Functions	78
5.3.2.2 Constraint Equations.....	79
6 RESULTS AND DISCUSSION	82
6.1 Calculation of the Scroll Chamber Volumes	82
6.2 Scroll Compressor Conversion into Expander	86
6.3 Cycle Results with Modified Scroll Geometry	88
6.3.1 Energy and Exergy Efficiency Improvements.....	88
6.2.2 Comparison of Exergy Destructions.....	93
6.3 Parametric Study and Design Optimization	105
6.3.1 Influence of the Scroll Geometry	105
6.3.2 Influence of Rotating Speed of Shaft	112
6.3.2 Influence of Boiler Outlet Temperature	116
6.4.3 Influence of Expander Inlet Pressure.....	120
6.4.4 Influence of Condenser Outlet Temperature	123
6.4 Model Verification	125
6.4.1 Validation of mass flow rate and suction temperature	125
6.4.2 Validation of the power output.....	126
6.5 Thermo-economic Optimization	127
7 CONCLUSIONS AND RECOMMENDATIONS	133
7.1 Conclusions	133
7.2 Recommendations	137
References.....	138

List of Figure Captions

Figure 1.1: World primary energy from different energy sources (IEA, 2006).	2
Figure 3.1: Carnot cycle efficiency as a function of hot temperature (T_H) for $T_0= 25^\circ\text{C}$... 9	9
Figure 3.2: Component diagram of a Kalina cycle.	10
Figure 3.3: Temperature profile through an evaporator pure fluid (left) and azeotropic (right) (Bombarda, 2010).	11
Figure 3.4: T-s diagram for a transcritical CO_2 cycle (Chen, 2006).	13
Figure 3.5: Qualitative P-v and T-s diagram for a Stirling engine (Harada, 2011).	14
Figure 3.6: Illustration of the different thermodynamic states of the Stirling cycle and system diagram (Thombare, 2008).	16
Figure 3.7: The arrangement of the P and N type semiconductors in a TEG (Fraas, 1982).	17
Figure 3.8: Basic Rankine cycle.	19
Figure 5.1: Fixed and orbiting scroll with working chambers.	54
Figure 5.2: General relation of the scroll (Chen,2002).	55
Figure 5.3: Geometrical parameters describing inner and outer involute.	57
Figure 5.4: Working chambers of the expander.	58
Figure 5.5: Scroll machine models for (a) compressor and (b) expander.	65
Figure 5.6: The Rankine cycle.	68
Figure 5.7: T-s diagram of a general organic Rankine cycle.	68
Figure 6.1 Change of the volume during suction, compression and discharge for compressor.	84
Figure 6.2: Change of the volume during suction, expansion and discharge for expander.	85
Figure 6.3: Compression and expansion processes determined by simplified model.	87
Figure 6.4: Rankine cycles with non-modified scroll machine and same working fluid. 88	88

Figure 6.5: Recommended cycle and scroll compressor modifications.	90
Figure 6.6: Energy Efficiency of the cycle for the modified and nonmodified geometry.	91
Figure 6.7: Exergy Efficiency of the cycle for the modified and nonmodified geometry.	92
Figure 6.8: Percentage of the exergy destruction in each component for R404a	94
Figure 6.9: Percentage of the exergy destruction in each component for R141b	95
Figure 6.10: Percentage of the exergy destruction in each component for R134a	97
Figure 6.11: Percentage of the exergy destruction in each component for NH ₃	98
Figure 6.12: Exergy wheel diagram for R404a and $\varphi_e = 57^\circ$	99
Figure 6.13: Exergy wheel diagram for R404a and $\varphi_e = 27^\circ$	100
Figure 6.14: Exergy wheel diagram for R141b and $\varphi_e = 69^\circ$	101
Figure 6.15: Exergy wheel diagram for R141b and $\varphi_e = 33^\circ$	102
Figure 6.16: Exergy wheel diagram for R134a and $\varphi_e = 57^\circ$	103
Figure 6.17: Exergy wheel diagram for R134a and $\varphi_e = 28^\circ$	103
Figure 6.18: Exergy wheel diagram for NH ₃ and $\varphi_e = 57^\circ$	104
Figure 6.19: Exergy wheel diagram for NH ₃ and $\varphi_e = 29^\circ$	104
Figure 6.20: Variation of the energy efficiency with the rolling angle of the scroll machine.	106
Figure 6.21: Variation of the exergy efficiency with the rolling angle of the scroll machine.	106
Figure 6.22: The influence of geometry on the mass flow rate.	107
Figure 6.23: The influence of geometry on the expander power output.....	108
Figure 6.24: The influence of geometry on the overall expander efficiency.....	109
Figure 6.25: The influence of geometry on the expander discharge temperature.	110
Figure 6.26: Leakage rate for n = 956 rpm.	111

Figure 6.27: Leakage rate for $n = 2847$ rpm.	111
Figure 6.28: Expansion ratio versus rotation speed for various inlet pressures.....	112
Figure 6.29: Mass flow rate versus rotation speed for various inlet pressures.	113
Figure 6.30: Expander isentropic efficiency for various inlet pressures and rotation speeds.....	114
Figure 6.31 Expander volumetric efficiency versus rotation speed for various inlet pressures.....	114
Figure 6.32: Theoretical expander work versus rotating speed for various inlet pressures.	115
Figure 6.33: Optimum expander work versus rotating speed for various inlet pressures.	116
Figure 6.34: Variation of the system thermal efficiency with the expander inlet temperature.	117
Figure 6.35: Variation of the system irreversibility with the expander inlet temperature.	118
Figure 6.36: Variation of the system second-law efficiency with expander inlet temperature.	119
Figure 6.37: Variation of the system energy efficiency with expander inlet pressure. ..	120
Figure 6.38: Variation of the system irreversibility with the expander inlet pressure....	121
Figure 6.39: Variation of the mass flow rate with the expander inlet pressure.	122
Figure 6.40: Variation of the irreversibility rate with the expander inlet pressure.....	123
Figure 6.41: Variation of the energy efficiency with the condenser outlet temperature.	124
Figure 6.42: Variation of the exergy efficiency with the condenser outlet temperature.	124
Figure 6.43: Validation of the mass flow rate.....	125
Figure 6.44: Validation of the suction temperature.	126
Figure 6.45: Validation of the power output.....	127

Figure 6.46: Optimum boiler efficiency as a function of exergy efficiency for various fuel prices.	129
Figure 6.47: Optimum expander efficiency as a function of exergy efficiency for various fuel prices and boiler temperatures.	130
Figure 6.48: Optimum condenser inlet pressure as a function of exergy efficiency for various fuel prices.	130
Figure 6.49: Cost of produced electricity as a function of exergy efficiency for various working fluids.	131
Figure 6.50: Net revenue generated as a function of exergy efficiency for various market prices of electricity and a fuel cost of \$2 per/MJ.....	131
Figure 6.51: Net revenue generated as a function of exergy efficiency for various market prices of electricity and a fuel cost of \$3 per/MJ.....	132
Figure 6.52: Net revenue generated as a function of exergy efficiency for various market prices of electricity and a fuel cost of \$4 per/MJ.....	132

List of Table Captions

Table 3.1: Summary of thermophysical properties of different refrigerants.	20
Table 3.2: Summary of atmospheric lifetime, GWP, and ODP of different fluids.....	20
Table 3.3: Summary of operating conditions and performance of different expander types.	42
Table 5.1: Costing equations for the Rankine cycle system.	75
Table 5.2: Fixed Parameters and Decision Variables for a cogeneration System.	80
Table 5.3: Equations of Constraint for the Cogeneration System.	81
Table 6.1: Technical parameters of the selected scroll compressor, Copeland ZF06K4E-PVF.	82
Table 6.2: Parameters defining scroll geometry.	83
Table 6.3: Scroll expander and Rankine cycle parameters with various working fluids..	89
Table 6.4: Parametrically varied fixed system parameters of the Rankine cycle.	128

Nomenclature

A	area, m ²
c_p	specific heat at constant pressure, J/kg.K
c_v	specific heat at constant volume, J/kg.K
C_d	discharge coefficient
C_f	specific flow coefficient
D	diameter, m
E	total internal energy, J
Ex	exergy, J
$\dot{E}x$	exergy rate, J/s
g	gravity of earth, m/s ²
h	specific enthalpy, J/kg
h_c	convective heat transfer coefficient, W/m ² -K
h_s	scroll height, m
k	specific heat ratio
L	length, m
m	mass, kg
\dot{m}	mass flow rate, kg/s
N	rotational speed, Hz
P	pressure, Pa
Q	heat, J
\dot{Q}	heat rate, J/s
r	radius, m

r_b	radius of the basic circle of the scroll, m
r_o	orbiting radius of the rotating scroll, m
r_v	built-in volume ratio
s	specific entropy, J/kg-K
t	scroll thickness, m
T	temperature, °C
u	specific internal energy, J/kg
U	internal energy, J
v	velocity, m/s
v	specific volume, m ³ /kg
V	volume, m ³
V_{ed}	expander discharge chamber volume, m ³
V_{ee}	expander expansion chamber volume, m ³
V_{ei}	expander intake chamber volume, m ³
W	work, J
\dot{W}	work rate, J/s
W_{in}	total work input to the compressor, J
W_{out}	net work output from the expander, J
W_s	total work output for the expander, J
z	height, m

Greek Letters

v	specific volume, m ³ /kg
w	rotational speed, rad/s
z	leakage flow coefficient
δ	gap, m
Δ	difference
ε	effectiveness
η	efficiency
θ	orbiting angle, rad
ρ	density, kg/m ³
φ	involute angle, rad
φ_e	rolling angle (involute ending angle), rad
$\varphi_{i,s}$	starting angle of the inner involute, rad
φ_{i0}	initial angle of the inner involute, rad
$\varphi_{o,s}$	starting angle of the outer involute, rad
φ_{o0}	initial angle of the outer involute, rad

Subscripts

a	actual
amb	ambient
b	base circle
c	Curvature
CB	cost of boiler

CC	cost of condenser
CE	cost per unit of electricity produced
CF	cost of fuel
CFUEL _f	fuel cost of producing hot fluid
conj	Conjugate
cp	Compressor
CTOT _f	cost of producing the hot fluid by the low pressure furnace
CV	control volume
d	discharge
diss	dissipated
e	expansion
en	ending
ex	exergy
exh	exhaust
exp	expander
FC _f	fixed charges for the low pressure furnace
fix	fixed
i	initial
l	low
leak	leakage
loss	mechanical loss
mot	motor
MPE	market price of electricity

N_{obj}	number of objectives
N_{param}	number of parameters
NRG	net revenue generated by the sale of the generated electricity
o	outer, orbiting radius
orb	orbiting
plen	plenum
rad	radial
s	isentropic
su	supply
suc	suction

1 INTRODUCTION

1.1 Energy and Environmental Impact

Energy demand before the industrial revolution was mostly provided by man power to meet the basic requirements of humanity. Over the last century, developments in science and concurrent technological advances helped to improve the quality of life for society. Unfortunately growing energy demand was mostly covered by fossil fuels, which caused environmental problems and forced the design of new energy conversion technologies like electricity production by sustainable sources such as solar, wind and geothermal power to eliminate global warming and atmospheric pollution problems.

The present global yearly energy consumption is about 500 EJ, which is equivalent to about 16 TW as the average rate of world primary energy consumption (IEA, 2006). Figure 1.1 shows the percentage contribution to world primary energy from different energy sources from 2000 to 2100 by performing a projection for the energy mix in the future. As shown in the figure, world demand for energy will be 60% more than it is now, which cannot be expected to met by fossil fuels because of the limited reservoirs of coal, oil and gas. Based on proven reserves, the current production level of oil can be maintained for over 40 years, gas over 66 years and coal for over 160 years. This picture requires developing production of electricity without generating environmental pollution.

The problem regarding the environmental impact of energy use is primarily caused by high atmospheric carbon dioxide (CO₂) concentrations as a result of burning fossil fuels. Earth's long term carbon cycle implies to keep CO₂ emissions below such a level that would cause environmental problems. The concern is the increasing

temperature of the planet caused by high levels of greenhouse gases in the atmosphere by burning fossil fuels. The greenhouse effect threatens the natural life on the planet. The level of carbon dioxide in the atmosphere was more or less stable at 280 ppm over the last few thousand years up to the onset of the industrial revolution at the beginning of the 19th century. Current CO₂ levels are 380 ppm and rising fast. Global CO₂ emissions in the alternative scenarios are 16% less in 2030 (IPCC, 2001) but are still more than 50% higher than 1990.

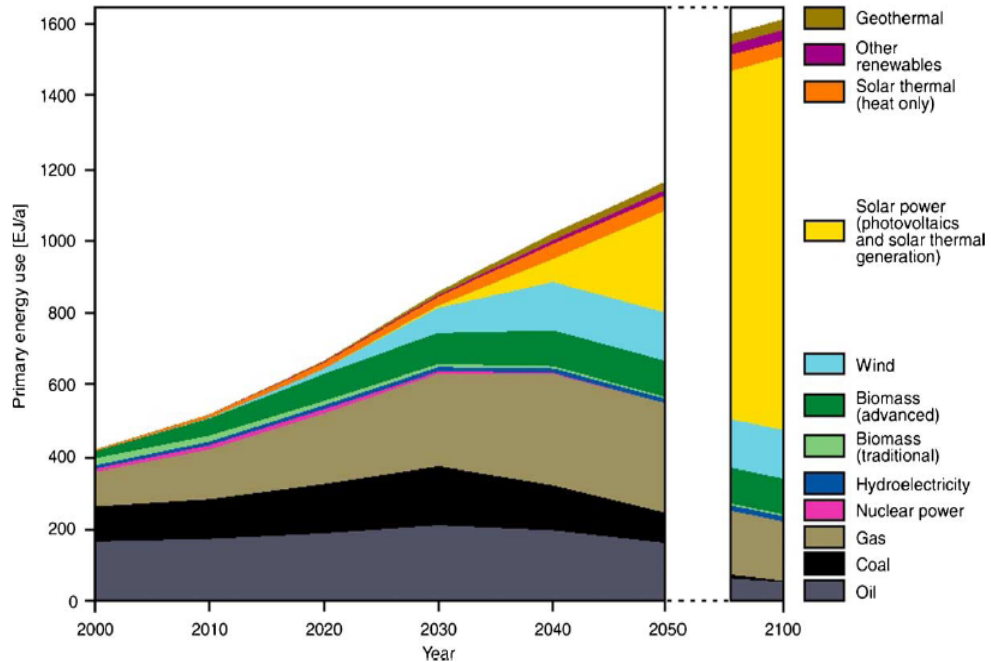


Figure 1.1: World primary energy from different energy sources (IEA, 2006).

In the present time, when there is a push toward sustainable energy based economy, externally driven heat engines which have been used for a long time for conversion of thermal energy to work are playing a major role. There are many sources of heat that can be considered sustainable. Examples are: geothermal reservoirs, solar heat,

ocean thermal energy, industrial waste heat recovery and power cogeneration. An important segment of the above mentioned applications is covered by low power heat generation systems that can be used, for example, for small scale residential or commercial settings. In such applications the generated power is typically below 10 kW. One common case is local generation of electricity and water/space heating from natural gas rather than only heating.

1.2 Low Temperature Power Generation

Generation of electricity from low temperature heat sources has become more popular in the last decade depending on its potential use for different types of applications such as solar thermal, waste heat, small scale cogeneration for residential purposes etc. Low capacity heat engines require appropriate selection of the thermodynamic cycle and of the prime mover.

The Rankine cycle has a relatively higher efficiency by using low temperature heat sources compared to other cycles (Harada, 2011). Solar energy and combustion heat can be used as a low temperature heat source for the cycle. In traditional power plants, Rankine cycle is used to produce useful work from expander mostly using water as a working fluid. The working fluid is pumped to a boiler where it is evaporated then passes through an expander generating shaft work and then finally condensed to be pumped again. Unlike conventional working fluids such as water, organic fluids that have lower boiling temperatures are more appropriate for low temperature Rankine cycle in terms of efficiency and environmental conditions. Water has a high vaporization because of its higher specific volume, which imposes larger installations and therefore higher cost.

There are several kinds of prime movers namely turbomachines and positive displacement machines. However, when it is about low capacity, positive displacement machines (scroll, screw, rotary vane expanders) become more attractive than turbomachines because (Quoilin, 2007):

- Performance of rotary machines depend on their peripheral speed, $v = 2\pi nR$ where n is the revolution speed per second and R is the radius of the rotary machine
- Typical peripheral speed for scroll machines is 1-10 m/s, while for turbomachines it is about 300 m/s
- For a similar radius, the revolution speed of the turbomachine must be the order of hundreds of thousands of RPM while the one of scroll expander it is of couple of thousands RPM. Therefore using turbomachines creates problems with bearings and coupling the electric generator
- Turbomachines have to be made with multiple expansion stages because they have low pressure ratio per stage, while a positive displacement expander would be preferred having one single expansion stage.
- Scroll or screw kind expanders are capable to expand in two phase vapor-liquid region which represents a clear advantage for Rankine cycle applications.

In this thesis, low temperature heat generation phenomenon is investigated for certain thermodynamic cycle and prime mover. The purpose is to achieve waste heat recovery for different purposes such as residential domestic heat supply when there is an electrical breakdown, which will decrease the fragility of the centralized large-scale power generation systems. A crucial part of the system is the design of the scroll

expander especially regarding the geometric and thermodynamics calculations in order to increase the efficiency to make it an alternative to conventional turbomachines.

2 MOTIVATION AND OBJECTIVES

Low capacity scroll machines are massively produced as compressors for refrigeration applications. Their use as expanders is not a new idea but has not yet been applied at a large scale. Because of their massive use in refrigeration, the technology of producing scroll machines is mature. However there is a need to develop know-how regarding a scroll expander design. The simplest approach is to use a refrigeration scroll compressors in reverse -as expanders- since they are reversible machines. For doing this, precautions must be made to use similar temperatures and pressure levels for the reversed operation. The only problem that occurs is in regards to the built-in volume ratio: when operating as an expander the built-in volume ratio must be modified to obtain a better heat engine efficiency. In what follows we aim to estimate how the compressor can operate as expander without any modifications.

In this thesis the feasibility of converting a scroll compressor into an expander to be used in heat recovery Rankine cycle of low capacity is modeled. The specific objectives of this research are given as follows:

1. To characterize the scroll machine in expander mode and searching the effect of geometry on the scroll performance in terms of built in ratio and leakages to evaluate the specific properties of the working fluid to be used in the thermodynamic model
2. To evaluate the geometric parameters of the scroll expander by optimization process to reduce the leakage loss caused by the gaps between the fixed and orbiting scroll and between the scrolls and plates.

3. To select an appropriate organic working fluid such as R404a, Toluene, R123, R141b, R134a and NH_3 which will ensure suitable temperature and pressure range to make the cycle realizable when converting scroll compressor to an expander.

3 BACKGROUND

Compressors are one of the main electricity consumers equipment used mostly in the refrigeration and HVAC industry. Approximately 17% of the world's electricity consumption belongs to compressors (Stosic, 2004). Scroll compressors which are generally used in air-conditioning industry has some advantages among other types of compressors in terms of low level of noise and vibration for human comfort and high efficiency (Lee , 2002).

3.1 Low Temperature Heat Recovery

There are several low temperature heat recovery cycles that include Carnot cycle, Kalina cycle, transcritical cycle, Stirling engine, and thermal electric generator (TEG). Both the Kalina and transcritical cycle are derivatives of the Rankine cycle. The Stirling engine aims to mimic the reversible processes of the Carnot cycle. TEGs are not power cycles but devices that produce a voltage from a heat flux (Harada, 2011).

3.1.1 Carnot Cycle

Carnot efficiency describes the maximum efficiency that and heat engine can achieve for the given temperature difference between two reservoirs as follows:

$$\eta_{Carnot} = \frac{T_H - T_L}{T_H} \quad (1)$$

where T_H is the average temperature of the heat source and T_L is the average temperature of the rejection sink. The region under the Figure 3.1 shows that the efficiency becomes more sensitive to changes in temperature with a decreasing hot side temperature and it can be observed that the thermal efficiency of the cycle will be lower for the low temperature heat recovery sources. Low temperature heat sources can be described by

their grade and separated into low, medium and high. Peterson (2008) categorized with 80-150 °C for low, 150-500 °C for medium and anything above 500 °C as high without giving actual definitions. Low energy recovery and its limitations for the Rankine cycle and other alternative cycles will be described depending on different working fluids, losses, cycle configurations and improvements.

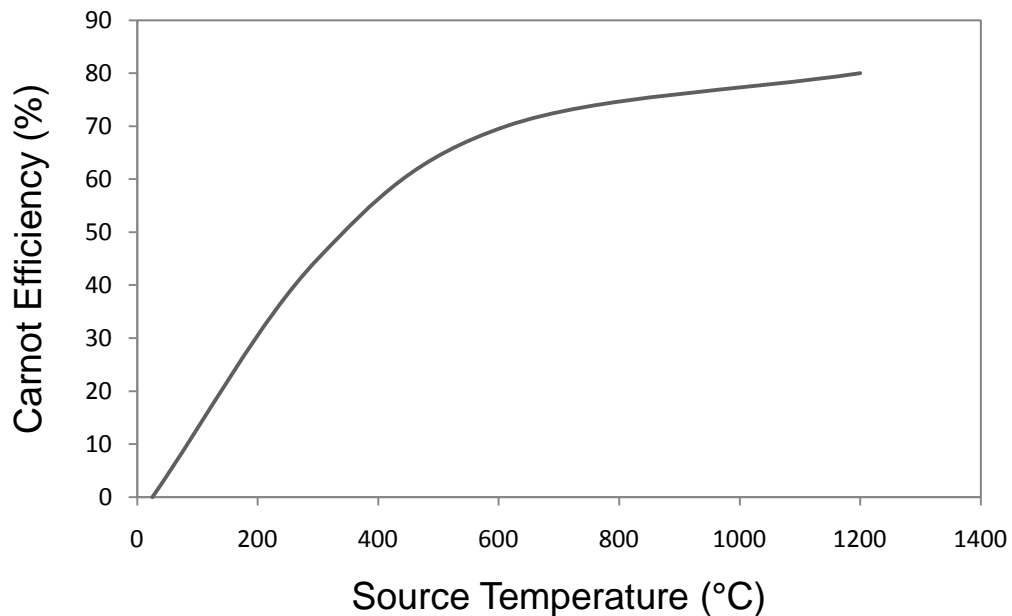


Figure 3.1: Carnot cycle efficiency as a function of hot temperature (T_H) for $T_0=25^\circ\text{C}$.

3.1.2 Kalina Cycle

The Kalina cycle is a modified absorption cycle. It is a relatively new cycle and has not had wide spread adoption (Harada, 2011). A component diagram of a Kalina cycle is given in Figure 3.2. It is similar to a Rankine cycle but with the inclusion of a separator and absorber. The cycle is described below:

- 1 \rightarrow 2: The sub-cooled mix is increased to P_{\max} .
- 2 \rightarrow 3: The mixture is preheated by heat from the separation process.

- 3 → 4: The fluid is evaporated into a high temperature-pressure vapor.
- 4 → 5: The mixture is separated into a rich ammonia-water vapor.
- 4 → 6: The mixture is separated into a weak liquid ammonia-water mixture.
- 5 → 9: The mixture is expanded and produces work.
- 6 → 7: The hot liquid is used to preheat the mixture coming out of the pump.
- 7 → 8: The liquid mixture is throttled to a lower pressure.
- 9 → 10: The liquid and vapor are mixed.
- 10 → 1: The vapor mixture is cooled and condensed into a liquid at P_{\min} .

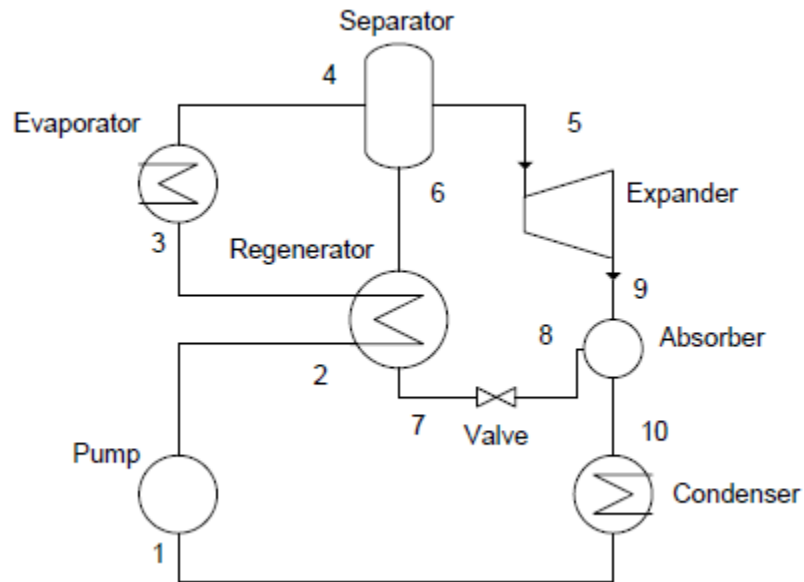


Figure 3.2: Component diagram of a Kalina cycle.

There are several variations of this cycle with the inclusion of additional regenerators, condensers, and pumps. These variations can increase performance but can also hurt the overall efficiency of the cycle (Saleh, 2007).

The main goal of this cycle is to reduce irreversibilities that occur within the heat exchangers by using an azeotropic working fluid like an ammonia-water mixture.

Azeotropic fluids have non-isothermal boiling temperatures at constant pressures, and their boiling curves better match the temperature profile of heat sources. The temperature profiles of the working fluid and heat source in an evaporator are shown in Figure 3.3.

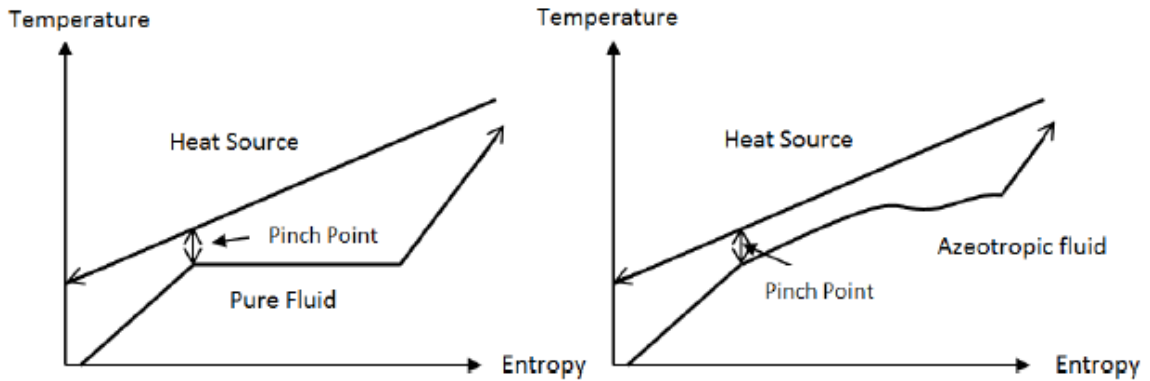


Figure 3.3: Temperature profile through an evaporator pure fluid (left) and azeotropic (right) (Bombarda, 2010).

With a pure fluid the maximum temperature it can achieve before boiling is referred to as the “pinch point.” This causes a large mismatch between the temperature profiles and the area between them is representative of the amount of exergy destruction.

The decrease in irreversibilities should theoretically give the Kalina cycle an advantage over ORCs. Bombarda et al. (2010) observed that a Kalina cycle only managed to offer marginal improvements over an optimized ORC but it required a more complex component layout. It provided large improvement in decreasing the irreversibility in the evaporator but its advantage was marginalized when the losses from the additional equipment were accounted for. For medium grade heat they stated that at a 100 bar the cycle components would have to be made of expensive materials to resist both the pressure and corrosive nature of ammonia-water mixtures. They also mentioned

that the small temperature differential of the Kalina cycle can be problematic in that large heat exchangers are required to achieve the desired high side temperature.

Hettiarachchi et al. (2007) modeled Kalina cycles with different ammonia-water mixtures and compared them to ORCs with ammonia and isobutene as working fluids. They found that the Kalina cycle provided better thermal efficiencies than the ORC for a given heat input. Their findings are summarized in Table 3.1.

Table 3.1: Kalina cycle and ORC simulation with a geothermal source at 90°C (Hettiarachchi, 2007).

Cycle	Pressure [MPa]	η [%]	Ammonia Fraction	Working Fluid
Kalina	2.6	8.9	0.8	Ammonia-water
Kalina	3.3	10.5	0.95	Ammonia-water
ORC	0.9	7.3	N/A	Isobutene
Rankine	3.4	10	N/A	Ammonia

Both Kalina cycles outperformed the ORC with isobutene but the ORC with ammonia remained competitive. The low 90°C heat source gives the advantage of requiring only moderate pressure for the Kalina cycle. This would allow it to be fabricated with more cost effective materials.

3.1.3 Transcritical CO₂ Cycle

The primary differences between this cycle and a supercritical ORC are that it operates closer to the triple point and uses CO₂ as the working fluid. Operating close to the triple point decreases the amount of work required to compress the working fluid. A T-s diagram of the cycle is shown in Figure 3.4. The benefits of using CO₂ as a working fluid is that it is non-toxic, inert, abundant, inexpensive, and is environmentally friendly

because of its lower GWP compared to hydrofluorocarbon-based refrigerants. In order to achieve supercritical conditions the P_{\max} of the cycle must be over 73.8 bar.

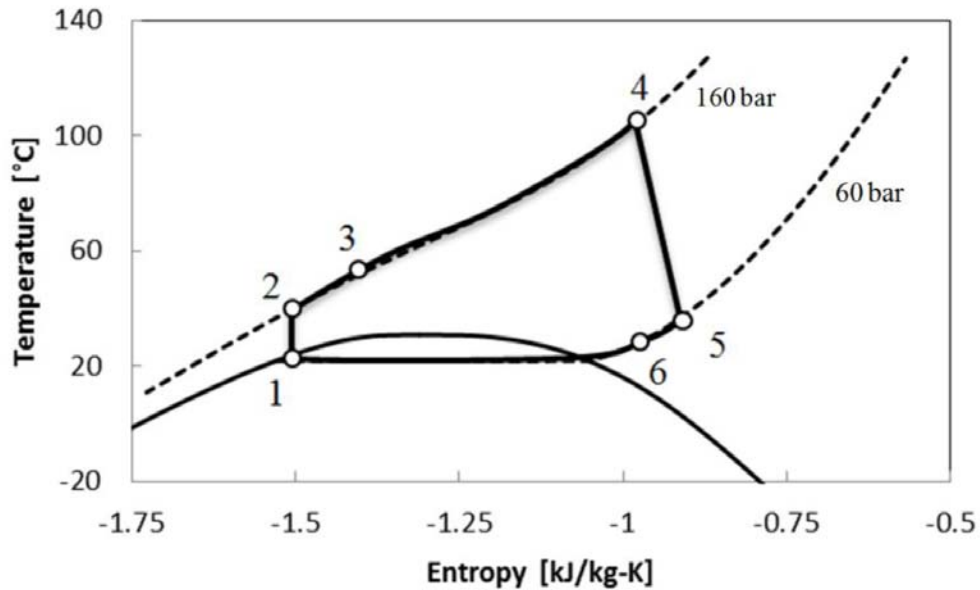


Figure 3.4: T-s diagram for a transcritical CO₂ cycle (Chen, 2006).

This cycle like the Kalina cycle reduces the irreversibilities in the evaporator through better temperature matching of the heat source. Theoretically this cycle should achieve better performance than an ORC (Chen, 2006). Super critical fluids give better agreement with source temperature profiles than azeotropic fluids.

Chen et al. (2006) modeled a transcritical CO₂ cycle with a 150°C heat source. They observed that it gave marginal improvements in performance over an ORC that used R123. The transcritical cycle operated at a P_{\max} of 160 bar which was described as an advantage because more compact components could be used. The high operating pressure also comes with the disadvantage of requiring thicker pressure vessels and piping which will increase the capital cost of the system (Fraas, 1982).

3.1.4 Stirling Engine

The Stirling engine is an old thermodynamic cycle that was patented by its inventor Robert Stirling in 1816. It is a closed reversible cycle and resembles the Carnot cycle in order to maximize thermal efficiency (Moran, 2004). The thermodynamic process of this cycle is shown in Figure 3.5.

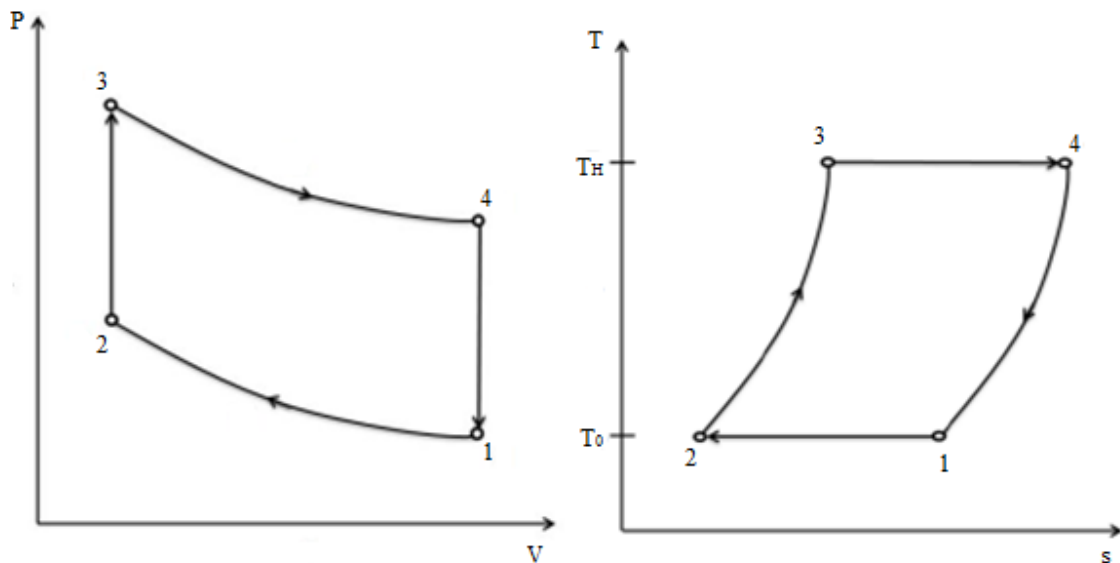


Figure 3.5: Qualitative P-v and T-s diagram for a Stirling engine (Harada, 2011).

The thermodynamic processes are described by:

- *Isothermal compression* $1 \rightarrow 2$: the compression piston moves forward to the regenerator and the working fluid stays at a constant temperature as heat is removed from T_C to the surroundings. The amount of work performed on the fluid is equal to the amount of heat that is removed.
- *Constant volume regeneration* $2 \rightarrow 3$: both pistons move to keep the volume constant. The fluid is transferred from the compression chamber to the expansion

chamber through the regenerator where it picks up heat and raises its temperature to T_H . The pressure increases and no work is done

- *Isothermal expansion* $3 \rightarrow 4$: the expansion piston moves outward increasing the volume and decreasing the pressure. The temperature is kept constant by adding heat externally. The amount of heat that is put into the system is equal to the amount of work taken out.
- *Constant volume regeneration* $4 \rightarrow 1$: again both pistons move to keep the volume constant and as the fluid moves back through the regenerator heat is removed and stored. This reduces the temperature of the working fluid to T_C .

The Stirling engine is composed of the following components: piston engine, heater, regenerator, and cooler. The piston engine has several different configurations and three common types are alpha, beta, and gamma. The regenerator itself is a porous matrix that stores heat from the working fluid during $4 \rightarrow 1$ and returns it in $2 \rightarrow 3$. It can be made of several materials like steel wool, steel felt, wire mesh, fine pipes, spring mesh, stacked screen, and metal foils (Thombare, 2008). A component diagram and illustration of the different thermodynamic processes are shown in Figure 3.6.

The main factors that affect the performance of the engine include regenerator effectiveness, volumes of un-swept gas that are known as dead volumes, thermal losses, and mechanical losses from seals, piston rings, bearings, and other frictional parts. Additionally ideal assumptions such as isothermal processes and a regenerator effectiveness of unity are not practical and would require infinitely slow heat transfer time or an infinitely long heat transfer area. From a material stand point a disadvantage of this cycle is its operating pressures which can reach 10-20 MPa (Thombare, 2008).

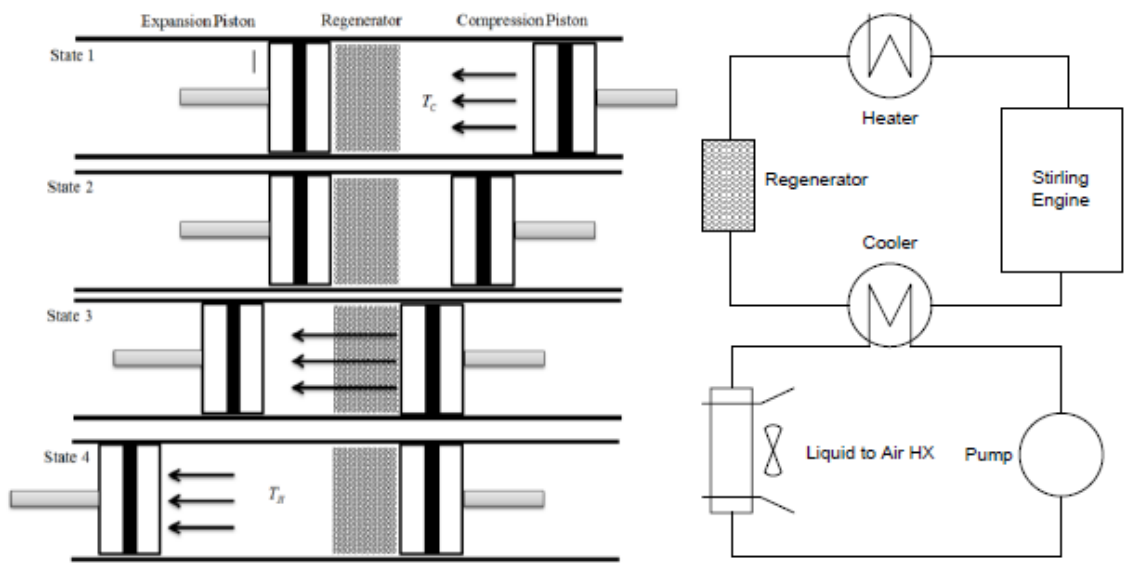


Figure 3.6: Illustration of the different thermodynamic states of the Stirling cycle and system diagram (Thombare, 2008).

Thombare (2008) made the following recommendations for the regenerator design. Desirable characteristics include maximizing heat capacity and heat transfer while minimizing dead space, flow losses, and contamination. The working fluid should have a high thermal conductivity, high specific heat capacity, low viscosity, and low density. Some common working fluids are helium and hydrogen.

They described the Stirling engine as one of the most complicated thermal cycles due to the interwoven motions of the compression-expansion pistons, heat transfer, and complicated control schemes. It requires joint thermal, fluid, and mechanical considerations in its design and optimization. It should be noted that the cycle when properly optimized can achieve efficiencies that are 65-70% of the Carnot efficiency.

3.1.5 Thermoelectric Generators

These devices produce a voltage potential from a heat flux. A simple form of this device would be comprised of several thermocouples connected in series to create a usable voltage (Fraas, 1982). This device would resemble a thermopile and would have a very low efficiency. To obtain improved efficiencies special materials are used to maximize this potential. The elements of a TEG (Thermoelectric generators) are shown in Figure 3.7.

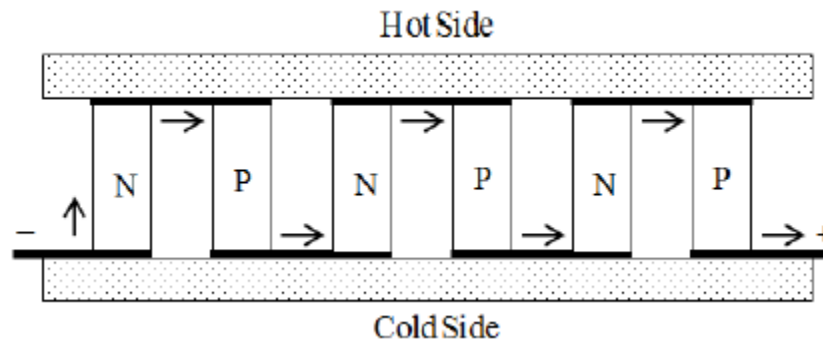


Figure 3.7: The arrangement of the P and N type semiconductors in a TEG (Fraas, 1982).

The N and P-type semiconductors are characteristically different. The N-type moves free electrons from the cold side to the hot and the P-type move them from the hot to the cold. A TEG is composed of a series of these devices.

The advantage of a TEG is that they have no moving parts and therefore have exceptional reliability. Unlike heat engines these devices are able to produce electricity directly from the flow of heat. An innovative application of TEGs is using them combined with an ORC (Miller, 2009).

3.1.6 Organic Rankine Cycle

The Rankine cycle is a closed power cycle that has been used for more than 150 years for the heat pumps. A Rankine cycle describes a model of steam powered heat engine for the power plants generally have four components, namely, condenser, boiler, pump and expander. Working fluid is heated by boiler where it becomes high-pressure vapor, it is then introduced in to expander to produce power by rotating generator. The low temperature working fluid from expander cooled and condensed in a heat exchanger and pumped to be able to perform the same process for power generation.

3.1.6.1 Cycle Configuration

Rankine cycle takes advantage of the small amount of work required to pump a liquid and the amount of energy that can be extracted from latent heat. An ORC differs from the basic Rankine cycle in that the working fluid is organic. Sahar et al. (2007) modeled 31 different working fluids in different ORC configurations. Types of organic working fluids modeled included alkanes, fluorinated alkanes, ethers and fluorinated ethers. These fluids can behave differently when used in an ORC and it is important to discuss the different configurations and working fluid characteristics together. Organic working fluids have performance advantages over water-steam at low power levels but these advantages disappear at 300 [kW] or more because of the poor heat transfer properties of organic fluids. The basic Rankine cycle is illustrated in Figure 3.8.

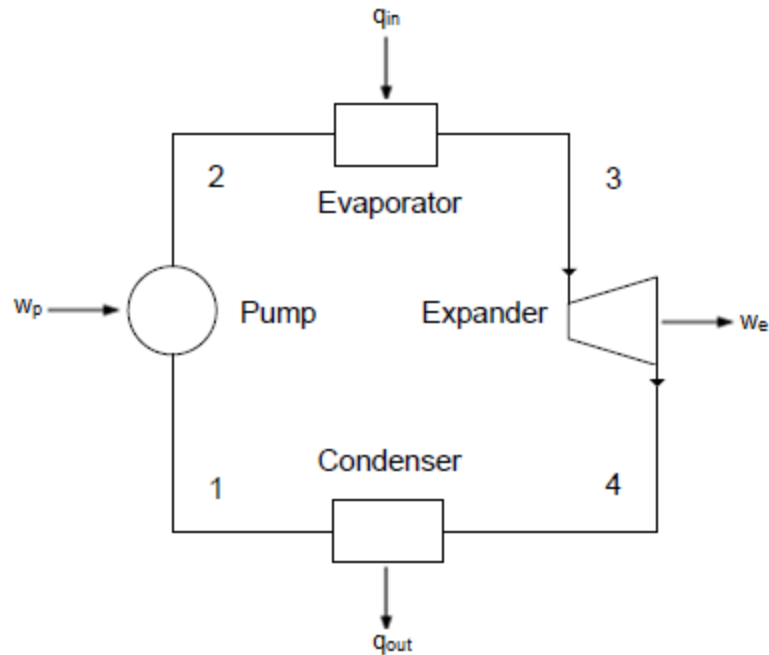


Figure 3.8: Basic Rankine cycle.

3.1.6.2 Working Fluids

Organic fluids should be considered since they have additional properties such as boiling temperature, latent heat, critical point, and stability temperature which are all important in ensuring good thermodynamic performance. Fraas (1982) mentions it also has effects on the expander type used as in the case of small turbines a high molecular weight is desired to maintain a high and optimal Reynolds number. A low critical point is useful when *s*-type cycles are considered. Boiling temperature and stability temperature are important when choosing a fluid for the heat source. Thermophysical properties of several refrigerants are summarized in Table 3.2.

Working fluid should also be considered in terms of environment and inhabitants beyond thermodynamic performance. Therefore global warming potential (GWP), ozone depletion potential (ODP), toxicity, flammability, material compatibility and atmospheric

lifetime are also important factors. Hung (2001) mentioned that refrigerants have a low toxicity in general. Table 3.3 shows some of these properties for different working fluids.

Table 3.1: Summary of thermophysical properties of different refrigerants.

Fluid		Type	Molecular Weight [g/mol]	Critical Point [C°] / [bar]	Boiling Temp. [C°]	Latent Heat@ 1 atm. [kJ/kg]
Water	H ₂ O	w	18.02	374 / 220.6	100	2257
Ammonia	CF ₃ -CH ₂ F	w	17.03	132.3 / 113.3	-33.3	1370
R11	CCl ₃ F	i	137.4	198 / 44.1	23.8	180.3
R123	C ₂ HCl ₂ F ₃	i	170.6	183.7 / 36.7	27.8	170.6
R134a	C ₂ H ₂ F ₄	w	217	101 / 40.6	-26.1	217
R245fa	C ₃ H ₃ F ₅	i	134	154 / 36.5	15.2	196
R601	C ₅ H ₁₂	d	357.8	196.5 / 33.4	35.9	357.8
n-hexane	C ₆ H ₁₄	d	86.17	234.7 / 30.6	69.27	329.9

Table 3.2: Summary of atmospheric lifetime, GWP, and ODP of different fluids.

Fluid	Lifetime [years]	GWP (20 years)	GWP (100 years)	ODP
CO ₂	-	1	1	-
R11	45	6,730	4,750	1
R22	12	5,160	1,810	0.055
R123	1.3	273	77	0.02
R134a	14	3,830	1,430	-
R152	0.6	187	53	-
R245fa	7.6	3,380	1,030	-

All HCFC refrigerants are scheduled to be phased out by 2030 as all countries agree in 2009, World Climate Conference and most CFCs are already prohibited. This makes these fluids poor choices as long term candidates for working fluids.

It can be observed from Table 3.2 that most fluids with simpler molecules have lower critical temperatures and also tended to be *w*- or *i*- types. Hung (2007) and Schuster (2010) found that complex molecules have higher critical temperatures in comparison and tend to be *d*- fluid.

Saleh (2007) showed that fluids with low critical temperatures had a low thermal efficiency when evaporated at subcritical conditions. He found that the low critical point of organic fluids makes the supercritical ORC a practical solution.

Saleh et al. (2007) also noticed that superheating *w*- and *i*- fluids is increasing the thermal efficiency. Through the use of both superheat and regenerator, more significant gains can be achieved. Pedro et al. (2008) and Mago et al. (2007) observed that *d*-working fluids show a decrease in thermal efficiency with superheat. They both noted that superheat would cause an increase in irreversibility and for maximum performance the cycle should be operated at saturated conditions.

Sahar et al. (2007) recommended R236ea, R245ca, R245fa, R600, R600a, R601a, RE134, and RE245 as working fluids in ORCs and stated that fluids with higher boiling temperatures showed better performance. Borsukiewicz-Gozdur et al. (2007) recommended both R245fa and R235ea as working fluids. Mago et al. (2007) concluded that *d*- working fluids such as R113, R123, R245ca, R245fa, and isobutene achieved better performance than *w*- working fluids such as R134a and propane.

3.1.6.3 Irreversibilities

The irreversibilities such as friction and leakage losses in the cycle cause reduction of cycle efficiency and of useful work output. Friction and leakage losses from expander contribute the highest portion of the irreversibilities with pressure drops and inefficiencies from the heat exchanger. The improvements regarding the geometry of the scroll machine will directly affect the cycle efficiency not only because of reducing the leakages but also to obtain appropriate built-in ratio for the compression/expansion process.

ORC has inherent irreversibilities as many processes. The losses may come in the form of friction-heat losses in the expander and pump. This is accounted in the isentropic efficiencies of each device. Valves, pipes and pressure drops are other sources. Hung (2001) stated that the largest source of irreversibility in the system is caused by the evaporator. The mismatch between the working fluid and the heat source causes this type of loss. Larjola (1995) showed that the organic working fluids due to their low latent heat match the source temperature profile better than water-steam.

There are some practical solutions to reduce losses for ORC. The liquid entering the pump should be sub-cooled to prevent cavitations. The fluid should be superheated when using turbines with w- type working fluids to prevent droplet formation during expansion. Moran (2004) stated that the quality at the turbine exit can be kept at 90%. Both cavitation and high speed droplets will corrode the pump and expander.

3.1.1.4 Cycle Improvements

There are a limited number of ways to improve the thermal efficiency of the cycle after the cycle configuration and fluid have been specified. Increasing the average high side

temperature or decreasing the average low side temperature is one of the approaches that can be used. The high side temperature is fixed in low temperature heat recovery and decreasing the condenser temperature below atmospheric conditions is not practical. Other approaches include increasing the isentropic efficiencies of the pump and expander. The pump work is significantly less than the expander work in a Rankine cycle. Therefore improvement of the efficiency of the expander will provide the greatest degree of cycle improvement.

Badr et al. (1984) modeled an ORC and performed a sensitivity study to show which of these parameters had the greatest effect on thermal efficiency. They varied the isentropic expander efficiency, evaporator temperature, and condenser temperature. They modeled both a basic and regenerative ORC with R113 as the working fluid. Their findings are shown in Figure 3.9.

The evaporator temperature and the expander efficiency are both important parameters in optimizing a ORCs performance. They noted that the expander efficiency was the most important parameter in low temperature energy recovery and that great care should be taken during expander selection in order to increase cycle efficiency.

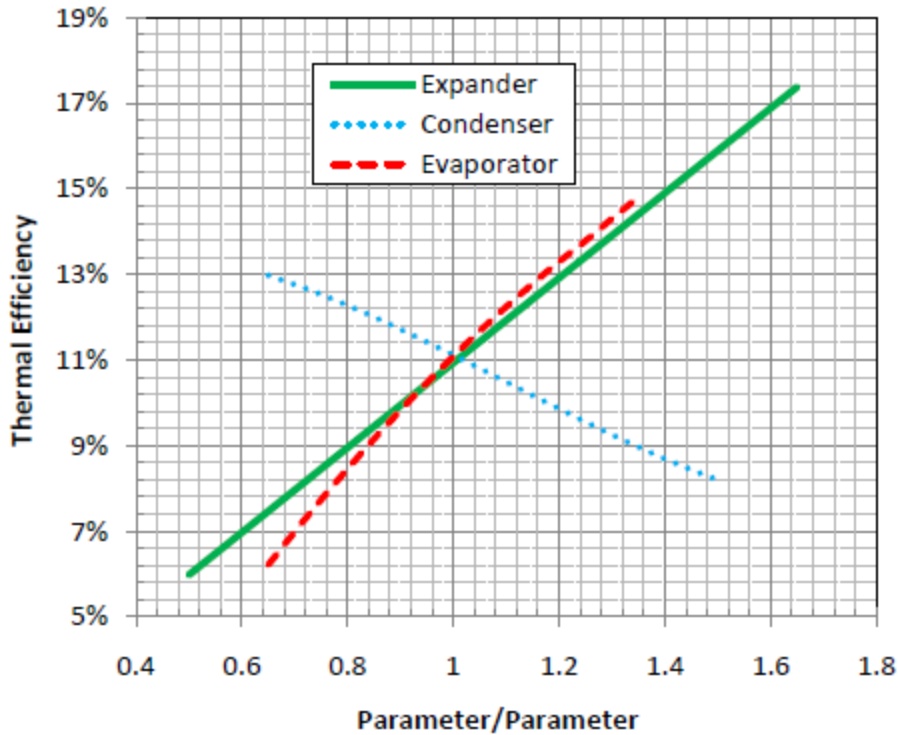


Figure 3.9: Sensitivity analysis of a regenerative ORC with varying expander efficiency, evaporator temperature and condensing temperature (Badr et al., 1984).

3.1.7 Comparison of Cycles

Power generation cycles and devices have their own advantages and disadvantages. The Kalina and transcritical CO₂ cycle show promise in thermodynamic performance but have not met widespread adoption and have not been proven. Both cycles have high operating pressures which introduces material limitations. The use of corrosive ammonia in the Kalina cycle limits the materials that can be used. There continues to be work on the Stirling engine and TEG and they hold promise of higher thermal performance. The Stirling engine has the disadvantage of operating at very high pressures and temperatures. The ORC requires a minimal number of components and is well established technology. The copious number of working fluids allows it to be optimized for a variety of heat

sources. Additionally it can operate efficiently over a wide range of pressures and temperatures.

3.2 Classification of Expanders

Expander is the one of the most important component in the efficient recovery of low temperature heat. Classification of Harada (2010) is used to describe expanders by their characteristics and operating parameters. The selection of the correct type as well as the optimization of its performance is paramount in achieving high thermal efficiencies. There are many important parameters when selecting an expander such as high isentropic efficiency, pressure ratio, power output, lubrication requirements, complexity, rotational speed, dynamic balance, reliability, and cost. In low temperature heat recovery the turbine, which is the dominant type of expander in conventional power plants, is not necessarily the most appropriate choice. Expanders can be categorized into dynamic and positive displacement types. Most compressors are positive displacement while turbo-machinery is dynamic. Research in the area of compressors has led to many devices that have been found to function efficiently as expanders. The expanders that will be discussed include turbine, reciprocating piston, rotary vane, rolling-piston, gerotor, and scroll types.

3.2.1 Turbines

Turbines are dynamic machines and can be broken up into impulse, reaction, and radial inflow types. Impulse turbines guide the flow into bucket shaped blades at which the kinetic energy of the fluid is converted into motion of the rotor. Reaction turbines in comparison use aerodynamic lift. Radial inflow turbines are like reaction turbines, but in

a different orientation. These different types are reported by Harada (2011) and illustrated in Figure 3.10.

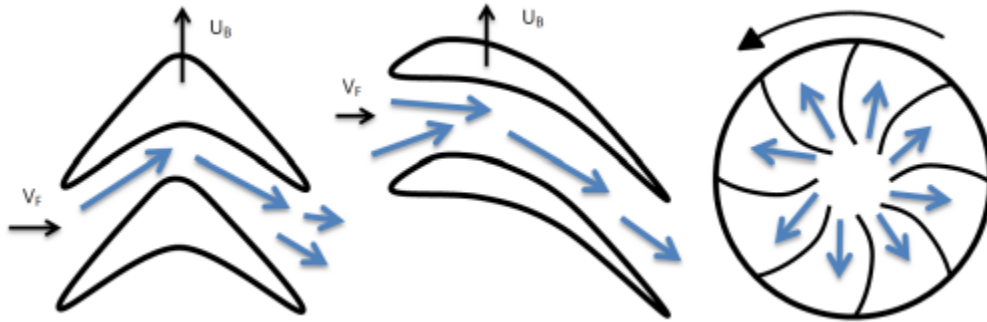


Figure 3.10: Impulse turbine (left), reaction turbine (middle), and radial inflow (right) (Harada, 2011).

Turbines dominate utility level power generation. Fraas (1982) showed that they are known to achieve isentropic efficiencies over 90% at this size. The most critical factor in turbine performance is the ratio of the rotor tip speed to the incoming fluid speed (U_B/V_f). The tip speed is defined as

$$U_B = \frac{\pi NR}{30}$$

where N is the rotational speed (RPM) and R is the radius of the turbine. It can be observed from the relation that for a given U_B/V_f ratio and a specified V_f a small machine must rotate at very high speeds to maintain optimal performance which makes turbine have a poor design performance. Froos (1982) found that turbines have tip speeds of 305 m/s in order to reduce the number of turbine stages in practice. The high speed of turbine is related to the blade Reynolds number which should be on the order of 10^6 . This is difficult to achieve in small turbines and organic fluids which have high molecular weights are used to maintain this parameter. Low pressure drop per stage is the another

characteristics of turbines. Froos (1982) presented that a pressure ratio of 2 is considered large and larger pressure ratios are achieved by using multiple stages and the cost increases due to that phenomena.

The losses in a turbine's performance primarily contributed from aerodynamic effects such as flow separation which can account for 10-30%. Other types of losses and their contribution include tip leakage (1-2%), bearings (1%), seal leakage (1%) and moisture churning (1% per 1% of moisture). For the small scale turbines certain losses increase (Froos, 1982). He reported that the tip leakage which is the amount of fluid that passes between the housing and the tip of the turbine blades increases to 10-15% in small machines. Other parameters for small scale turbines which produces power between 10-100 (kW) are small blade height, low Reynolds number effects, tip clearance, surface finish and manufacturing tolerances which are described by McDonald (2008).

The condensate formation from wet expansion is one of the most common problems with turbines. These droplets impact the blades and over time cause erosion which results in poor performance and mechanical failure. It was mentioned that a quality of 90% or higher is optimal at the turbine exit. The problem caused by condensation takes place when the turbines are used with d-fluids in ORC.

Yamamoto (2001) investigated the performance of small scale vapor turbines. He designed a small scale turbine for an ORC that used R123 as a working fluid. The turbine was a radial inflow type with 18 blades, 30 mm in diameter, 4.5 mm thick and achieved a maximum isentropic efficiency of 46%. The study also searched the effect of operating conditions on turbine performance and showed that by changing the heat input from 13 kW to 9 kW the turbine efficiency drops to 15%. The reason of the performance drop was

the change in volumetric flow rate. It can be observed that power output of the turbine is highly sensitive to changes in operating conditions and any deviation can cause high amount of decrease in power output.

Yogoub (2006) designed a turbine for ORC and achieved isentropic efficiency of 85% at 60.000 rpm when used with HFE-301. He investigated the effect of the working fluids rather than operating conditions and showed that the efficiency decreases to 40% when n-Pentane used as a working fluid. The power output was approximately 1 kW. That means small scale turbines are capable to achieve high isentropic efficiencies but it should be noted that they have high capital cost.

3.2.2 Reciprocating Piston Engines

Pistons are positive displacement machines used in a Rankine cycle which is composed of three processes; intake, expansion and exhaust as illustrated in Figure 3.11. Harada (2010) explained the working principles of reciprocating pistons.

When the piston is at top dead center (TDC) the intake valve opens. High temperature-pressure vapor fills the chamber until the piston reaches the location of expansion (LOE) and the intake valve closes. The vapor expands driving the piston down to bottom dead center (BDC) and the exhaust valve opens. The piston rises to TDC to expel the low temperature-pressure vapor. Upon reaching TDC the exhaust valve closes and the cycle repeats.

Reciprocating pistons are complex devices that require precise timing of the intake and exhaust valves. They also require both primary and secondary balancing. Primary balance is the effect caused by a mass rotating about the shafts center and secondary is the effect of a mass that rotates around a center that is not concentric with

the shaft. They are also known to have large friction losses from the large number of interacting surfaces. A primary contribution is friction between the piston rings, piston, and cylinder wall. An ORC could decrease the impact of these losses by dissolving oil into the working fluid.

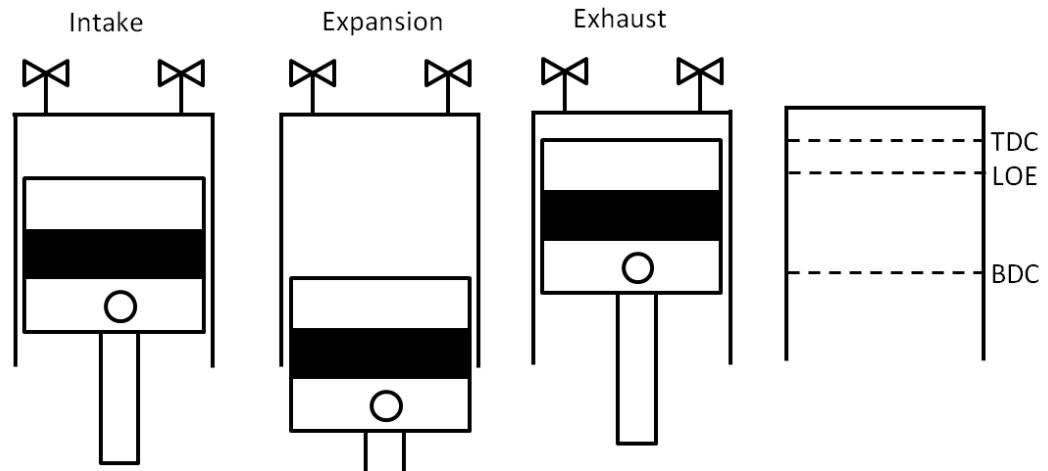


Figure 3.11: Different processes of a reciprocating piston (Baek, 2005).

Baek et al. (2005) design a transcritical CO₂ heat pump and replaced the expansion valve with a piston expander in an effort to increase the COP. The expander was a modified four cycle two cylinder gasoline engine. To limit the requirement of a flywheel the two pistons were modified to operate out of phase. The valve timing was controlled by electronic solenoid valves. The displacement volume of the device was 26.52 cm³. The expander achieved a low isentropic efficiency of 11%. The lower performance was contributed to internal leakages.

Zhang et al. (2007) also developed a transcritical CO₂ cycle but fabricated a free piston expander to replace the expansion valve. This device combines the compressor and expander into one unit. This eliminates the need for a camshaft. Instead a slider controls

the opening and closing of the intake and exhaust valves. It was expected to achieve a compressor and expander efficiency of 60% and 70% respectively. Extrapolating data from the P-V diagram and their expert opinion they estimated the expander efficiency to be 62%. Under expansion was estimated to account for 10.3% of the loss while 8.4% was contributed to the large pressure drop in the discharge process.

3.3.3 Rotary Vane Expander

Rotary vane expanders (RVE) are positive displacement devices. The makeup includes housing, rotor, vane slots, and vanes which are shown in Figure 3.12. In operation a high pressure-temperature vapor enters the inlet (1) which expands causing the rotor to move. Harada (2010) described the opponents and working principles of rotary vanes in details.

As the rotor moves the expansion volume increases (2→3). The volumes are kept isolated by the vanes which slide out to form a seal. High pressure behind the vanes keeps them in place. At the end of expansion the vapor is exhausted (4). Badr (1984) stated that they have several positive characteristics such as simple construction, low noise- vibration, high volumetric expansion ratios as large as ten, and are tolerant of wet expansion. Tahir et al. (2010) described in their study that they are also capable of handling high pressures.

In operation the device must be lubricated to minimize wear and enhance sealing. A low number of contacting surfaces minimizes friction loss in these devices. Leakage has been found to be a larger contributor in performance loss than friction by Tahir (2010) and Yang (2009). This occurs in two locations; between the vanes and housing as well as in between the rotor ends and sealing faces. Badr et al. (1984) claimed that the

pressure drops during intake account for 65% of the loss in efficiency while leakage only accounts for 20%.

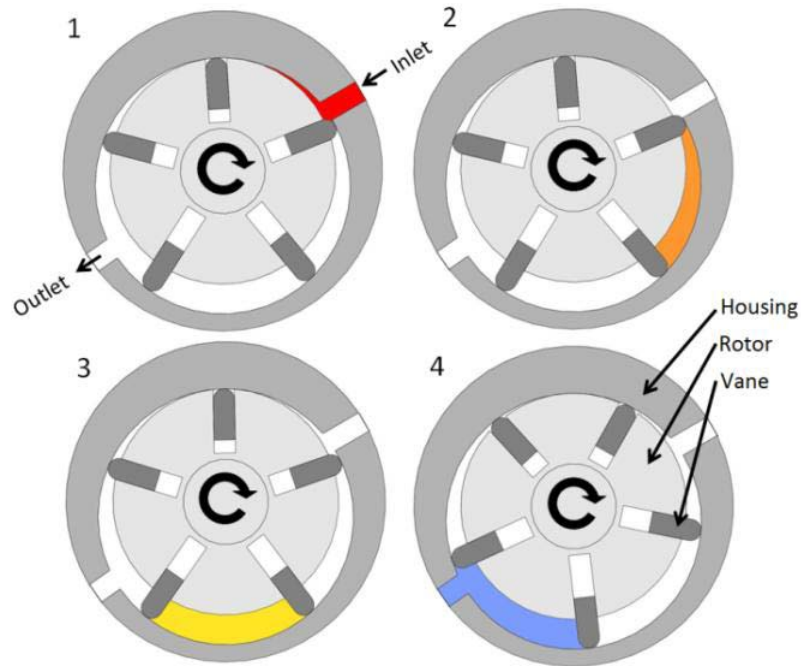


Figure 3.12: Rotary vane expander with intake (1), expansion (2-3), and exhaust (4). Leakage and friction are the primary causes for loss in performance RVE (Harada, 2010).

Yang et al. (2009) tested a double acting RVE in a vapor compression cycle where it replaced the expansion valve to improve the COP. A double acting RVE has two inlets and exits which is beneficial because it creates balanced loading and low vibrations. In its design particular attention was given to leakage. Springs were placed behind the vanes to ensure good sealing. The expander achieved a maximum isentropic efficiency of 23% at 800 [RPM]. The efficiency decreased at higher speeds and was contributed to the increase in frictional losses. In some cases with RVEs the vanes will impact the cylinder wall. The authors concluded the main cause of this was by incoming

vapor pushing the vanes to the bottom of the slots which then bounce back and strike the cylinder wall.

Mohd et al. (2010) tested a RVE in an ORC with a source temperature that ranged between 60-80°C. The RVE achieved a maximum isentropic efficiency of 48% with a power output of 32 W.

3.3.4 Rolling Piston Expander

The rolling piston expander is a positive displacement device in which the piston and the vane are one part. In Figure 3.13 the rolling piston is shown during expansion. The piston begins to roll when the high-temperature vapor enters the inlet (1). This rolling houses the expansion of the vapor (2→3) . The vapor is exhausted at the end of the expansion through the outlet (4). The sealing vane is in constant contact with the rolling piston and is held in place by a spring. These devices are commonly used as compressors in the vapor compression cycles. Haiqing (2006) mentioned that the development of these devices has continued since the 1970's due to their ability to handle large pressures at low compression ratios.

Rolling piston expanders have some advantages including simple construction, few parts and the ability to handle high pressures. They require tight tolerances to minimize leakage due to their constrained nature and lubrication is needed to minimize wear and enhance sealing. Friction and leakage are the main losses. Large pressure difference between the neighboring chambers causes leakage between the rolling piston and the cylinder wall.

Wang et al. (2010) used a rolling piston expander in a solar powered ORC that used R245fa as the working fluid. It achieved a maximum isentropic efficiency of 45.2%

at 800-900 rpm. Haiqing et al. (2006) used a swing piston expander to replace the expansion valve in a transcritical CO₂ cooling cycle. They claimed that a swing piston should have superior performance over a rolling piston because of a reduction in friction and leakage. It achieved a maximum isentropic efficiency of 44% at 1,800 rpm. In contrast this device performed no better than the aforementioned rolling piston expander. Subiantoro and Ooi (2010) modeled the performance of a revolving vane expander and claimed that it should provide superior performance to both the rolling piston and swing arm expanders. They recommended a revolving vane expander where the sealing vane is attached to the rotor and the rotor is the driving mechanism.

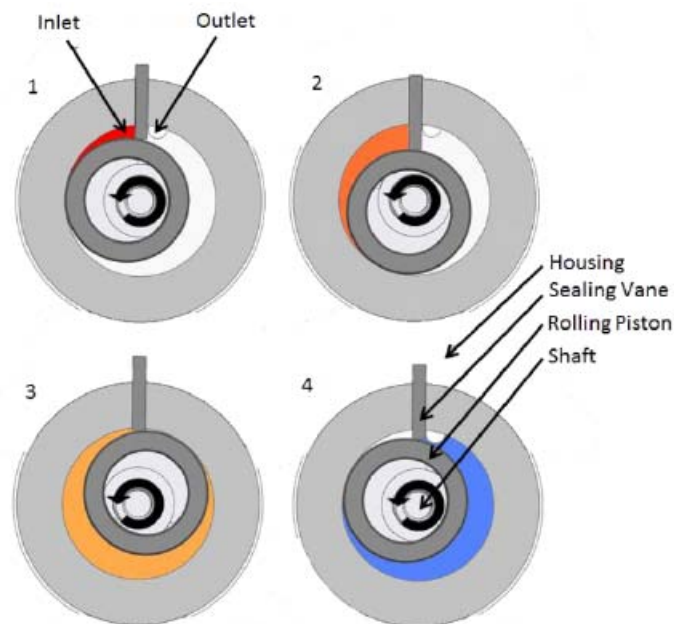


Figure 3.13: Rolling piston expander with intake (1), expansion (2-3), and exhaust (4) (Harada, 2010).

3.3.5 Gerator

The gerator is a positive displacement device. It consists of an outer stator and inner rotor that have eccentric centers to each other. Both of these components share a common shaft and are illustrated in Figure 3.14. The rotor has four teeth and the stator has five. The

contact points between the two form a sealed chamber for the expanding vapor. It has the advantage of a reduction in friction between the rotor and stator. The rotor and stator do not rotate at the same speed. A five tooth stator will move at one-fifth the shaft speed relative to the rotor (Sabiontoro, 2010). This means that a shaft rotating at 3,000 [RPM] would result in a relative shaft speed of 600 [RPM] between the rotor and stator. The gerotor also benefits from a simple construction. This device shares many of the advantages of the rotary vane and rolling piston expanders but with a reduction in friction losses.

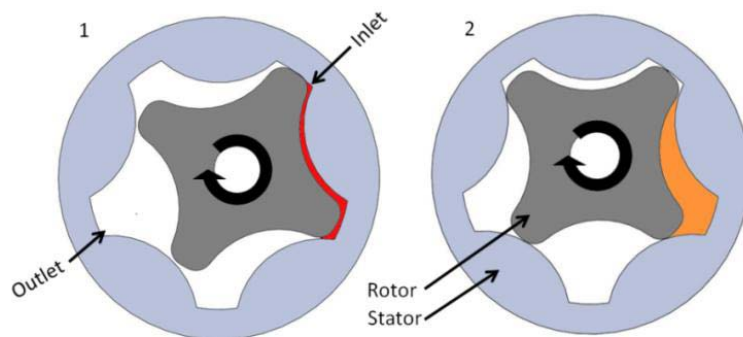


Figure 3.14: Gerotor expander with intake (1) and expansion (2) (Harada, 2010).

Mathias et al. (2009) demonstrated a gerotor in an ORC. They tested three different gerotors which they identified as A, B, and C. Gerotor A had a large spacing between the stator and rotor. This resulted in excessive leakage and poor performance. It achieved a maximum isentropic efficiency of 66%. Gerotor B in contrast had insufficient spacing between the rotor and stator which was contributed to thermal expansion. It eventually failed due to excessive wear but achieved an isentropic efficiency of 66%. Gerotor C showed good performance and achieved a high isentropic efficiency of 85%.

An interesting quantity they used to optimize the performance of their expanders was the expansion-matching ratio (EM_{ratio}). It is a figure of merit of how close an expansion process comes to a device's ideal expansion. A value close to unity represents an ideal expansion. Alternatively the ideal expansion can be determined through a qualitative evaluation of expander performance as a function of pressure ratio. Evaluating the data we can see that with an EM_{ratio} of 1.07 gerotor C achieved an isentropic efficiency of 85%. The efficiency drops to 45% when the EM_{ratio} is 1.39. This shows that the gerotor has poor off design performance.

3.3.6 Scroll Expander

Scroll machine is first invented by Croux (1905) and main characteristics, working principle has been known since then for more than a century. But it took almost 70 years for the industry to provide machine tools with small enough tolerances to be able to manufacture scroll pairs. Since then development and technical studies have been growing regarding environmentally friendly working fluid search, possible heat engine applications and improvement of geometry to reduce leakages for an efficient compression and expansion process.

The scroll expander is a positive displacement device and is commonly used as a compressor in vapor compression cycles. Common to all positive displacement devices it has a fixed volumetric ratio. Compared to the aforementioned positive displacement expansion devices it has the most complicated geometry. It is made up of two involute curves in opposing directions. They are called the orbiting and fixed scrolls. The fixed scroll does not move and the orbiting scroll always keeps its orientation while it orbits around the shaft's center. The high pressure-temperature vapor enters the suction port (1).

It then expands steadily increasing the expansion volume (2-5). At the end of the expansion the low pressure-temperature vapor is exhausted (6). This process is shown in Figure 3.15.

Scrolls can be categorized into two types; compliant and kinematically constrained. Constrained scrolls are fixed in their position. They can be constrained radially, axially, or both. Commonly they are composed of three cranks that are separated by 120° (Peterson, 2008). The three cranks are then linked to a common shaft. It is because of this additional gearing that the scroll and shaft can have different speeds (Kim, 2007). Manufacturing tolerances are a critical parameter in the effective sealing of constrained scrolls. A compliant scroll in contrast is not constrained and uses a centrifugal effect to keep the orbiting scroll in continuous contact with the fixed scroll. Compliant scrolls require lubrication to operate efficiently without causing significant wear. Constrained scrolls in contrast can operate without lubrication.

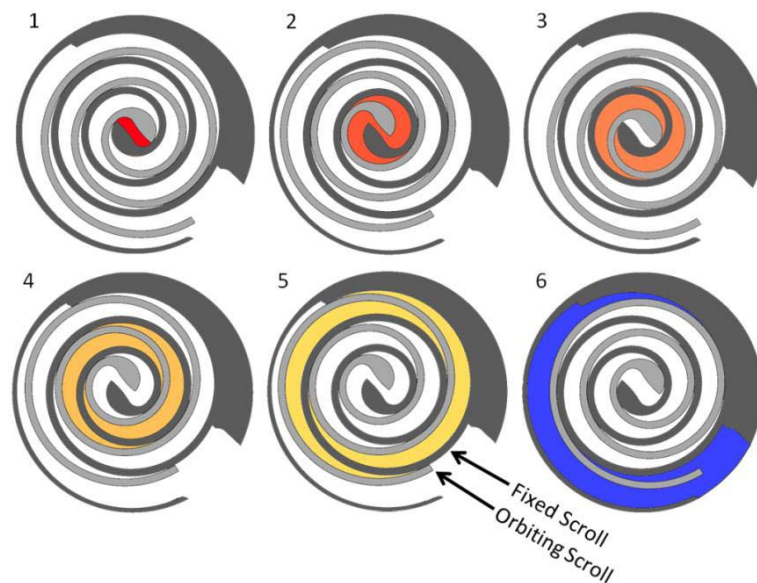


Figure 3.15: Scroll expander with fixed and orbiting scroll. Intake (1), expansion (2-5), and exhaust (6) (Harada, 2010).

Like the aforementioned positive displacement expanders scrolls are negatively impacted by leakage. The two leakage passages in a scroll assembly are shown in Figure 3.16.

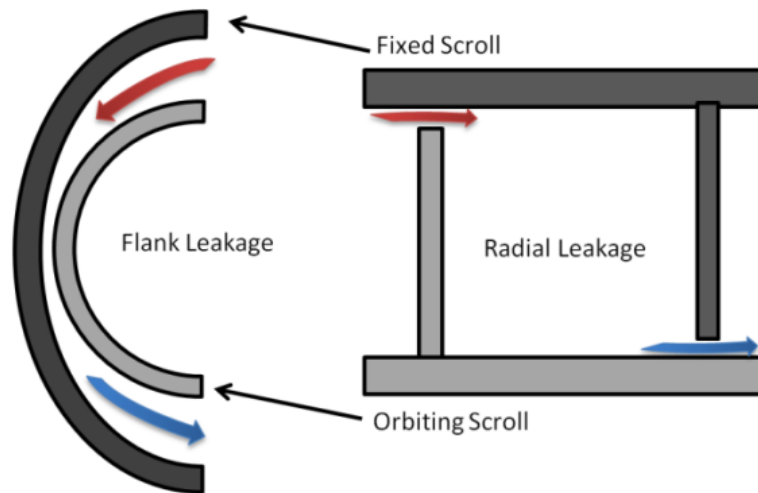


Figure 3.16: The two passages for leakage in a scroll assembly (Xiajun, 2004).

An advantage of compliant scrolls over constrained types is that they can provide better radial and flank sealing. The scroll wraps are only separated by an oil film. They also have the advantage of being tolerant of liquids which allows them to increase the gap size if excessive pressure builds up inside the device (Peterson, 2008).

In constrained scrolls a low friction material is used to form a tip seal between the plates which resists radial leakage. Only the tight tolerances between wraps minimize the amount of flank leakage. This sealing can be improved by using oil which acts as a gap filler. Peterson et al. (2008) mentioned that constrained scrolls that operate as expanders have a tendency to washout this oil. When they operate as compressors it is swept in.

The primary modes of loss are both leakage and friction. Peterson et al. (2008) determined that the poor performance of constrained scroll expanders was caused by

excessive leakage. Lemort et al. (2009) created a semi-empirical model for the performance of a scroll expander. They concluded that internal leakage is the largest contributing factor in efficiency loss. The lesser but second largest contributor was mechanical losses. Other publications have also concluded that leakage is the primary cause for decreased performance (Kim, 2007).

In constrained scroll expanders internal leakage can be controlled to an extent by increasing the speed of the expander. This is why their efficiency increases with speed (Xiajun, 2004) because of the time the vapor has to escape decreases. There is a point where increasing the speed will have a negative impact on performance. At excessive speeds frictional losses will become noticeable.

Scroll expanders have demonstrated high performance over a variety of working conditions. They consistently achieve isentropic efficiencies over 50% and have achieved efficiencies as high as 83%. They also have demonstrated good partial load performance (Schuster, 2010).

Scroll geometry is one of the key components affecting the scroll machine efficiency defining chamber areas and volumes. The parameters to describe scroll geometry have to be understood to generate equations for volume and area of the expander chambers as a function of angle in terms of obtaining specific characteristics of the working fluid. The shape of the scroll expander is an involute of a circle with a constant distance of wraps.

The geometry of the scroll machine was defined by Halm (1997). The goal of the geometrical modeling is to define pocket volumes for intake, expansion and discharge chambers as a function of orbiting angle (θ) to obtain volume-angle functions. The

orbiting angle describes the number of turns of the orbiting scroll around the fixed scroll for a complete cycle of expansion. The study of Wang (2005) evaluates the chamber volumes as a function of orbiting angle throughout the compression process in a scroll machine. In this thesis analytic expressions calculated for scroll compressor by Wang is converted for the expander operation to use in organic Rankine cycle application since they are reversible machines.

In order to define the position of fixed and orbiting scroll, conjugacy of the scroll profiles is given by Bush (1992). Calculation of the chamber volumes between the fixed and orbiting scroll with respect to orbiting angle for suction, compression/expansion and discharge is investigated by Hirano (1988) and Yanagisawa (2001). In this thesis the expressions given by Wang (2005) have been used to generate the expander model.

3.3.7 Comparison of Expansion Devices

There are many different expanders that can convert a high pressure-temperature vapor into mechanical work. This review has shown that not all expanders are created equal and that each has their own limitations and trade-offs. Some are applicable to small-scale operation while others (such as turbines) are not. These considerations are presented in summary below and in Table 3.4.

Turbines: turbo-machinery is a well proven technology at large scale but they require excessively high speeds to operate efficiently at small speeds. They have poor off design performance and have poor compatibility with wet fluid types. Single turbine stages are characteristic of low pressure ratios. They have been shown to have isentropic

efficiencies as high as 85% in a low temperature ORC. Limited literature exists on their performance in small scale ORCs.

Reciprocating Piston: reciprocating pistons are a mature technology but they are characteristic of high friction losses. They require both primary and secondary balancing as well as a cam system to ensure proper valve timing. They have been reported to have an isentropic efficiency of 62% in a transcritical CO₂ cooling cycle but no literature exists on their performance in ORCs.

Rotary Vane: they are simple and robust in design but they are susceptible to high friction losses from the large number of interacting components. They are also susceptible to leakage through the vanes as well as through the end faces of the rotor. They are tolerant of wet expansion and can handle high pressures. A rotary vane has been recorded to have an isentropic efficiency of 48% in a low temperature ORC but they have not been extensively researched in this application.

Rolling Piston: these devices are simple and robust in design. They have a reduction in the overall number of moving parts as compared to a RVE and therefore should have a reduction in frictional losses. There are several variations that aim to minimize leakage paths and friction. They are also tolerant of wet expansion and high pressures. Isentropic efficiencies as high as 45.2% have been achieved in a solar powered ORC but they have not been extensively researched as expanders in ORCs.

Gerotor: it is more complicated than the rolling piston and rotary vane in operation but it is still a simple and robust device. Due to the low relative velocities between the rotor and stator it benefits from a decreased frictional loss when compared to rotary vane and rolling piston types. It like other positive displacement types it can

handle wet fluids and high pressures. It has been shown to have a very high isentropic efficiency of 85% but it has not been tested extensively. Current results show that it has poor off design performance. Only one literary source has documented its performance as an expander.

Scroll: of the positive displacement types the scroll has the most complicated geometry and requires tight manufacturing tolerances. With both axially and radially compliant scrolls the effect of leakage, which is the primary cause of loss of performance, can be minimized. It can handle wet expansion. It has been shown to achieve isentropic efficiencies as high as 83% over a variety of working conditions and has been tested extensively in literature. It has shown good off design performance.

The gerotor is shown to have a higher maximum efficiency than the scroll but it has not been tested as extensively in literature. The scroll has shown a high efficiency over a variety of working conditions. For this reason it is chosen to develop a high efficiency axially and radially compliant scroll expander for use in an ORC.

Table 3.3: Summary of operating conditions and performance of different expander types.

Type	Isentropic Efficiency [%]	Expander Inlet Temperature [°C]	Expander Inlet Pressure [bar]	Pressure Ratio	Power Output [W]	Speed [RPM]	Working Fluid	Reference
Turbine	46	701	3.41	21	1501	17,0001	R123	Yamamoto (2001)
Turbine	85	70	2.21	1.1	1500	60,000	HFE-301	Yagoub (2006)
Turbine	40	95	2.71	1.1	1500	60,000	n-Pentane	Yagoub (2006)
Piston (Recip.)	10.5	87	60.5	2.1	24.35	114	CO ₂	Baek (2005)
Piston (Free)	62	-	7.8	2.4	-	3069	CO ₂	Zang (2007)
Rotary Vane	48	808	2.9	24.2	32.1	2,0951	R245fa	Tahir (2010)
Rotary Vane	23	-	90-75	1.5	-	800	CO ₂	Yang (2009)
Swing Piston	44	42	82.3	-	500	18001	CO ₂	Haiqing (2006)
Rolling Piston	45.2	831	6	2.2	1,730	800-900	R245fa	Wang (2010)
Gerotor A	66	84	4.1	3.0	28010	3,670	R123	Mathias (2009)
Gerotor B	66	146	18.8	8.3	48010	3,670	R123	Mathias (2009)
Gerotor C	85	150	12.3	4.2	1,96010	3,670	R123	Mathias (2009)
Scroll A	67	127	13.5	8.8	1,20010	3,670	R123	Mathias (2009)
Scroll B	81	149	18.2	5.5	1,38010	3,670	R123	Mathias (2009)
Scroll C	83	155	17.9	3.1	1,75010	3,670	R123	Mathias (2009)
Scroll D	83	120	11.9	3.0	1,040	3,670	R123	Mathias (2009)
Scroll Con.	49.9	170	6.4	3.82	256	1,287	R123	Peterson (2008)
Scroll	65	136	8.311	-	350	2,8001	R113	Saitoh (2007)
Scroll Con.	33	145	13	11.4	-	2,355	Water	Kim (2007)
Scroll	65	65	1311	-	2,050	2,000	R134a	Manolakos (2007)
Scroll Con.	68	142	10.03	5.0	-	2,296	R123	Lemort (2009)
Scroll	45.12	70	3.2511	-	2111	8911	R134a	Manolakos (2009)

4 LITERATURE REVIEW

In this section the previous studies regarding scroll geometry, scroll compressor and scroll expander reviewed. First, the studies performed in the field of scroll geometry and dynamic analysis reviewed for the geometric analysis. In the second phase, scroll compressor and scroll expander models are reviewed in terms of compression and expansion processes, leakage flow, heat transfer, noise and vibration for the analysis of the expansion process to be able to develop a thermodynamic model.

4.1 Scroll Geometry

Scroll geometry is one of the key components affecting the scroll machine efficiency defining chamber areas and volumes. The parameters to describe scroll geometry have to be understood to generate equations for volume and area of the expander chambers as a function of angle in terms of obtaining specific characteristics of the working fluid. Therefore significant amount of research regarding the scroll machine involves the investigation of scroll geometry. Bush (1992) gave the relations in terms of generating expressions for the conjugacy of the scroll profiles to define the relative position of the fixed and orbiting scroll. Yanagisawa et al. (2001) and Hirano et al. (1988) have also worked on how to calculate the volume in suction, compression/expansion and discharge chamber and the length of a vane separating two chambers with respect to orbiting angle.

4.2 Dynamic Analysis

Dynamic modeling including equations of motion for the crank shaft, the orbiting scroll and the Oldham coupling and taking into account motor torque, frictional torque, gas forces and frictional forces is very important to determine mechanical losses which are

the main factor on the efficiency of a scroll machine. Hayano et al. (1988) developed a mathematical model for the orbiting scroll and Oldham coupling based on the analysis of various forces acting on each moving element of scroll machine and calculated frictional losses at ten locations of the scroll machine validating his results with experimental data afterwards. Ishii et al. (1986) has also studied dynamic behavior of the scroll machine including the calculation of crank shaft load fluctuations, the crank shaft rotary behavior, the unbalanced inertia forces, the compressor vibrations and the mechanical efficiency. The study performed by Morishita (1984) focused on calculating the overturning moment that acts on the orbiting scroll due to the unbalanced forces and to clarify stability conditions with respect to overturning moment.

4.3 Compressor Process

4.3.1 Suction Process

The volumetric efficiency of the scroll machine is strongly depends on the suction process for compressor and discharge process for expander since the pockets starts from volume of zero and increase to the maximum displacement volume while the pressure of the pockets stay constant during the suction/discharge process in an ideal case. Hence the pressure in suction chamber increase due to a decrease of suction pocket volume and suction port resistance just before the suction pockets are closed. The pressures of the suction pockets are higher than the suction line pressure for a small time interval. DeBlois (1988) worked on this phenomenon and assumed the pressure in the suction chamber is lower than suction line pressure and claimed that additional work must be done to recompress the refrigerant as an energy loss. While designing a simplified model for this study, the idea of DeBlois taken into account to analyze the scroll compressor

converting into expander. Unlike DeBlois (1988), Yanagisawa (1988) related the pressure rise at the end of suction process to an optimum operating pressure ratio. Nieter (1988) and Li (1992) investigated the suction pre-compression and reported the volumetric efficiency can be increased by 4.3% under the influence of oil-rejection to avoid the leakage flow.

4.3.2 Compression Process

Built-in compression ratio of a scroll machine depends on the geometric characteristics of the scroll wraps. Assuming the pressure directly to the compression chamber volume, ideal compression can be defined as isentropic compression process. However in real compression process some of the work will be dissipated into heat and increase the isentropy and other properties of the working fluid. Leakages, heat transfer, two phase flow and dynamic behavior of the refrigerant are the reasons to need for designing the model to obtain accurate results.

The thermodynamic model of scroll compressor is developed by Kim (1998) by considering real gas behavior for the compression process based on the first law of thermodynamics. The other model developed by Li (1992) took leakage and losses into account applied the first law of thermodynamics assuming ideal gas behavior and constant volume pressure rising process. In this thesis first law of thermodynamics is applied for the compression chambers in order to calculate organic working fluid properties as a function of orbiting angle. The model is developed for calculating the built-in volume ratio from the properties of working fluid and converting scroll compressor into expander using the real technical data obtained by manufacturer catalogue.

4.3.3 Discharge Process

When the compression process ends, discharge process starts at an angle defined as discharge angle and working fluid is not compressed anymore. Unlike the theoretical case in which the pressure is constant in discharge region, in real case the pressure at any moment of discharge could be different than discharge pressure due to losses and flow resistance at the discharge port when compression chamber combined with the discharge chamber. Nieter (1992) introduced an effective area for the discharge process to calculate the mass flow rate assuming steady-state, one-dimensional flow. Caillat (1988) computed the flow rate of discharge gas using Bernoulli equations by the computer model which concluded by the determination of similar results compared to measured results.

4.4 Evaluation of Losses

Evaluation of compressor losses is very important since the real performance of a scroll machine will be different than the ideal case by the effect of leakages, heat transfers, frictional losses and other motor losses. These kinds of losses should be investigated in order to improve the volumetric efficiency of the scroll machine characterized by geometrical model.

4.4.1 Leakage

Leakage is one of the most significant losses. There are two kinds of leakages formed by two different paths. One is the path formed by the gap between the plate and scrolls which is called radial leakage. The other path is formed by a gap between flanks of orbiting and fixed scrolls called as a tangential leakage. Puff and Mogolis (1992) developed a model which is based on simulation using the isentropic nozzle. They

calculated the volumetric efficiency of the scroll machine for different flank clearances. As a result, volumetric efficiency decreased by 87.5% for the flank clearance more than 0.1 mm in their study. Suefuji et al. (1992) applied Fanno flow in the leakage model and calculated volumetric efficiency to be within 3% of the measured data. Tojo et al. (1986) showed that radial leakage is affecting the volumetric efficiency more than the flank leakage which means having similar results with Puff's (1992) model of a diverging nozzle. Zhu et al. (1992) has also modeled radial leakage flow between two plates. Yong (1994) calculated the detailed flow field in a clearance using two-dimensional Navier-Stokes equations and developed the model by reducing it to quasi-one-dimensional model assuming pressure, temperature, density change only in one direction for small clearances. The model is applied for radial and flank leakage in order to calculate leakage flow rate.

4.4.2 Heat Transfer

There are several places in a scroll machine that heat transfer is taking place. The density of the working fluid increases during the suction/intake process for the scroll expander. Heat rejection during the expansion process and the heat addition during the compression process will cause compression and expansion processes to go to further away from the ideal isentropic process.

Jand and Jeong (1999) studied the heat transfer through experiments and measured the temperature distribution within the chambers to see how the geometry is affecting the heat flux along the fixed scroll wrap. They reported that temperature is distributed linearly from the center of the scroll machine to the end. Wagner and Marchese (1992) developed an analytical method to investigate the thermal process

within the components of the scroll machine based on temperature and heat flux measurements. Suefuji et al. (1992) also worked on the heat transfer mechanism in the suction pipe for the scroll compressor. Bush (1998) suggested to reduce suction gas heating to improve the efficiency of the scroll compressor. Although there are lots of studies in the literature regarding the investigation of heat transfer mechanism of scroll machine none of those studies could develop a convective heat transfer coefficient between the scroll and refrigerant that would be useful for the thermodynamic analyses of the scroll compressor/expander.

4.4.3 Frictional Losses

Frictional losses can occur at different locations of the scroll machine: bearings, orbiting and fixed scroll, Oldham coupling and frame. Hayano et al. (1988) calculated frictional losses for major locations based on analytical model developed for orbiting scroll and Oldham coupling. Mechanical losses and mechanical efficiency were also investigated by Ishii et al. (1990, 1992, 1994) at moving parts of the scroll such as the crank pin, and the thrust bearing. In the model Ishii compared scroll compressor with rotary compressor for the same capacity and showed that in spite of obtaining lower efficiencies for the scroll compressor it can be improved by selection of appropriate dimensions using geometrical optimization of variables as well as scroll expanders.

Hayano et al. (1988) calculated losses due to heat exchange and fluid resistance at the orbiting scroll and reported that mechanical losses are 30% of the total losses (motor losses). Liu et al. (1998) investigated working parameters of the different types of scroll mechanisms and developed a theoretical approach for the working principle of radial mechanisms. Hasegawa (1998) applied a new method for the joint and no joint

mechanisms and showed that Oldham rings can be used as a joint for higher efficiency although the noise and vibration could be a problem for HVAC applications.

4.5 Noise and Vibration

The level of noise and vibration in a scroll machine is one of the advantages it has since simultaneous compression/expansion within several chambers reduces the load fluctuations. Depending on the gas which is releasing from high pressure to low pressure at the discharge process for expander the level of noise and vibration may increase by the contact of the metal between orbiting and fixed scroll. Another reason of the vibration and noise could be the forces of inertia of the Oldham coupling. The vibration analysis of the scroll compressor due to the dynamic characteristics of the scrolls is performed by Ishii (1986). Hasegawa (1998) claimed the level of noise and vibration can be reduced by using a mechanism with no joint between the fixed and orbiting scroll in his dynamic analysis. Shu (1992) investigated the natural frequency of the scroll machine to be able to avoid from high level of noise and vibration. Nieter (1992) and Itoh (1994) were also performed investigation regarding noise and vibration models at the discharge process.

4.6 Comprehensive Modeling of Scroll Compressors

Halm (1997) performed comprehensive analysis of the scroll machine taking all the processes mentioned before into account. He applied conservations of energy equations for the each chamber of the scroll compressor and calculated temperature and pressure distribution as a function of the orbiting angle. The predictions he made through his model for the mass flow rate and power consumption were similar to the measured

results. Halm validated his model through an experiment and showed the motor and frictional losses can be calculated assuming isentropic efficiency by regression.

4.7 Experimental Investigations

There are also experimental investigations in the literature for the validation of theoretical models. Jang et al. (1999) used thermocouples and flux gauges to measure the temperature distribution along the fixed scroll wrap. He showed that the temperature is distributed linearly at the scroll wrap from high level to the low level as a result of increased involute angle. They concluded that rotational speed is also effecting the wrap temperature linearly. Wagner (1992) has used thermocouples and flux gauges in a similar manner of Jang but this time he mounted them on different locations of scroll compressor to determine the temperature at different components such as shell, bearing, oil etc. DeBlois (1988) used piezoelectric pressure transducers to measure the pressure in the compression chamber in the experiment. Marchese (1992) presented a measurement technique for the pressure and orbiting scroll motion using appropriate transducers which has a high response capability.

Scumann (1994) measured scroll motion using strain gauges which are in contact with the Oldham coupling as a part of beams. Drost (1992) explained a method to measure the oil flow rates in scroll compressor using an experimental rig. The visualization of the fluid flow during discharge and compression process was performed by Rodgers (1990) by conducting computational fluid flow analysis.

4.8 Design Variations

There are many different scroll compressor/expander designs, depending on the type of improvement made on various geometries. Hagiwara et al. (1998) conducted a study which compares a conventional scroll compressor with a high pressure housing compressor and showed that by using asymmetric scroll wrap mechanism heat loss can be reduced and volumetric efficiency can be improved by 4.5%. Hasegawa et al. (1998) performed a dynamic analysis which focused on the structure of a drive scroll and driven scroll (fixed and orbiting scroll) and investigated the way of combining them eccentrically by a certain distance. The drive scroll is rotated by a motor via drive shaft while driven scroll is driven directly by the drive scroll or via Oldham ring. He showed that using Oldham ring higher efficiencies and low level of noise can be ensured instead of using drive scroll directly.

Hase et al. (1994), Sawai (1992), Richardson (1992) and Kawabe (1992) reported different types of mechanisms such as horizontal and vertical or high and low side compressors which are called as 2-in-1 compressors. Ahn et al. (1988) designed a check valve which has an unstable motion compared to conventional valves during operation and analyzed the scroll machine through the performance improvement perspective.

4.9 Scroll Expander Modeling

Yanagisawa et al. (2001) worked on modeling scroll expander. He expressed crank angle evolution of the pressure and temperature in the pockets of scroll type oil-free air expander and validated the model measuring the pressures in the pockets. The papers dealing with the modeling of a scroll expander include the analysis of control volumes in terms of conducting volume expressions as a function of orbiting angle and applying

conservation of energy equation for the chambers. Xiajun et al. (2004) simulated a scroll expander to use in fuel cell. The model took the radial and flank leakage into account as mechanical losses neglecting suction pressure loss. Yuanyang et al. (2006) developed a model for the conversion of compressor into expander to use in automotive fuel cell which focused on leakages and under/over compression and expansion losses applying conservation of mass and energy equations.

Halm (1997) defined the geometry of the scroll machine. The goal of the modeling is to define the pocket volumes for intake, expansion and discharge chambers as a function of orbiting angle in order to apply conservation of energy and mass equations and solve them numerically for each chamber. Wang et al. (2005) gave analytical expressions for the scroll compressor chambers as a function of orbiting angle. The study of Halm (1997) and Wang (2006) used in this thesis converting the expressions developed for the compressor into expander operation to evaluate the built-in volume ratio and specifications of the working fluid in order to apply mass and energy balance equations for the control volumes of the working chambers of the scroll expander.

5 ANALYSIS AND MODELLING

5.1 Geometric Analysis

The aim of the geometric modeling is to obtain expressions for areas and volumes of different working chambers as a function of the orbiting angle to be able to analyze the compression/expansion process. Additionally change of volume and pressure as a function of the orbiting angle will be investigated. Since the volumes define the compression/expansion process, it is very important to derive the expressions by performing careful analysis because of the geometric complexity. Some approximations have to be made to reduce the number of geometrical variables to reach exact expressions.

Scroll expanders are positive displacement machines that comprise two interfitting spiral-shaped scroll members, one being fixed and the other having an orbital motion (see Figure 5.1). One scroll is inverted, rotated 180 degrees, and inserted into the gaps of the second scroll. The magnitude of the orbital motion depends on the base circle radius r_b and the scroll flange thickness t , which will be explained later. A specially designed coupling, called an Oldham coupling, holds the lower scroll at a fixed angular position, preventing rotation and allowing radial movement in an orbital path. The intake gas is brought in the central region of the scrolls. Thereafter, the two symmetric crescent shaped pockets are moved towards scroll periphery as the orbiting scroll rotates. These two pockets progressively decrease (or increase) in size toward the center. Positive displacement process increases (or decreases) the pressure of the fluid by reducing (or increasing) the internal volume of the compression (or expansion) chambers. Generally, it

takes two or three shaft rotations, depending on the scroll rolling angle, to bring the fluid from the intake to discharge state.

There is no valve on the scroll machine to control suction and discharge processes since the scroll geometry and the orbital motion defines the timing of these processes forcing the refrigerant into pockets by eccentric motion.

The built-in volume ratio (r_v) by the design for the expander is the ratio between the suction chambers volume at the end of the suction and the discharge chambers volume at the beginning of the discharge.

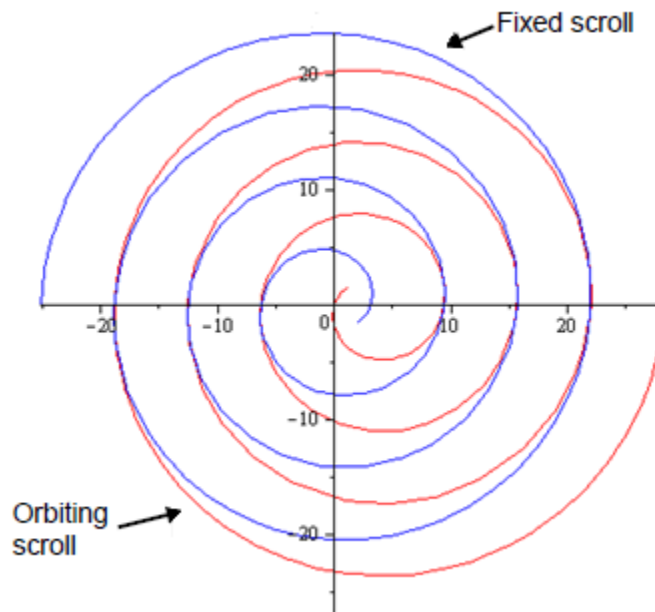


Figure 5.1: Fixed and orbiting scroll with working chambers.

The scroll geometry is defined by two involutes that develop around a common basic circle and are offset by a constant distance by Bush (1992). Assuming the base vector pointing away from the center of the wraps is constant, a pair of involutes in polar coordinates can be written as follows (see Figure 5.2):

$$L_i = r_b(\varphi - \varphi_{i0}) \quad (5.1)$$

$$L_o = r_b(\varphi - \varphi_{o0}) \quad (5.2)$$

where L_i is the length of the inner involute, L_o is the length of the outer involute, φ_{i0} is the initial angle of the inner involute and φ_{o0} is the initial angle of the outer involute.

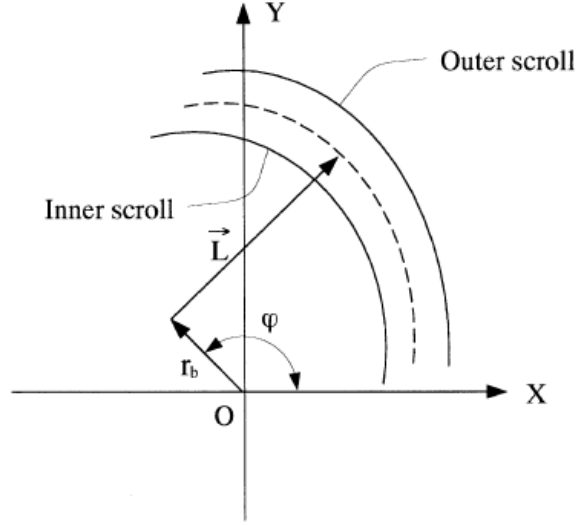


Figure 5.2: General relation of the scroll (Chen,2002).

The thickness t of the scroll is given by

$$t = L_o - L_i = r_b(\varphi_{o0} - \varphi_{i0}) \quad (5.3)$$

The orbiting and fixed scrolls are in contact at their point of conjugacy, which is defined by the k -th point of conjugacy angle (φ_k) and given by the following equation:

$$\varphi_k = \varphi_e - \theta - (k - 1)2\pi \quad (5.4)$$

where φ_e is the rolling angle (involute ending angle). The outer and inner involutes end at the rolling angle, θ is the orbiting angle, which is defined such that $\theta=0$ at the volume of the suction chamber and starts to increase from minimum position.

The scrolls which have a form of involute, starts at an inner starting angle φ_{is} and outer starting angle φ_{os} are connected by a circular arc with radius r and thickness t as shown in Figure 5.3.

In the compressor or expander two symmetrical scrolls are always assembled together which are offset by 180° and are in conjugacy. In fact the ending angle of the inner involute of the fixed scroll is larger than that of the orbiting scroll. The inner involute of the fixed scroll should be extended which leads to asymmetry between the fixed scroll and the orbiting scroll.

Scroll geometry is one of the key components affecting the scroll machine efficiency. The parameters that describe scroll geometry have to be understood to generate equations for working fluid pocket volume and leakage areas as functions of rotating angle (denoted here with θ). Figure 5.3 introduces the main geometrical parameters of the scroll expander. The scroll is a free standing strip of metal machined in the form of an involute spiral (see Figure 5.3).

The spiral, as a geometrical curve, can have a number of volutions which is defined as the number of turns around its centre, denoted by a rolling angle (φ_e), which is illustrated for the orbiting scroll (dashed line) in Figure 5.4.

The machine tools which will give the final shape of scrolls are set to finish the surface as it is shown in the figure but since two symmetrical shape scrolls which offset by 180° will touch to each other before their conjugacy points between φ_i and φ_o , some part of the inner and outer involute of the fixed and orbiting scroll will be rubbed off after some number of rotation. In order to overcome this problem, the part of the scroll

between φ_i and φ_o as it is shown by the dashed lines in Figure 5.3 should be machined not to apply cutting forces to each other.

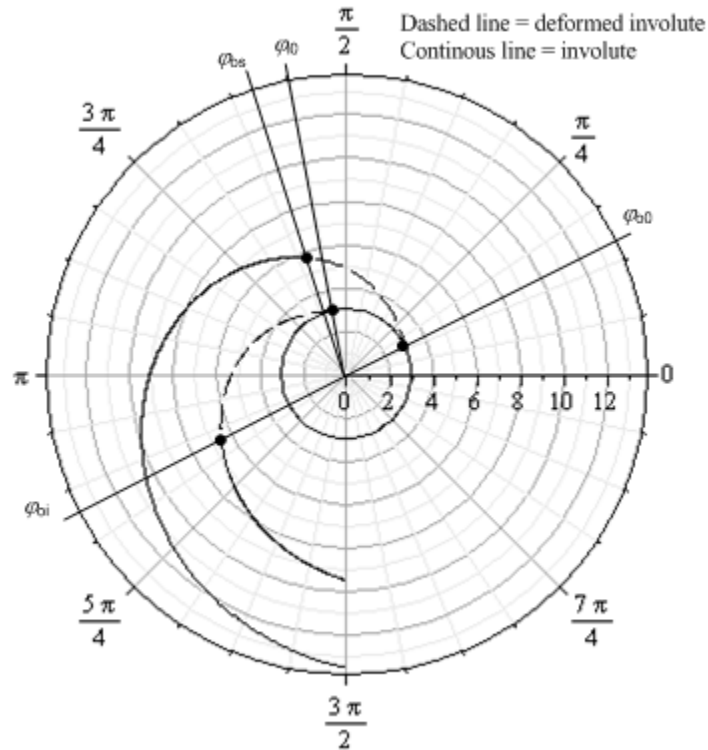


Figure 5.3: Geometrical parameters describing inner and outer involute.

The working chambers of the scroll expander are defined by relative positions of the fixed and orbiting scroll. Two symmetrical and diametrically opposed fluid pockets are formed, which move from centre to periphery during the expansion process. The natural symmetry in the scroll set balanced radial gas forces against the vanes, providing a smooth expansion cycle. Moreover, each orbit begins the expansion cycle anew so that at any given time there are three types of symmetrical crescent-shaped pockets that can be found: at high-(intake) \rightarrow chamber 1, medium-(expansion) \rightarrow chambers 2'-4' and 2''-4'', and low-pressure (discharge) \rightarrow chambers 5', 5'' conditions as shown in Figure 5.4.

Therefore, expansion is a smooth and continuous process without vibration or strong pulsations as in reciprocating expanders.

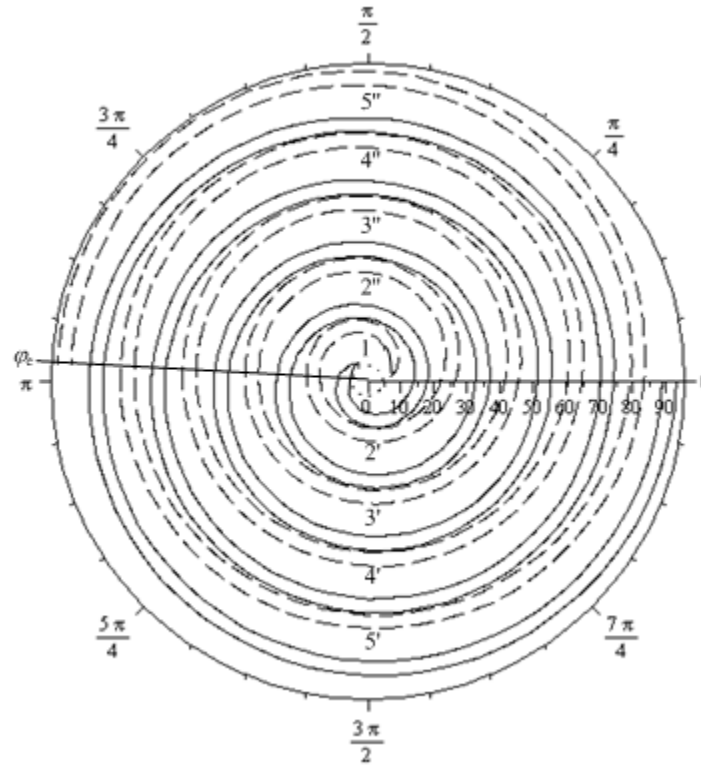


Figure 5.4: Working chambers of the expander.

The geometry of the scroll machine was defined by Halm (1997). The goal of the geometrical modeling is to define pocket volumes for intake, expansion and discharge chambers as a function of orbiting angle (θ) to obtain volume-angle functions. The orbiting angle describes the number of turns of the orbiting scroll around the fixed scroll for a complete cycle of expansion. The study of Wang (2005) evaluates the chamber volumes as a function of orbiting angle throughout the compression process in a scroll machine.

In the expander model, the scroll machine works in exactly the opposite direction of scroll compressor. The intake of high pressure gas from the center of the expander (intake chamber) can be considered the discharge chamber of compressor. In a same manner, the discharge of low pressure gas from the periphery (discharge chamber) of the expander can be considered the suction chamber of the compressor. Therefore the equations for the suction, compression and discharge volumes as a function of orbiting angle and involute angle (which defines the spiral) can be applied to scroll machine operation as expander.

Wang et al. (2005) give analytical expressions for scroll compressor chambers as function of orbiting angle. We converted these expressions as for the expander operation as follows. Expander intake chamber volume is given by

$$V_{ei}(\theta) = hr_b r_o \theta (\theta - \varphi_{i0} - \varphi_{o0} + 3\pi) \quad (5.5)$$

where $0 \leq \theta < 2\pi$ for the intake; that is the intake process extends for one full orbit. The expander's expansion chamber volume is given by

$$V_{ee}(\theta) = 2\pi hr_b r_o (2\theta - (\varphi_{i0} - \varphi_{o0} - \pi)) \quad (5.6)$$

where $2\pi \leq \theta < \varphi_e - 2\pi$. The last orbiting corresponds to discharge process $\varphi_e - 2\pi \leq \theta < \varphi_e$ when the volume of the chamber reduces according to

$$V_{ed}(\theta, \varphi_e) = hr_b r_o \left((2\varphi_e - 2\theta)\varphi_e - (\varphi_e - \theta)^2 - (\varphi_e - \theta)(\varphi_{i0} + \varphi_{o0} + \pi) + 2 \left(1 - \cos(\varphi_e - \theta) \right) - 2(\varphi_e - \pi) \sin(\varphi_e - \theta) - \frac{\pi}{4} \sin(2(\varphi_e - \theta)) \right) \quad (5.7)$$

The built-in volume ratio of the expander is defined as the volume of the expansion chamber at the end of the expansion process over the volume of the expansion chamber at the beginning of the expansion process. The built-in volume ratio can be expressed with the help of equations. (5.5-5.7), more specifically

$$\tilde{r}_v = \frac{V_{ee}(\varphi_e - 2\pi)}{V_{ei}(2\pi)} = \frac{2\varphi_e - \varphi_{i0} + \varphi_{o0} - 3\pi}{5\pi - \varphi_{i0} + \varphi_{o0}} \quad (5.8)$$

The built-in volume ratio is the most important parameter of scroll machine because it directly influences the expansion or compression process, whichever is the case. For the analysis of the expansion and compression processes with positive displacement machines – as of scroll type – it is important to possess simplified models(thermodynamic model) that relate the built-in volume ratio and leakage flow coefficients with the isentropic and volumetric efficiency of the machine. In what follows we introduce simplified models for positive displacement machines that are used in this paper to predict the operation of the scroll compressor as expander.

The whole change process of the volume during suction, compression and discharge can be plotted in the Maple software for the scroll compressor. In an expander mode the volume of the chambers can be obtained as a function of orbiting angle by converting the expressions and range of the angles for intake, expansion and discharge processes. The volume expression of the discharge chamber for the compressor can be applied to evaluate the intake chamber of the expander for the same range of angle ($0 \leq \theta < 2\pi$). In a same manner the expansion chamber volume can be plotted by calculating the range of angle from the end of suction to the start of discharge for the compressor ($2\pi \leq \theta < \varphi_e - 2\pi$). Lastly the volume of the discharge chamber of an expander can be equated to the expression for suction chamber of the compressor by modifying the range of orbiting angle ($\varphi_e - 2\pi \leq \theta < \varphi_e$) to be able to plot the whole process as a function of the orbiting angle by adding the volume curves by order using the Maple software.

5.2 Thermodynamic Analysis

The geometrical model and volume expressions for the chambers will be used to model the thermodynamic process of the working fluid from the beginning of suction ($\theta=0$) to the end of the discharge process ($\theta=2\pi$ rad)

5.2.1 Differential Equations Governing the Expansion Process

The first law of thermodynamics for the control volume with a mass balance can be applied to calculate the temperature, mass and pressure in the working chambers with respect to orbiting angle.

The conservation of energy for the control volume is:

$$\frac{dE_{cv}}{dt} = \dot{Q} + \dot{W} + \sum \dot{m}_{su} \left(h + \frac{v^2}{2} + gz \right)_{su} - \sum \dot{m}_{ex} \left(h + \frac{v^2}{2} + gz \right)_{ex} \quad (5.9)$$

where $\frac{dE_{cv}}{dt}$ is the rate of total internal energy increase (W), \dot{Q} is the heat transfer rate

(W), \dot{W} is the power output from expander (W), \dot{m} is the inflow or outflow rate (kg/s),

$h + \frac{v^2}{2} + g$ is the total enthalpy (J/kg).

The mass balance for the control volume is:

$$\frac{dM}{dt} = \sum \dot{m}_{su} - \sum \dot{m}_{ex} \quad (5.10)$$

The total energy of the control volume E_{cv} can be reduced to internal energy U_{cv} neglecting kinetic and potential energies. The left side of the conservation of energy equation can be written as

$$\frac{dE_{cv}}{dt} = \frac{dU_{cv}}{dt} = m \frac{du}{dt} + u \frac{dm}{dt} \quad (5.11)$$

The change of the specific internal energy u for the control volume is

$$du = C_v dT + \left[T \left(\frac{\partial P}{\partial T} \right)_v - P \right] dv \quad (5.12)$$

The specific internal energy u can be written as $u = h - Pv$, where h is the specific enthalpy, such that equation (5.11) can be written as

$$\frac{dU_{cv}}{dt} = mC_v \frac{dT}{dt} + T \left(\frac{\partial P}{\partial T} \right)_v \left(\frac{dV}{dt} - V \frac{dm}{dt} \right) - P \frac{dV}{dt} + h \frac{dm}{dt} \quad (5.13)$$

Uniform pressure and temperature can be assumed for each control volume and the work term $\dot{W} = \frac{\partial W}{\partial t}$ on the right hand side of equation (5.9) can be expressed as

$$\dot{W} = -P \frac{dV}{dt} \quad (5.14)$$

The first law of thermodynamics for the control volume becomes

$$mC_v \frac{dT}{dt} + T \left(\frac{\partial P}{\partial T} \right)_v \left(\frac{dV}{dt} - V \frac{dm}{dt} \right) + h \frac{dm}{dt} = \dot{Q} + \sum \dot{m}_{in} h_{in} - \sum \dot{m}_{out} h_{out} \quad (5.15)$$

Equation (5.15) can be arranged to

$$\frac{dT}{dt} = \frac{1}{mC_v} \left\{ -T \left(\frac{\partial P}{\partial T} \right)_v \left[\frac{dV}{dt} - v(\dot{m}_{in} - \dot{m}_{out}) \right] - \sum \dot{m}_{in} (h - h_{in}) + \dot{Q} \right\} \quad (5.16)$$

by applying mass balance equation (5.10) for $h = h_{out}$. The temperature change with respect to orbiting angle can be obtained from equation (5.16) if angular speed w is expressed as

$$w = \frac{d\theta}{dt} \quad (5.17)$$

Substituting equation (5.17) in to equation (5.16) yields

$$\frac{dT}{d\theta} = \frac{1}{mC_v} \left\{ -T \left(\frac{\partial P}{\partial T} \right)_v \left[\frac{dV}{dt} - (v/w)(\dot{m}_{in} - \dot{m}_{out}) \right] - \sum (\dot{m}_{in}/w) (h - h_{in}) + (\dot{Q}/w) \right\}$$

And the mass balance equation becomes

$$\frac{dM}{d\theta} = (\sum \dot{m}_{in} / w) - (\sum \dot{m}_{ex} / w) \quad (5.18)$$

In equation (5.16), independent variables temperature T and mass m should be integrated for the first order differential equation. Applying the mass balance equation (5.18) and the equation of temperature distribution with respect to orbiting angle (5.17)

the thermophysical properties in each chamber can be evaluated as a function of the orbiting angle (θ).

5.2.2 Heat Transfer

There are different types of heat transfer mechanisms in a scroll compressor including between:

1. The shell of the scroll compressor and the fluid in suction
2. The fluid and motor, oil, scrolls (electromechanical losses)
3. The shell of the scroll compressor/expansion and the fluid in discharge
4. The fluid and the ambient

It can be assumed that the wall of the temperature is constant at T_w through the thickness of the fluid to be able to present the heat transfer and conservation of energy equations.

The steady state balance for the wall can be given as

$$\dot{Q}_{ex} - \dot{Q}_{su} - \dot{Q}_{amb} - \dot{W}_{loss} = 0 \quad (5.19)$$

The suction heat transfer assuming constant envelope temperature for the isothermal heat exchanger and uniform wall temperature is

$$\dot{Q}_{su} = \dot{m}c_p(T_{su,1} - T_{su}) = \varepsilon_{su}\dot{m}c_p(T_w - T_{su}) = [1 - e^{\left(-\frac{AU_{su}}{Mc_p}\right)}]\dot{m}c_p(T_w - T_{su}) \quad (5.20)$$

The discharge heat transfer under the same conditions and assumptions:

$$\dot{Q}_{ex} = \dot{m}c_p(T_{ex} - T_{ex,1}) = \varepsilon_{su}\dot{m}c_p(T_{ex} - T_w) = [1 - e^{\left(-\frac{AU_{su}}{Mc_p}\right)}]\dot{m}c_p(T_{ex} - T_w) \quad (5.21)$$

where AU_{su} can be written in terms of nominal heat transfer coefficient ($AU_{su,n}$) which is given by Dewitt (2002) to develop the model for a turbulent flow through a pipe by the Reynolds number as follows:

$$AU_{su} = AU_{su,n}(\dot{m}/\dot{m}_n)^{0.8} \quad (5.22)$$

The ambient heat transfer can be evaluated by the following equation introducing a global heat transfer coefficient (AU_{amb}):

$$\dot{Q}_{amb} = AU_{amb}(T_w - T_{amb}) \quad (5.23)$$

5.2.3 Expander Model

After defining the properties of the fluid and the volume of the chambers as a function of the orbiting angle there is a need to develop a model to analyze and describe the main features of the machine regarding the energy and exergy efficiencies and fluid flow characteristics with a limited number of parameters.

The model proposed by Winandy et al. (2002) was modified to be able to predict the characteristics of the flow and the thermodynamic process of the scroll machine converting from scroll compressor to scroll expander and to improve the modeling of heat pump systems.

The schematic representation of the evolution of the refrigerant through the scroll machine is given for both the compressor and expander case in Figure 5.5. In this study the heat up in suction and cool down in discharge are not taken into account considering the compression and expansion process of the refrigerant in a scroll machine.

The compression process can be decomposed into two parts:

1. Isentropic compression (1→2s)
2. Isochoric pressure rising (2s→2a)

The expansion process can be decomposed into two parts:

1. Isentropic expansion (1→2s)
2. Constant volume pressure rebuild (2s→2a)

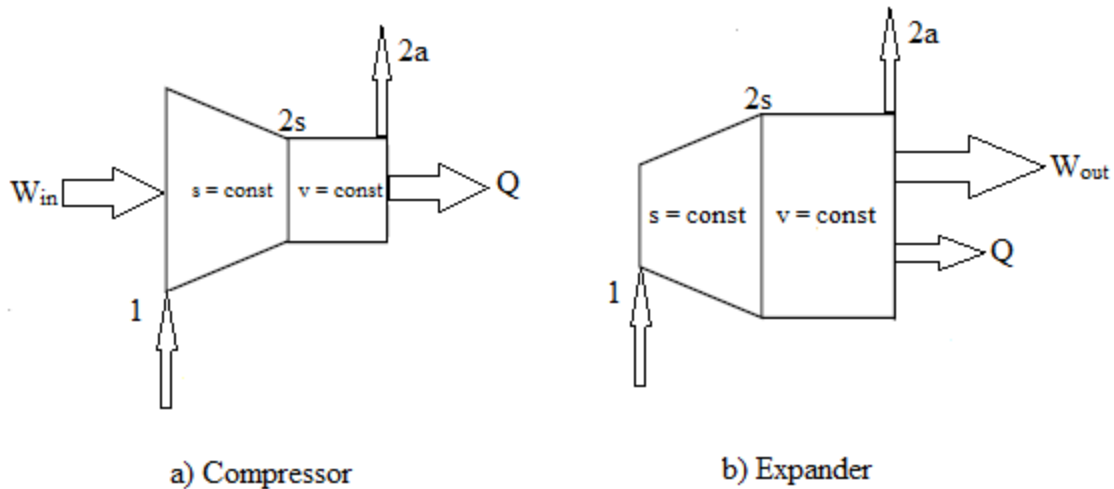


Figure 5.5: Scroll machine models for (a) compressor and (b) expander.

The equations describing the thermodynamic model will be given in terms of heat transfer, the internal leakage and pressure drop to describe the compression and expansion processes separately.

Figure 5.5 introduced scroll machine models functioning as compressor (a) and expander (b). Assume that a low pressure gas is to be compressed (Figure 5.5.a) from state 1. The compression process in positive displacement compressors implies closing the volume of gas in a compression chamber, which reduces its volume according to the built-in volume ratio. One assume that no leakages and no heat transfer occurs during the theoretical compression process represented from state 1 to state 2s as an isentropic one. Figure 6.1.a illustrates the process in a T - s diagram. The amount of work required for this part of compression process is denoted W_s .

In real compression processes the gas does not evolve isentropically and more work is consumed. The additional work is in fact transformed into heat that increases the entropy and enthalpy of the gas. Therefore, after the isentropic process 1-2s it follows an isochoric process with rising pressure driven by heat addition. The added heat originates

from the input work, which is partially destroyed such that $Q = W_{\text{in}} - W_s$ (see Figure 5.5.a). After the isochoric process the working fluid achieves state 2a. Eventually a part of the discharged gas flows back to suction as leakage flow. The leakage flow rate can be estimated from energy balance applied to simplified model. The energy balance can be written as it follows, in the compressor case (see Figure 6.1.a). The isentropic compression work is

$$\dot{W}_s = (\dot{m} + \dot{m}_{\text{leak}})(h_{2s} - h_1) \quad (5.24)$$

where \dot{m} is the net mass flow rate, and \dot{m}_{leak} represents the internal leakage flow rate. The summation $\dot{m} + \dot{m}_{\text{leak}}$ is the mass flow rate actually circulated through the compressor. In order to compensate the irreversibilities (leakages and heat exchange) more work input is needed to drive the compressor, such that $\dot{W}_{\text{in}} = \dot{W}_s + \dot{Q}$. Assuming that most of the irreversibilities are due to leakage flows, it becomes possible to calculate the leakage flow rate from an energy balance:

$$\dot{Q} = \dot{W}_{\text{in}} - \dot{W}_s = (\dot{m} + \dot{m}_{\text{leak}})(h_{2a} - h_{2s}) = \dot{m}_{\text{leak}}(h_{2a} - h_1). \quad (5.25)$$

Therefore, noting also that $v_{2a} = v_{2s}$ one solves for \dot{m}_{leak} and obtains

$$\frac{\dot{m}_{\text{leak}}}{\dot{m}} = \frac{h_{2a} - h_{2s}}{h_{2s} - h_1}. \quad (5.26)$$

A leakage flow coefficient $\zeta = C_f A_{\text{leak}}$ can be determined if one solves equation (5.7) for known pressure difference across the compressor

$$\dot{m}_{\text{leak}} = \zeta \sqrt{P_{2a}/v_{2a} - P_1/v_1} \quad (5.27)$$

where C_f is the specific flow coefficient per average leakage area A_{leak} .

The simplified model for the expander is introduced in Figure 5.5.b. In this case, a part of the main flow by-passes the expander and dissipates power as it flows over the expander's "flow resistance"; this is the leakage flow, $\dot{m}_{e,\text{leak}}$. The expansion process

according to the simplified model, evolves first isentropically from state 1 to 2s followed by, a constant volume pressure rebuild 2s-2a (see Figure 6.1.b). At the reverse operation – as expander – a reasonable assumption is to consider that the leakage coefficient remains the same. Therefore, denoting expander's states with index “e” one has the following equations can be written for the expander to apply for the thermodynamic modeling.

$$\begin{cases} v_{e,2a} = v_{e,2s} \\ \dot{m}_{e,leak} = \zeta \sqrt{\frac{P_{e,1}}{v_{e,1}} - \frac{P_{e,2a}}{v_{e,2a}}} \\ \dot{W}_{e,s} = (\dot{m}_e - \dot{m}_{e,leak})(h_{e,1} - h_{e,2s}) \\ \dot{Q}_{e,diss} = \dot{m}_{e,leak}(h_{e,1} - h_{e,2s}) \\ \dot{W}_{e,out} = \dot{W}_{e,s} - \dot{Q}_{e,diss} = \dot{m}_e(h_{e,1} - h_{e,2a}) \end{cases} \quad (5.28)$$

From Eqs.(28) one can determine the ratio

$$\frac{\dot{m}_e}{\dot{m}_{e,leak}} = 2 \times \frac{h_{e,1} - h_{e,2s}}{h_{e,2a} - h_{e,2s}}, \quad (5.29)$$

which is important for calculating the mass flow rate through the expander.

5.2.4 Cycle Analysis

Energy balance equation, entropy balance equation and exergy balance equation will be used to determine the energy and exergy efficiency of Organic Rankine Cycle (ORC). The performance of an ORC will be analyzed for different working fluids under diverse working conditions using the first and second laws of thermodynamics. There will be assumptions regarding the system as follows: steady-state conditions, no pressure drop in the evaporator, condenser and pipes and isentropic efficiencies for the turbine and pump. The heat engine to produce electrical power with ORC is shown in Figure 5.6. There are four different processes in ORC as can be observed from Figure 5.6: process 1-2

(constant-pressure transfer of heat), process 2-3 (expansion process), process 3-4 (constant-pressure heat transfer), and process 4-1 (pumping process). A T - s diagram of the typical ORC is given in Figure 5.7.

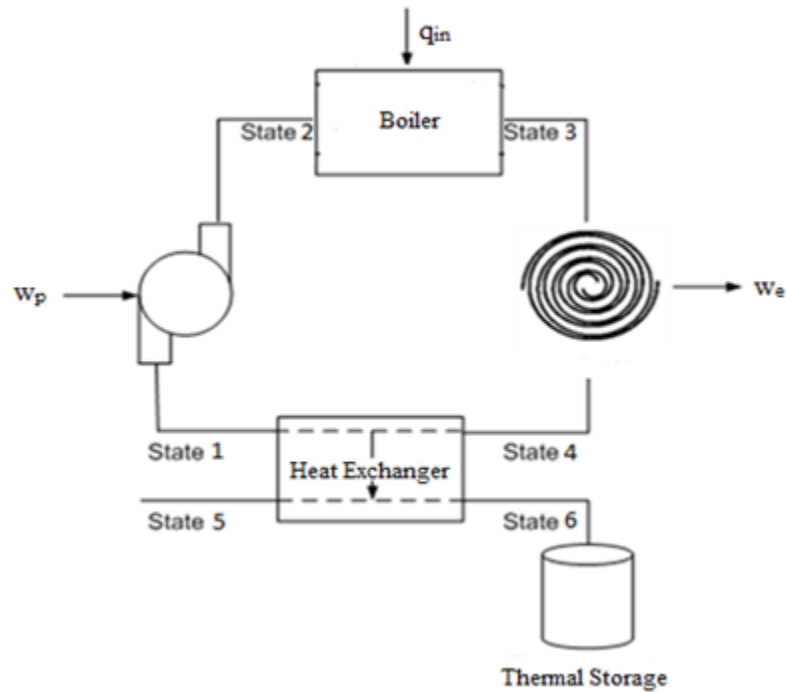


Figure 5.6: The Rankine cycle.

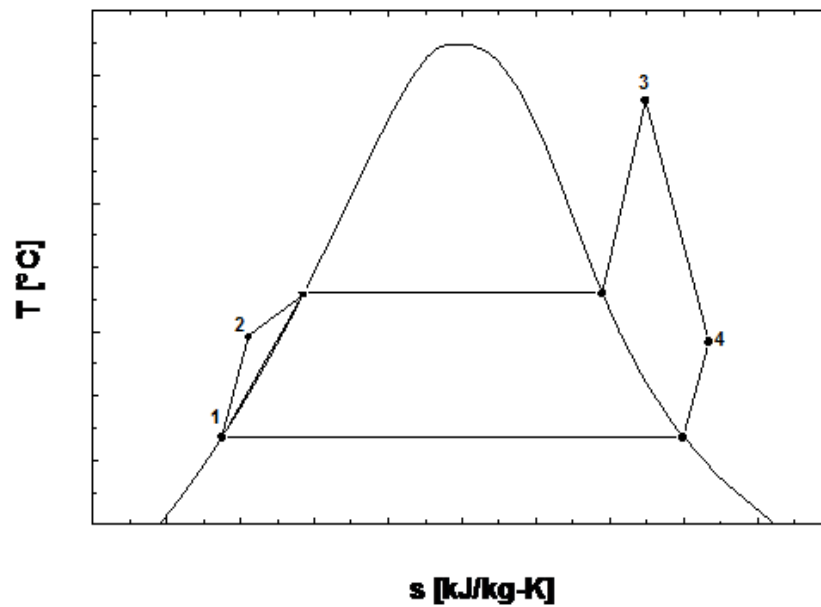


Figure 5.7: T - s diagram of a general organic Rankine cycle.

5.2.4.1 Pump

Process 1→2 implies an increase in the pressure resulting from using the pump. The driving mechanism of the ORC is the pump since it ensures the circulation.

The energy balance equation for the pump is

$$\dot{m}_1 h_1 + \dot{W}_p = \dot{m}_2 h_2 \quad (5.30)$$

The entropy balance equation for the pump is

$$\dot{m}_1 s_1 + \dot{S}_{gen} = \dot{m}_2 s_2 \quad (5.31)$$

The exergy balance equation for the pump is

$$E\dot{x}_1 + \dot{W}_{in} = E\dot{x}_2 + E\dot{x}_d \quad (5.32)$$

$$\text{where } E\dot{x}_1 = \dot{m}_1 h_1 - \dot{m}_0 h_0 - T_0 \dot{m}_1 (s_1 - s_0) \quad (5.33)$$

The pump power can be expressed as

$$\dot{W}_p = \frac{\dot{W}_{p,ideal}}{\eta_p} = \frac{\dot{m}(h_1 - h_{2s})}{\eta_p} \quad (5.34)$$

where $\dot{W}_{p,ideal}$ is the ideal work that should be supplied for the pump, η_p is the isentropic efficiency of the pump, \dot{m} is the flow rate of the working fluid, h_1 and h_{2s} are the inlet and outlet enthalpies of the refrigerant for the ideal case.

The actual specific enthalpy can be given as

$$h_2 = h_1 - \frac{\dot{W}_p}{\dot{m}} \quad (5.35)$$

The exergy destruction rate for the uniform flow can be expressed as

$$E\dot{x}_d = T_0 \frac{dS}{dt} = T_0 \dot{m} [\sum S_{exit} - \sum S_{inlet} + \frac{dS_{system}}{dt} + \sum_j \frac{q_j}{T_j}] \quad (5.36)$$

where j represents the heat transfer for different reservoirs. Applying the steady-state conditions ($\frac{dS_{system}}{dt} = 0$) equation (36) becomes

$$\dot{E}x_d = T_0 \frac{dS}{dt} = T_0 \dot{m} [\sum s_{exit} - \sum s_{inlet} + \sum_j \frac{q_j}{T_j}] \quad (5.37)$$

And the exergy destruction rate for the pump is

$$\dot{E}x_{d,p} = T_0 \dot{m} (s_2 - s_1) \quad (5.38)$$

where s_1 and s_2 are the specific entropies of the working fluid at the inlet and exit of the pump for the actual conditions.

5.2.4.2 Boiler

The pressure of the working fluid stays constant during the heat addition process in boiler. The boiler heats the working fluid at the pump outlet to the turbine inlet condition, which can be saturated or superheated vapor.

The energy balance equation for the boiler is

$$\dot{m}_2 h_2 + \dot{Q}_{in} = \dot{m}_3 h_3 \quad (5.39)$$

The entropy balance equation for the boiler is

$$\dot{m}_2 s_2 + \frac{\dot{Q}_{in}}{T_H} + \dot{S}_{gen} = \dot{m}_3 s_3 \quad (5.40)$$

The exergy balance equation for the boiler is

$$\dot{E}x_2 + \dot{Q}_{in} \left(1 - \frac{T_0}{T_H}\right) = \dot{E}x_3 + \dot{E}x_d \quad (5.41)$$

The heat transfer rate from the boiler into the working fluid is given by

$$\dot{Q}_b = \dot{m} (h_3 - h_2) \quad (5.42)$$

where h_3 and h_2 are the enthalpies of the working fluid at the exit and inlet of the boiler.

Using equation (5.36), the boiler exergy destruction rate can be determined as

$$\dot{E}x_{d,b} = T_0 \dot{m} \left[(s_3 - s_2) - \frac{h_3 - h_2}{T_H} \right] \quad (5.43)$$

where s_3 and s_2 are the specific entropies of the working fluid at the inlet and exit of the boiler and T_H is the temperature of the high temperature heat source.

5.2.4.3 Expander

In the expander, the superheated or saturated vapor working fluid passes through the scrolls of the expander to rotate the shaft to generate mechanical power. The pressure decreases in the expansion process due to the volume increase of the chambers between the fixed and orbiting scroll.

The energy balance equation for the expander is

$$\dot{m}_3 h_3 = \dot{m}_4 h_4 + \dot{W}_e \quad (5.44)$$

The entropy balance equation for the expander is

$$\dot{m}_3 s_3 + \dot{S}_{gen} = \dot{m}_4 s_4 \quad (5.45)$$

The exergy balance equation for the expander is

$$E\dot{x}_3 = \dot{W}_e + E\dot{x}_4 + E\dot{x}_d \quad (5.46)$$

The expander power can be given as

$$\dot{W}_e = \dot{W}_{e,ideal} \eta_e = \dot{m}(h_3 - h_2) \eta_e \quad (5.47)$$

where $\dot{W}_{e,ideal}$ is the ideal power of the expander, η_e the expander isentropic efficiency, and h_3 and h_{4s} the enthalpies of the working fluid at the inlet and outlet of the expander for the ideal case. The actual specific enthalpy of the working fluid at the expander exit is

$$h_4 = h_3 - \frac{\dot{W}_e}{\dot{m}} \quad (5.48)$$

And the exergy destruction rate for expander is

$$E\dot{x}_{d,e} = T_0 \dot{m}(s_4 - s_3) \quad (5.49)$$

where T_0 is the ambient temperature which can be assumed as 298.15 K, s_3 and s_4 are the specific entropies of the working fluid at the inlet and exit of the expander for the actual conditions.

5.2.4.4 Condenser

The low pressure and temperature working fluid leaving the expander rejects latent heat to the environment or condenser coolant by heat exchanger through a constant-pressure phase change process.

The energy balance equation for the condenser is

$$\dot{m}_4 h_4 = \dot{Q}_{out} + \dot{m}_1 h_1 \quad (5.50)$$

The entropy balance equation for the condenser is

$$\dot{m}_4 s_4 + \dot{S}_{gen} = \dot{m}_1 s_1 + \frac{\dot{Q}_{out}}{T_L} \quad (5.51)$$

The exergy balance equation for the condenser is

$$\dot{E}x_4 = \dot{Q}_{out} \left(1 - \frac{T_0}{T_L}\right) + \dot{E}x_1 + \dot{E}x_d \quad (5.52)$$

The condenser heat rate, \dot{Q}_c , which is the rate of latent heat rejection from the condensing working fluid, can be expressed as

$$\dot{Q}_c = \dot{m}(h_1 - h_4) \quad (5.53)$$

The condenser exergy destruction rate can be determined from equation (5.36) as follows

$$\dot{E}x_{d,c} = T_0 \dot{m}(s_1 - s_4) - \frac{h_1 - h_4}{T_L} \quad (5.54)$$

where s_1 and s_4 are the specific entropies of the working fluid at the inlet and exit of the condenser, and T_L is the temperature of the low-temperature reservoir where the heat is rejected for $T_1 > T_c > T_0$.

5.2.4.5 Cycle Energy Efficiency

The thermal efficiency is defined as the ratio between the net power output of the cycle to the boiler heat rate. It can be expressed as

$$\eta_{en} = \frac{\dot{W}_e - \dot{W}_p}{\dot{Q}_{in}} \quad (5.55)$$

5.2.4.6 Total Cycle Exergy Destruction

The total exergy destruction can be obtained by adding equations (5.38), (5.43), (5.49), and (54) as follows:

$$\dot{E}x_{d,cycle} = \sum_j \dot{E}x_{d,j} = \dot{E}x_{d,p} + \dot{E}x_{d,b} + \dot{E}x_{d,e} + \dot{E}x_{d,c} \quad (5.56)$$

$$\dot{E}x_{d,cycle} = \dot{m}T_0 \left[\left(-\frac{h_3 - h_2}{T_H} \right) - \left(\frac{h_1 - h_4}{T_L} \right) \right] \quad (5.57)$$

5.2.4.7 Cycle Exergy Efficiency

The second-law exergy efficiency can be calculated using the following equation

$$\eta_{ex} = \frac{\dot{W}_{net}}{\dot{Q}_{in} \left[1 - \left(\frac{T_0}{T_H} \right) \right]} \quad (5.58)$$

5.3 Thermo-economic Optimization

Thermo-economic optimization is the final stage of the design procedure which, for defined boundary conditions, makes it possible to find the optimal values of independent variables. The values that minimize or maximize the chosen optimization criteria are considered to be optimal in this case. It may be the annual net profit, time of return of investment or any other economic profitability criterion. In this thesis, the cost per unit of net electric power generated by the cycle was chosen as the primary measure of the

performance of the system. It is considered to be the most universal optimization criterion since the other two mentioned are dependent on price at which electricity can be sold. This price may vary depending on the country and the type of application.

5.3.1 Economic Model

5.3.1.1 Cost Estimation

The capital costing equations generated in the model (Garceau, 1983) have been used to yield approximate capital and maintenance expenditures and to reflect the consequences of changing the system's variables on these costs. The form of these equations expresses equipment costs in terms of stream and performance variables. In all cases a Capital Recovery Factor (CRF) is used to account for the cost of capital ($i = 15\%$) and estimated useful life ($n = 40$ years). The approach taken to develop these costing equations was to single out the most important parameters that influence cost, and use them to yield a base cost, designating them with a prime. This base cost is then adjusted by multiplication factors so as to incorporate the influence of other factors. The form of these equations has been suggested in the literature (Clark, 1978) and by experienced engineers, then curve fit to available data. The costing equations for this system are listed in Table 5.1.

5.3.1.2 Fixed Charges

The costing equations previously discussed determine the cost associated with each component of the system. The total system cost is composed of the sum of the component costs plus any other charges attributable to the system.

Table 5.1: Costing equations for the Rankine cycle system.

Component	Function
Boiler	$CB = f(STM, P3, T3, AN, AR)$ $CB = X11 \times FAP \times FAM \times FAT \times FAN \times FAR$ $X11 = CRF \times C11$ $FAP = e^{(B11 \times P3)}$ $FAM = e^{(B12 \times \log STM)}$ $FAT = 1.0 + C12 \times e^{[(T3 - T3S)/B13]}$ $FAN = 1.0 + [(1.0 - ANS)/(1.0 - AN)]^{B14}$ $FAR = 1.0 + [(1.0 - ARS)/(1.0 - AR)]^{B15}$
Expander	$CE = f(STM, P3, P4, T3, T4, BN)$ $CE = X21 \times FBW \times FBT \times FBN$ $T3R = T3 + 460$ $T4R = T4 + 460$ $X21 = CRF \times C21$ $FB1 = B22 \times BN \times STM$ $F2T = CPS \times (T3R - T4R - T4R \times \log(T3R/T4R))$ $F2P = R \times T4R \times \log(P3/P4)$ $FBW = e^{\{B21 \times \log[FB1 \times (F2T \times F2P)]\}}$ $FBT = 1.0 + (C22 \times e^{[(T3 - T3S)/B23]})$ $FBN = 1.0 + [(1.0 - BNS)/(1.0 - BN)]^{B24}$
Condenser	$CC = f(CA, P1, P4, PB, PC, T4, TB)$ $CC = X31 \times FCA1 \times FCR \times FCPW \times FCP \times FCB$ for $100 < CA < 3000 \text{ ft}^2$ $CC = X31 \times FCA2 \times FCR \times FCPW \times FCP \times FCB$ for $CA > 3000$ $X31 = CRF$ $FCA1 = CA \times C31 \times e^{(B31 \times \log CA)}$ $FCA2 = CA \times C36$ $FCR = [(P1 \times (1/CR) - 1.0)/C35]^{B32}$ $FCPW = [(PC - PB)/C35]^{B33}$ $FCP = C32 + C33 \times P4 + C34 \times (P4^2)$ $FCB = \exp(B34/(T4 - TB - 5))$
Pump	$CP = f(STM, P1, P2, DN)$ $CP = X42 \times FD1 \times FDN$ $X41 = CRF \times C41$ $Y2 = B42 \times STM \times V34 \times (P2 - P1)/DN$ $FD1 = \exp^{[B41 \times \log Y2]}$ $FDN = 1.0 + [(1.0 - DNS)/(1.0 - DN)]^{B43}$
Fuel	$CF = CF \times HF$

These other charges, called fixed charges, include such costs as the piping between components, foundation charges, building charges, operating personnel charges, etc. Fixed charges are estimated at 1.5 times the sum of the component costs. These costs are considered constant for a specified heat and work output requirement. Because the optimization scheme is at fixed product, these costs do not need to be incorporated into this part of the optimization. However, these charges must be considered in order to select the optimum exergy efficiency from the set of optimizations (each at constant product).

5.3.1.3 Comparison with Alternative and Selection of Overall Optimum Cost

The alternative to the system is typically taken as a low pressure boiler and purchasing electricity from the utility. It is when the economy of the optimally designed system is compared to the alternative, that a system's true potential can be shown. The amortized capital cost attributable to the low pressure boiler is estimated using the relation

$$Z_f = CRF \times 153.964 \times 10^{0.89476 \log HP} \quad (5.59)$$

where the boiler horsepower is given by

$$HP = 33500 \times Q \quad (5.60)$$

The fixed charges for the low pressure furnace, FC_f , are estimated in the same manner as the system, at one and a half times the equipment cost. The fuel cost of producing hot fluid, $CFUEL_f$, is estimated using the unit cost of fuel, CF , the heat input to the fluid, Q , and the estimated boiler efficiency

$$CFUEL_f = CF \times Q / \eta_b \quad (5.61)$$

where the boiler efficiency, η_b is taken to be 0.80. The total cost of producing the hot fluid by the low pressure furnace, $CTOT_f$, is estimated by

$$CTOT_f = CFUEL_f + FC_f + Z_f \quad (5.62)$$

The cost per unit of electricity produced, CE , can be calculated as the difference of the total cost of the system and the cost allocated to the hot fluid, all divided by the amount of electricity produced:

$$CE = (ZTOT + FC - ZTOT_f)/E \quad (5.63)$$

In order to select the electricity production that maximizes the profit returned from its sale, the market price of electricity, MPE , must be known. The net revenue generated by the sale of the generated electricity, NRG , is then expressed as

$$NRG = (MPE - CF) \times E \quad (5.64)$$

For a particular hot water requirement the optimal work output will correspond to the point where net revenue generated is a maximum.

5.3.2 Multi-objective Optimization

A multi-objective problem consists of optimizing (i.e. minimizing or maximizing) several objectives simultaneously, with a number of inequality or equality constraints. Ahmadi et al. (2000) mentioned that the problem can be formally written as follows:

Find $x = x_i$,

$$\forall i = 1, 2, \dots, N_{param} \text{ such as } f_i(x) \text{ is a minimum (respectively maximum)} \quad (5.65)$$

$$\forall i = 1, 2, \dots, N_{obj} \text{ subject to:} \quad (5.66)$$

$$g_j(x) = 0, \forall j = 1, 2, \dots, M, \quad (5.67)$$

$$h_k(x) < 0, \forall k = 1, 2, \dots, K, \quad (5.68)$$

where x is a vector containing the N_{param} design parameters, $(f_i)_{i=1,\dots,N_{\text{obj}}}$ the objective functions and N_{obj} the number of objectives. The objective function $(f_i)_{i=1,\dots,N_{\text{obj}}}$ returns a vector containing the set of N_{obj} values associated with the elementary objectives to be optimized simultaneously.

Deb (2000) gave the definition that an individual $X^{(a)}$ is said to constrain-dominate an individual $X^{(b)}$, if any of the following conditions are true,

1. $X^{(a)}$ and $X^{(b)}$ are feasible with
 - (a) $X^{(a)}$ is no worse than $X^{(b)}$ in all objective and
 - (b) $X^{(a)}$ is strictly better than $X^{(b)}$ in at least one objective
2. $X^{(a)}$ is feasible while individual $X^{(b)}$ is not.
3. $X^{(a)}$ and $X^{(b)}$ are both infeasible, but $X^{(b)}$ has a smaller constraint violation.

5.3.2.1 Objective Functions

The aim of the optimization is to minimize the total cost of owning and operating the system (at fixed product output) while maximizing the exergy efficiency of the system. Two objective functions including exergy efficiency (to be maximized), the total cost rate of product (to be minimized) are considered for multi-objective optimization. The objective function for this analysis is considered as:

Exergy Efficiency of the Expander:

$$\eta_{ex} = \frac{(h_3 - h_4) \times \left\{ \frac{n_e}{n_e - 1} \times \left(\frac{P_4}{\rho_4} \right) \times \left[\left(\frac{2\varphi_e - \varphi_i + \varphi_0 - 3\pi}{5\pi - \varphi_i + \varphi_0} \right)^{\frac{n_e}{n_e - 1}} - 1 \right] \right\}}{(h_3 - h_2) \times \left(1 - \frac{T_0}{T_3} \right)} \quad (5.69)$$

where

- $h_1 = f(T_1, P_1)$
- $h_2 = f(T_2, P_2)$

- $h_3 = f(T_3, P_3)$
- $h_4 = f(T_4, P_4)$

Total Cost of the Rankine Cycle System

$$C_{total} = C_{boiler} + C_{expander} + C_{condenser} + C_{pump} + C_{fluid} \quad (5.70)$$

where

$$C_{boiler} = f(STM, P3, T3, AN, AR)$$

$$C_{expander} = f(STM, P3, P4, T3, T4, BN)$$

$$C_{condenser} = f(CA, P1, P4, PB, PC, T4, TB)$$

$$C_{pump} = f(STM, P1, P2, DN)$$

$$C_{fluid} = f(HF)$$

5.3.2.2 Constraint Equations

The selection of fixed parameters and decision variables is given in Table 5.2. The equations of constraint link the cost estimate through the system's thermodynamic performance to fuel costs. The thermodynamic analysis must relate the variables used to describe the system's performance to those used in the cost estimate. In this problem, costing equations are used which are generally in terms of stream and performance variables. Thus the thermodynamic analysis need only be in terms of these variables. Sixteen equations of constraint have been developed from a thermodynamic analysis of the cycle, and are given in Table 5.3. Some constraints use stream variables to describe the thermodynamic state of the working fluid.

The problem has now been reduced to five independent variables. The form of the constraint equations has been arranged such that each state variable can be obtained explicitly and the order selected such that the resulting matrix is diagonalized. In order to

obtain equations for the solution of the shadow and marginal prices, various derivatives of the constraint equation matrix should be evaluated. However, because not all the constraints are in algebraic form (those constraints that are functions of steam table properties) numerical derivatives must be evaluated. One other note, there are two condenser costing equations. This means that two separate derivatives must be taken and the derivative corresponding to whichever costing equation is valid for that value of condenser area, is the one that should be used.

Table 5.2: Fixed Parameters and Decision Variables for a cogeneration System.

Code	Fixed Parameters (y_f)
TB	Condenser hot water outlet temperature
TC	Condenser hot water inlet temperature
PB	Condenser hot water outlet pressure
PC	Condenser hot water inlet pressure
HWM	Required hot water mass flow rate
WA	Net turbine shaft work output
CR	Condenser shell-side pressure loss coefficient
X2	Expander exit quality
U	Condenser overall heat transfer coefficient
CPW	Specific heat of water at constant pressure
CN	Condenser First Law efficiency
	Decision Variables (y_k)
AN	Boiler efficiency
AR	Boiler pressure drop coefficient
P3	Expander inlet pressure
P4	Condenser inlet pressure
DN	Pump isentropic efficiency

The solution procedure requires the designer to select a feasible set of decision variables (y_k) for the first iteration. Once this initial set of five decision variables has been chosen, entire design (for that iteration) is fixed and the set of state variables (x_i), and cost estimates are determined.

Table 5.3: Equations of Constraint for the Cogeneration System.

State Variable(x_i)	Thermodynamic Constraint Defining Relation (Φ_i)
H4	$f(P4, X4)$
T4	$f(P4, \text{quality})$
P1	$P4 \times CR$
H1	$f(P1, \text{SAT}, \text{LIQ})$
P2	$P3/AR$
H2	$H1 + CF3 \times V34 \times (P2 - P1)/DN$
STM	$HWM \times CPW \times (TB - TC)/[CN \times (H4 - H1)]$
WP	$STM \times (H2 - H1)$
H3	$(WA + WP)/(STM + H4)$
T3	$f(H3, T3)$
H4S	$f(P3, P4, T3)$
BN	$(WA + WP)/[STM \times (H3 - H4S)]$
HF	$STM \times (H3 - H2)/AN$
T1	$f(P1, \text{SAT}, \text{LIQ})$
TM	$[(T1 - TC) - (T4 - TB)]/\log[(T1 - TC)/(T4 - TB)]$
CA	$HWM \times CPW \times (TB - TC)/(TM \times U)$

6 RESULTS AND DISCUSSION

6.1 Calculation of the Scroll Chamber Volumes

The purpose of the presented analysis is to establish a reasonably accurate method to predict the operation of a scroll compressor in reverse, namely the expander. Furthermore, as aforementioned, one intends to investigate how the scroll geometry must be modified for better efficiency of the expansion process. In this respect, we selected a low capacity scroll compressor from a refrigeration equipment manufacturer, namely Copeland ZF06K4E-PVF (liquid injected) of which parameters are given in Table 6.1.

Table 6.1: Technical parameters of the selected scroll compressor, Copeland ZF06K4E-PVF.

Mechanical		Electrical		Thermodynamic	
Parameter	Value	Parameter	Value	Parameter	Value
Swept volume	34 cm ³ /rev	No of Phases	1 ph	Refrigerant	R404A
Displacement	7.14 m ³ /hr	Voltage	208/230V	Tevap	-31.7°C
Suction	¾"	Frequency	60 Hz	Tcond=Tinj.liq.	40.6°C
Discharge	½"	LRA	61 A	T return gas	18.3°C
Oil charge	1 litre	RLA	12.2 A	Cooling cap.	1960W
Net weight	28 kg	MCC	19.0	Electric power	1730 W
Intern free vol.	3.36 cm ³	RPM	3500	Drawn current	8.1 A
Shaft power	2 HP	Start capacitor	107µF/330V	Mass flow rate	15 g/s
Housing diam.	191 cm	Run capacitor	40µF/370V	Isentr.efficiency	40%

LRA = locked rotor amperes; RLA = rated load amperes; MCC = maximum continuous current

Using the equations (5.24-5.29) for simplified modeling of positive displacement compressors and the compressor manufacturer data for nominal operation, we determined the compressor's isentropic efficiency, built-in volume ratio and the flow coefficient.

In order to obtain a better design, certain strategies can be pursued – separately or simultaneously- by modifying the scroll geometry with respect to rolling angle and changing the working fluid. The aim is to adapt the thermodynamic cycle to the imposed external conditions better at sink and source. Based on the literature survey, Halm (1997),

Winandy et al. (2001), Lemort et al. (2008) the geometric parameters of scroll machines are given in Table 6.2.

Table 6.2: Parameters defining scroll geometry.

Symbol	Value
r_b/h	0.09-0.013 (0.11)
r_o/h	0.17-0.23 (0.20)
$\varphi_{o,0}$	0 rad
$\varphi_{i,0}$	1.3-1.5 (1.4) rad
$\varphi_{o,s}$	1.4-1.8 (1.57) rad
$\varphi_{i,s}$	3-5 (3.5) rad
φ_e	20-60 rad

* The values in parenthesis are adopted for the study

The volumes of the different chambers calculated by the geometric equations and selected parameters are plotted as a function of the orbiting angle θ in Figures 6.1 and 6.2. The whole change process of the volume during suction, compression and discharge can be plotted in Maple Software. In the compressor mode suction volume increases until it reaches a maximum and decreases again until the suction chamber is closed where the compression process starts at the orbiting angle of 4 rad. The change of suction chamber volume is initially positive and decreases afterwards since the suction chambers become closer. After the suction chamber is closed, the compression process takes place as the volume between the fixed and orbiting scroll decreases depending on the specific geometry of the scroll and the orbiting motion. The compression chamber continues from

the end of the suction process at 4 rad to the start of the discharge process at 23 rad as the shaft rotates 2.7 times to produce useful work.

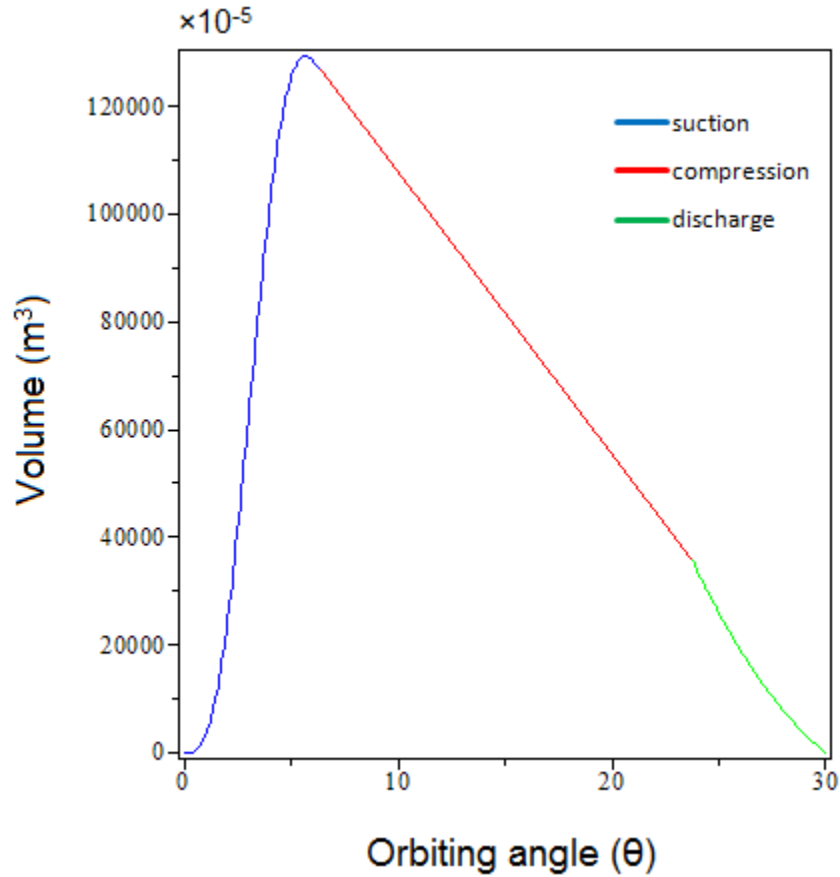


Figure 6.1 Change of the volume during suction, compression and discharge for compressor.

The decrease of the compression chamber volume is linear as shown in Figure 6.1 since the working fluid is forced to compress by the orbiting scroll at a constant number of revolutions per minute in terms of the change in orbiting angle and shaft rotation during the compression process. Finally discharge takes place and the volume decreases simultaneously from the end of compression at 23 rad to the end of discharge process at 30 rad in order to send the working fluid at a high pressure and temperature. The sudden pressure drop occurs at the end of the discharge process when the working fluid is

transferred to the discharge port which should be taken into account in order to specify the conditions at the compressor exit. In an expander mode, the volume of the suction chamber increases as the orbiting angle increases from 0 rad to 7 rad as shown in Figure 6.2.

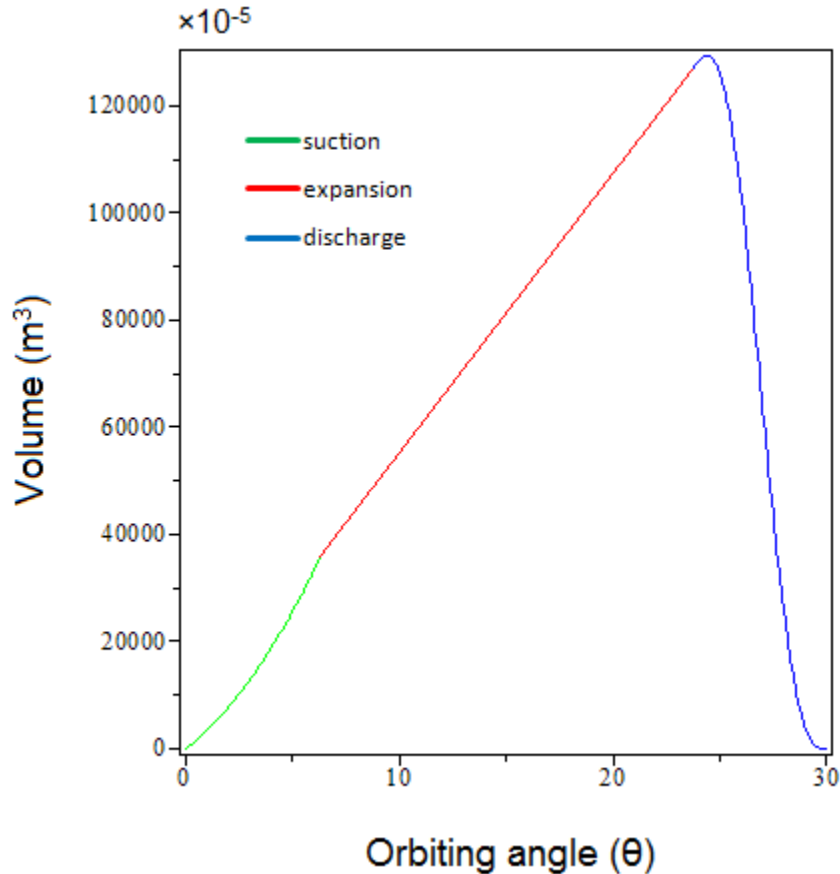


Figure 6.2: Change of the volume during suction, expansion and discharge for expander.

The suction chamber volume at the beginning of the suction process ($\theta=0$) is not zero due to the clearance volume which is equal to the volume of chamber 1 shown in Figure 5.4. After 1.114 times of shaft rotation, the working fluid is transferred to the expansion chambers and the volume increases linearly until the discharge starts at the orbiting angle of 24 rad and produces power by approximately 3 times of the shaft

rotation through the expansion process reaching a maximum volume of $130000 \times 10^{-5} \text{ m}^3$ just before the discharge starts. Finally expansion chambers open to the discharge chamber and the volume decreases as the same rate as the suction process in compressor mode. As a result, it takes 30 rad or 4.77 shaft rotations to bring the fluid from suction to discharge, making 63% of total shaft work produced through the expansion process.

6.2 Scroll Compressor Conversion into Expander

After these determinations, the expander model has been used to predict the operation of the same machine operating in reverse. It has been imposed that the expansion process evolves from a state having the same temperature and pressure as that of the discharge at operation as an expander ($T_{e,1} = T_{2a}$; $P_{e,1} = P_{2a}$). The results are indicated graphically in Figure 6.3. The calculated built-in pressure ratio was 7.34, while the leakage flow coefficient was $\zeta = 1.365 \times 10^{-6} \text{ m}^{-2}$.

Assume that the scroll compressor geometry is not modified and the maximum nominal pressure and temperature are kept the same as in the manufacturer data sheet; meaning that the thermodynamic state at the expander intake is defined by the aforementioned values. The corresponding Rankine cycle can be easily determined. The resulting Rankine cycle configuration is shown in Figure 6.4 and the corresponding efficiency is 14%. It can be observed that the sink temperature for this cycle must be far below the normal environment temperature (except when the cycle is operating in deep winter condition); in other words, this thermodynamic cycle is non-realizable.

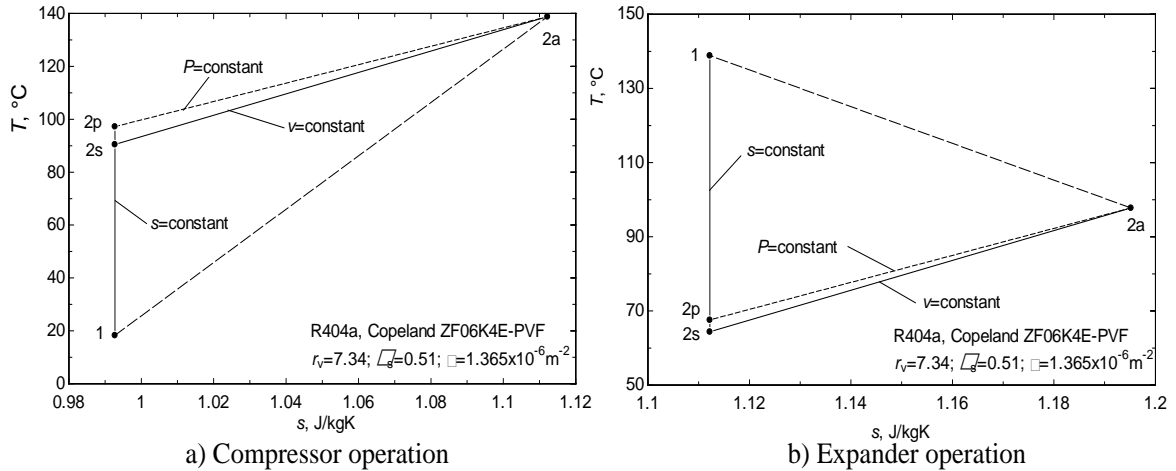


Figure 6.3: Compression and expansion processes determined by simplified model.

In order to run a feasible Rankine cycle with the selected expander without changing the scroll geometry and the working fluid, the upper pressure and temperature must be increased. Through a trial and error procedure, we found out that by increasing the pressure and temperature at the expander intake to the supercritical value of 68bar and 264°C, the cycle becomes realizable and achieves an efficiency of 18%; when the internal heat regeneration is applied. The cycle performs well, but the only inconvenience which arguably arises is that the pressure and temperature values are high. This implies redesigning the expander shell to resist such conditions; which is a measure that must be taken regardless, since other modifications, except the scroll, are necessary: e.g., recoiling the electric motor into a generator.

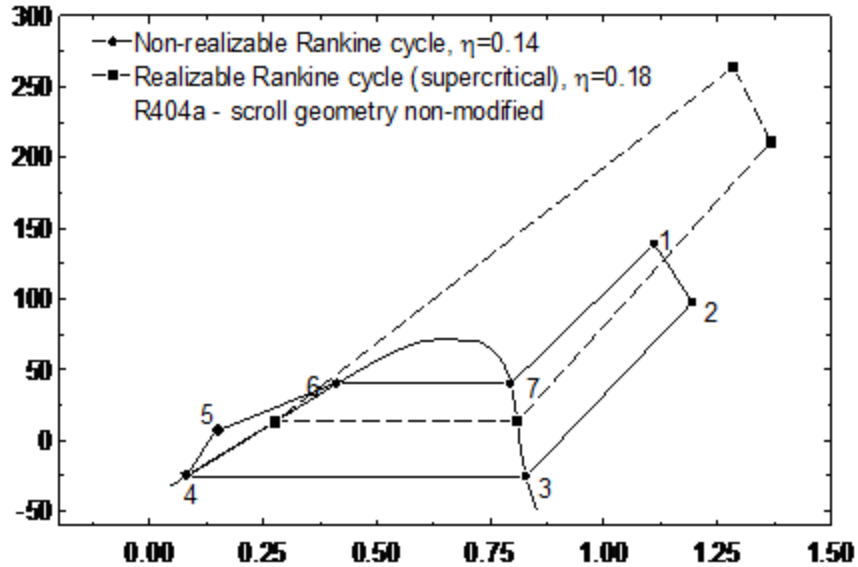


Figure 6.4: Rankine cycles with non-modified scroll machine and same working fluid.

6.3 Cycle Results with Modified Scroll Geometry

6.3.1 Energy and Exergy Efficiency Improvements

Several working fluids for Rankine cycle were investigated. For each studied case the expander geometry has been adjusted with respect to the rolling angle only. The rolling angle and Rankine cycle parameters were determined by a trial and error method. The results are summarized in Table 6.3 where 6 working fluids were investigated. The working fluid is originally used for the scroll compressor, R404a, that gave the best performance. Two cases were analyzed with R404a. In the first case the rolling angle has been reduced to 27 rad. The corresponding built-in pressure ratio in this case becomes 3.0. In this situation, a supercritical Rankine cycle has been implemented for a maximum pressure and temperature values of 38 bar and 139°C. The cycle is illustrated in Figure 6.5, and the corresponding efficiency is 25%. The cycle configuration offers a good

opportunity for internal heat regeneration between streams 2-3 and 5-1. For this reason, the resulted efficiency is exceptionally high.

Table 6.3: Scroll expander and Rankine cycle parameters with various working fluids.

Working Fluid	φ_e rad	r_v	V_{suc} ml/rev	P_{max} bar	T_{max} °C
R404a	27	3.0	54	38	139
R404a	57*	7.3	128	68	264
R141b	33	3.8	68	30	178
R141b	69*	9.2	161	54	338
NH₃	57*	7.3	128	60	173
NH₃	29	3.3	61	33.5	91
R134a	57*	7.3	128	40	170
R134a	28	3.1	59	22.3	89.4
R123	185*	25	447	21	230
R123	90	10.6	206	11.7	121
Toluene	725*	100	1790	20	273
Toluene	352	42.4	824	11.1	143

* no modification of scroll geometry

First and second laws analysis is performed and corresponding energy and exergy efficiencies are evaluated for modified and nonmodified scroll geometries with different organic fluids and the results are given in Figures 6.6 and 6.7. The configuration given in Figure 6.4 with R404a involves no modifications of the scroll geometry. This configuration is described above achieves 18% efficiency. The other working fluid that shows a good performance is R123a; however, Table 6.3 shows that the rolling angle is

very high which results in a less compact design with 17% efficiency. Toluene requires an expansion ratio of 100, leading to a massive expander with 725 rad rolling angle, which is not practical. All other studied fluids show lower efficiency and therefore appear to be less attractive for implementation. Note that the efficiency listed in Figure 6.6 and Figure 6.7 is the general efficiency of Rankine cycle, defined as useful output over heat input.

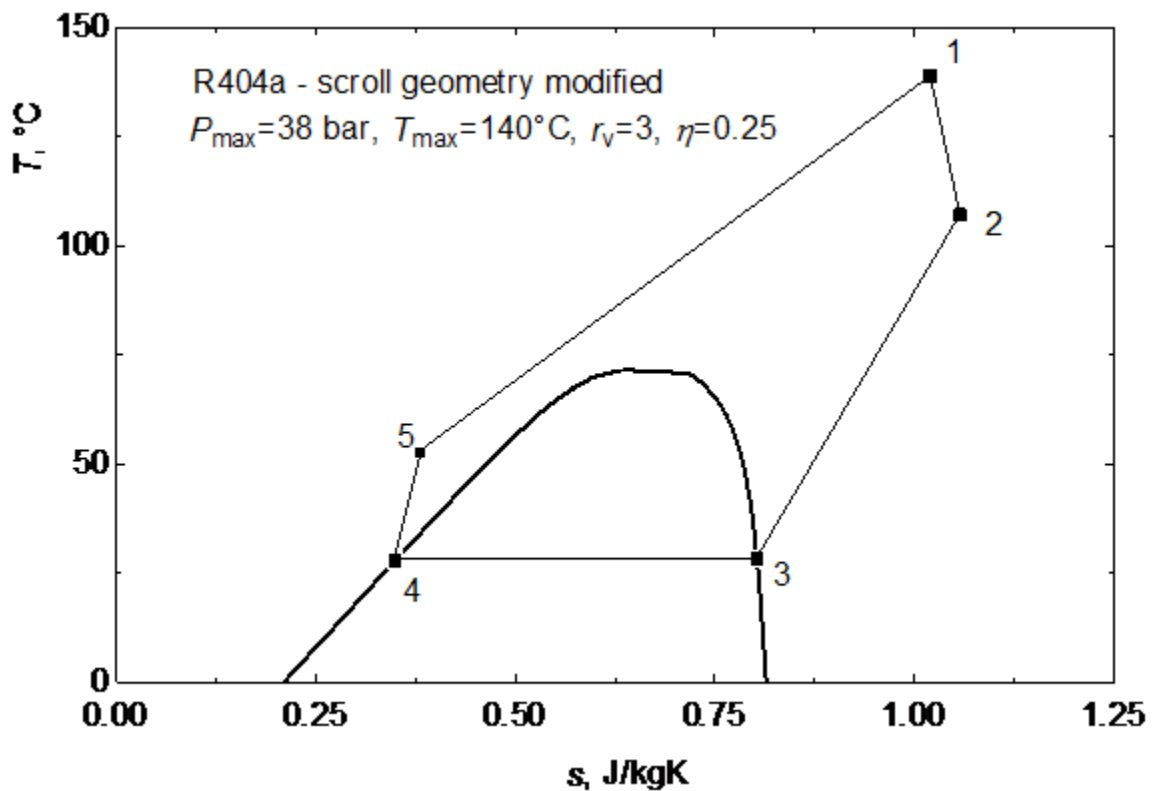


Figure 6.5: Recommended cycle and scroll compressor modifications.

Table 6.3 indicates that if no modifications are made to the scroll machine, the appropriate choice of working fluid for Rankine cycle is R134a because the resulted efficiency is good (12%) and the maximum level of pressure and temperature in the system does not require modification of the housing. If modification of the housing is to

be considered only with respect to maximum pressure and temperature but not to the scroll geometry modifications, then the original working fluid can be used. In this case, the pressure that needed to be withstood is more than triple and the temperature is 100°C higher, while the cycle efficiency is 18%. The best results are obtained with R404a and the built-in ratio is reduced from 7.3 to 3. The scroll rolling angle is 27 rad, the temperatures and pressures in the system are reasonably low and are suitable for low temperature heat engine and the energy efficiency will reach 25%. The T-s diagram of the cycle for R404a with modified scroll geometry is given in Figure 6.5. It can be observed from Figure 6.6 and Figure 6.7 that the energy and exergy efficiencies of the Rankine cycle is strongly depended on the scroll expander geometry.

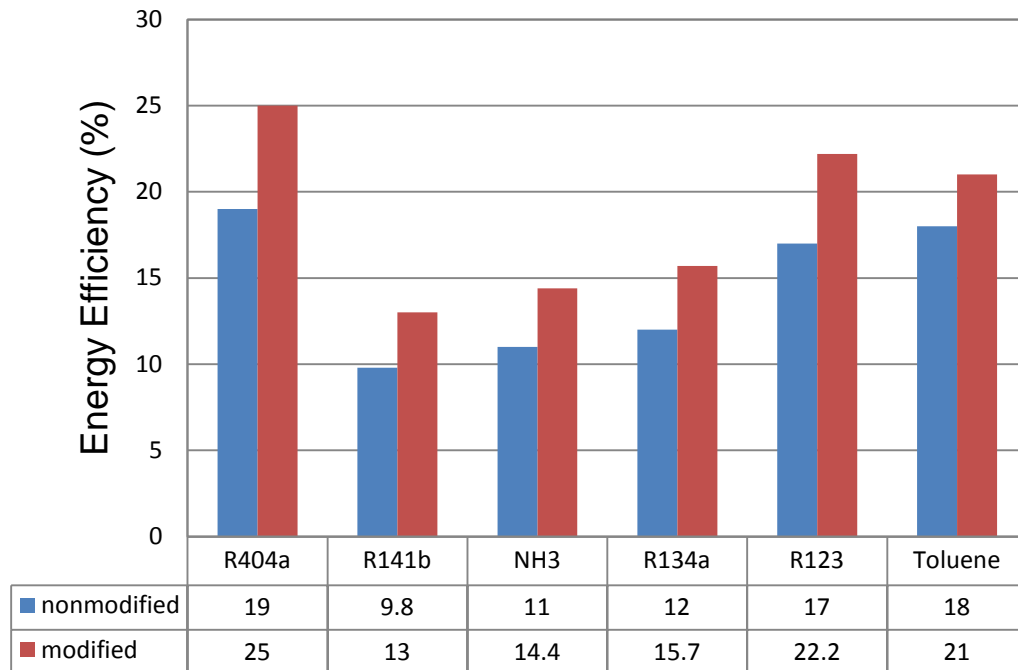


Figure 6.6: Energy Efficiency of the cycle for the modified and nonmodified geometry.

For all the organic working fluids, the efficiency can be improved by modifying the geometry in order to be able to calculate the most appropriate built-in volume ratio for the scroll machine. The rolling angle is the most important geometric parameter since it defines the length of the scroll and the number of loops through the expansion process. Built-in volume ratio of the scroll expander is modified with respect to the rolling angle and influence of the modified geometry on the efficiency is evaluated for different working fluids as shown in Figure 6.6 and 6.7. It can be observed that exergy efficiencies are higher than energy efficiencies because of the temperature difference between sink and source times heat input term at the denominator in equation 5.58.

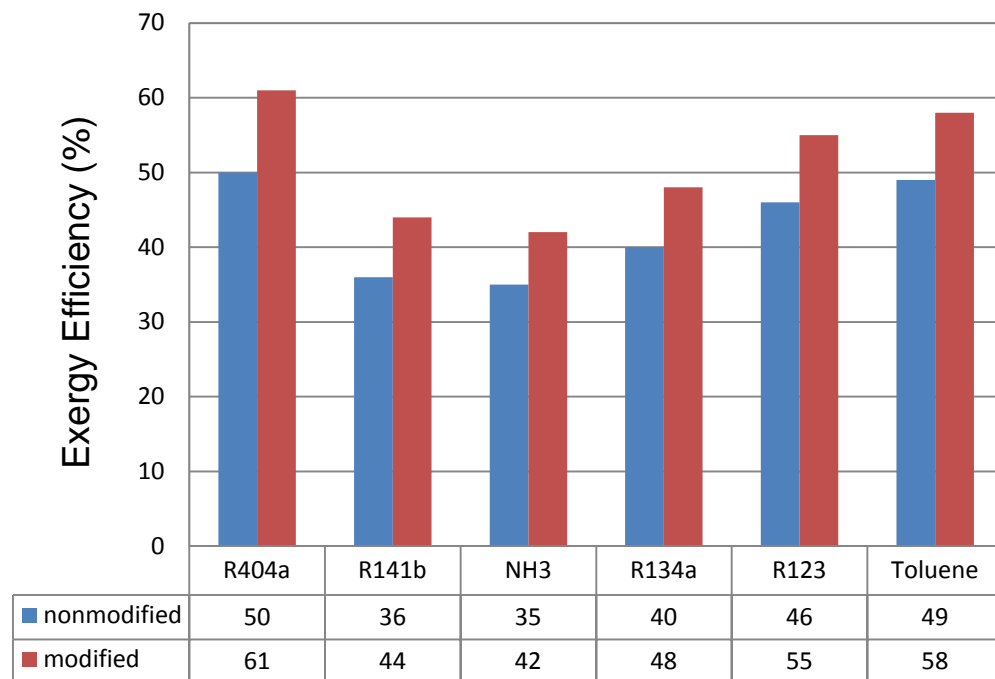


Figure 6.7: Exergy Efficiency of the cycle for the modified and nonmodified geometry.

The optimum rolling angle of the scroll expander for each organic fluid is evaluated and results are given in Table 6.3 to obtain an appropriate built in volume ratio for the best possible cycle efficiency. The results are provided in Figures 6.6 and 6.7, and

the modified geometry is shown by the columns labeled in red. R404a clearly gives the best result for the modified geometry and the energy efficiency is increased from 19% to 25% while the exergy efficiency is increased from 50% to 61% (see Figures 6.6 and 6.7). R123 and Toluene are the other working fluids which have relatively higher energy and exergy efficiencies compared to other organic fluids for the modified and unmodified cases of the scroll expander geometry as can be observed in the figures.

6.2.2 Comparison of Exergy Destructions

Figure 6.8 illustrates the percentage of the exergy destruction in each component with respect to the total system exergy destruction for both configurations. Figure 6.8 demonstrates that the evaporator is the component with the highest exergy destruction contribution (76%) followed by the expander with 22.1% for the ORC that has an expander with a rolling angle of 57° . For the ORC with modified expander, the evaporator is still the highest contributor to the total exergy destruction of the system, contributing 81.2% of the total exergy destruction. However, the exergy destruction in the expander reduced from 22.1 to 17.3% by using expander with the rolling angle of 27° . This exergy reduction is mainly due to reduced leakage which is implied by the rolling angle geometric modification that accounts for 4.8% of the exergy destruction.

Figure 6.9 illustrates the percentage of the exergy destruction in each component with respect to the total system exergy destruction for both configurations. Figure 6.9 demonstrates that the evaporator is the component with the highest exergy destruction contribution (75.3%) followed by the expander with 23.2% for the ORC with expander rolling angle of 69° . For the ORC with modified expander, the evaporator is still the highest contributor to the total exergy destruction of the system contributing 78.7% of the

total destruction. However, the exergy destruction in the expander is reduced from 23.2 to 19.8% by using expander with the rolling angle of 33° . This exergy reduction is mainly due to reduced leakage which is implied by rolling angle geometric modification that accounts for 3.4% of the exergy destruction.

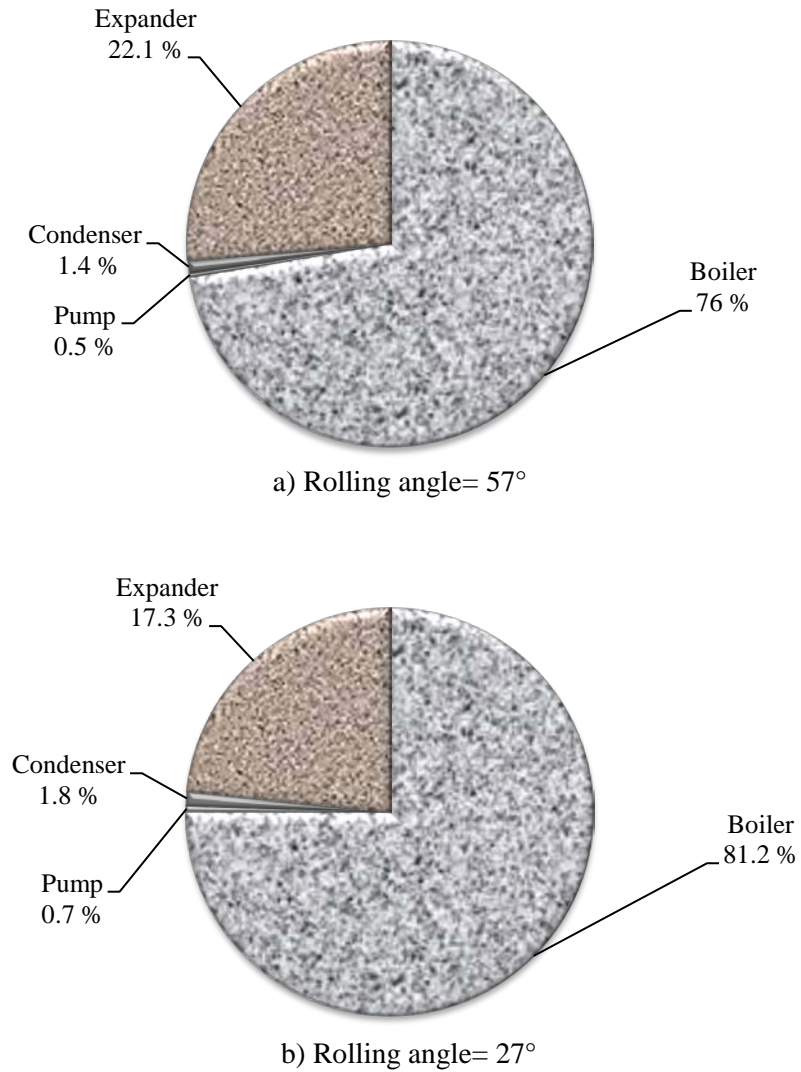
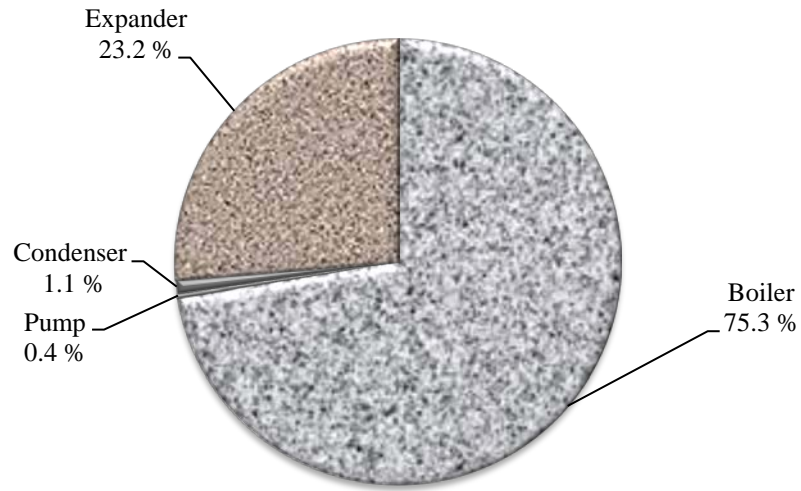
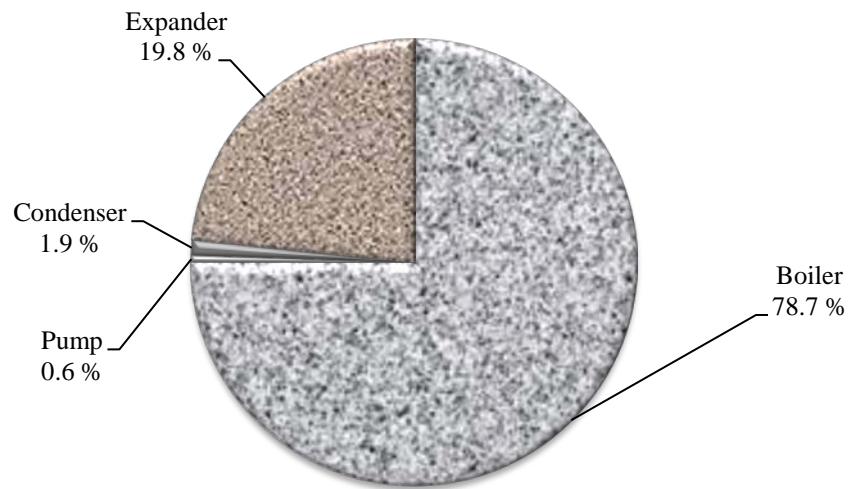


Figure 6.8: Percentage of the exergy destruction in each component for R404a

(a) $\phi_e=57^\circ$ and (b) $\phi_e=27^\circ$.



a) Rolling angle= 69°



b) Rolling angle= 33°

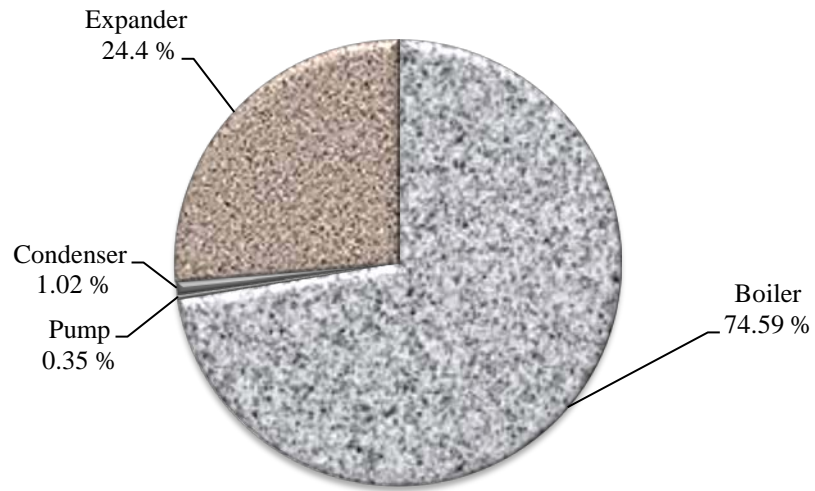
Figure 6.9: Percentage of the exergy destruction in each component for R141b

(a) $\phi_e=69^\circ$ and (b) $\phi_e=33^\circ$.

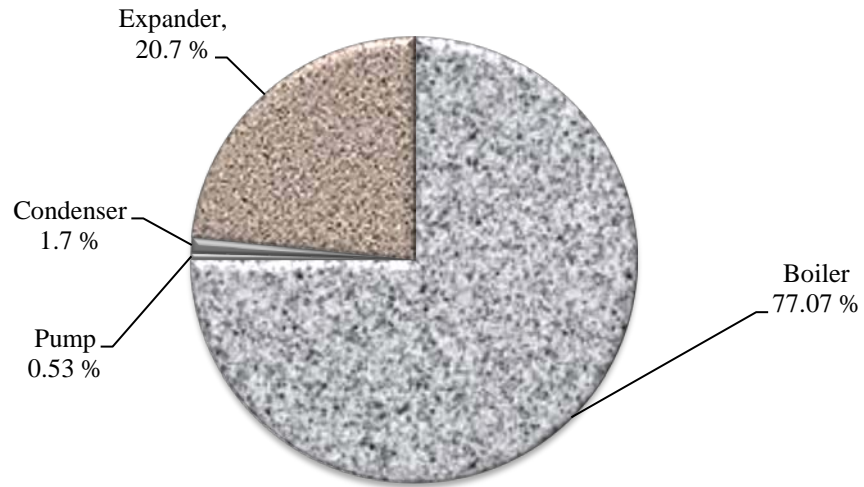
Figure 6.10 illustrates the percentage of the exergy destruction in each component with respect to the total system exergy destruction for both configurations. It clearly demonstrates that the evaporator is the component with the highest exergy destruction contribution (74.59%) followed by the expander with 24.4% for the ORC with expander rolling angle of 57°. For the ORC with modified expander, the evaporator is still the

highest contributor to the total exergy destruction of the system contributing 77.07% of the total destruction. However, the exergy destruction in the expander reduced from 24.4 to 20.7% in comparison by using expander with the rolling angle of 28° . This exergy reduction is mainly due to decreased leakage destruction which is implied by geometric modification in rolling angle that accounts for 3.7% of exergy destruction.

Figure 6.11 illustrates the percentage of the exergy destruction in each component with respect to the total system exergy destruction for both configurations. Figure 6.11 demonstrates that the evaporator is the component with the highest exergy destruction contribution (72.41%) followed by the expander with 26.29% for the ORC with expander rolling angle of 57° . For the ORC with modified expander, the evaporator is still the highest contributor to the total exergy destruction of the system contributing 75.02% of the total destruction. However, the exergy destruction in the expander reduced from 26.29 to 23.37% in comparison by using expander with the rolling angle of 28° . This exergy reduction is mainly due to decreased leakage destruction which is implied by geometric modification in rolling angle that accounts for 2.92% of exergy destruction.



a) Rolling angle= 57°



b) Rolling angle= 28°

Figure 6.10: Percentage of the exergy destruction in each component for R134a

(a) $\varphi_e=57^\circ$ and (b) $\varphi_e=28^\circ$.

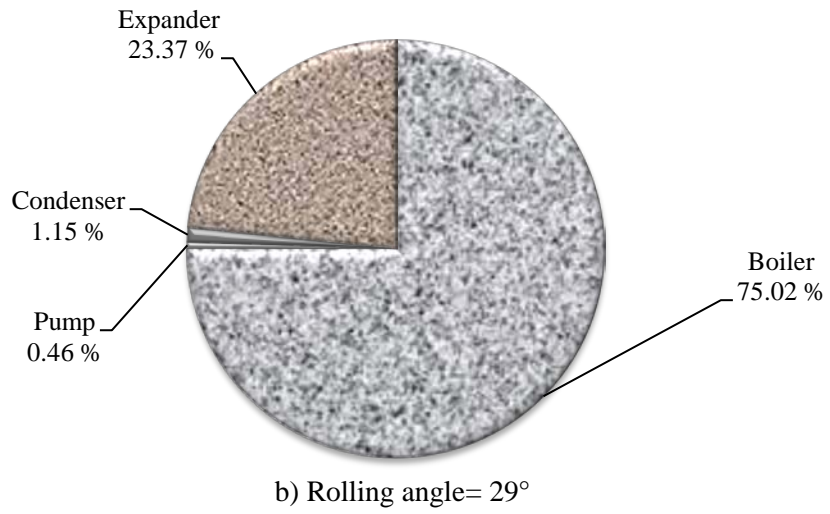
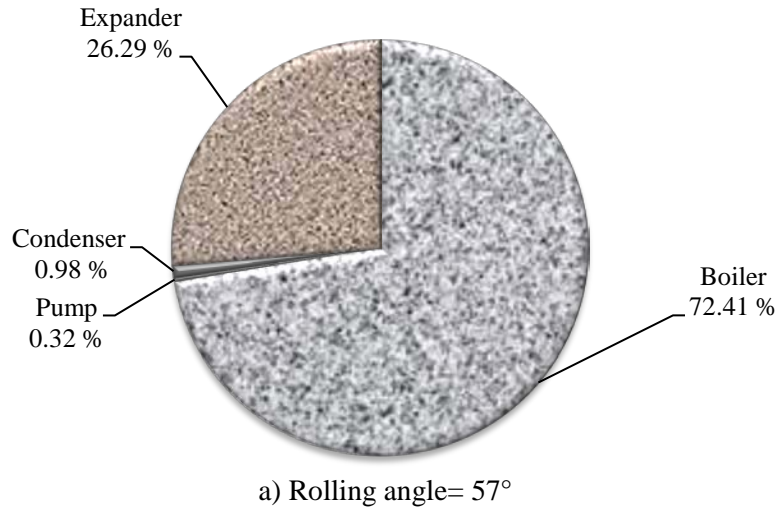


Figure 6.11: Percentage of the exergy destruction in each component for NH₃
(a) $\varphi_e=57^\circ$ and (b) $\varphi_e=29^\circ$.

Figure 6.12 shows the exergy wheel graph of ORC using R404a as an organic fluid that has an expander rolling angle of 57° . It can be observed that boiler and the expander have the highest contribution of exergy destructions with 3.02 kW and 0.55kW, respectively.

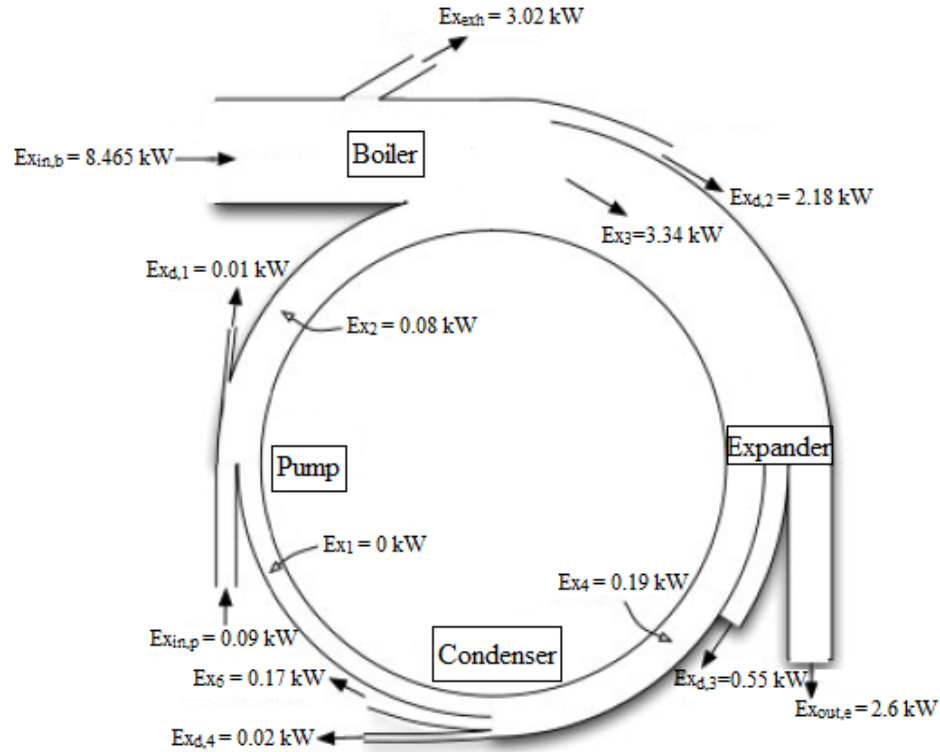


Figure 6.12: Exergy wheel diagram for R404a and $\phi_e = 57^\circ$.

Figure 6.13 shows the exergy wheel graph of ORC for R404a using an organic fluid and expander rolling angle of 27° . It can be from the figure that boiler and expander have the highest contribution of exergy destructions with 3.02 kW and 0.43 kW, respectively. It can be observed that exergy destruction in the expander is reduced from 0.55 kW to 0.43 kW by decreasing the rolling angle of expander from 57° to 27° and therefore the exergy output from the expander is increased from 2.6 kW to 2.72 kW.

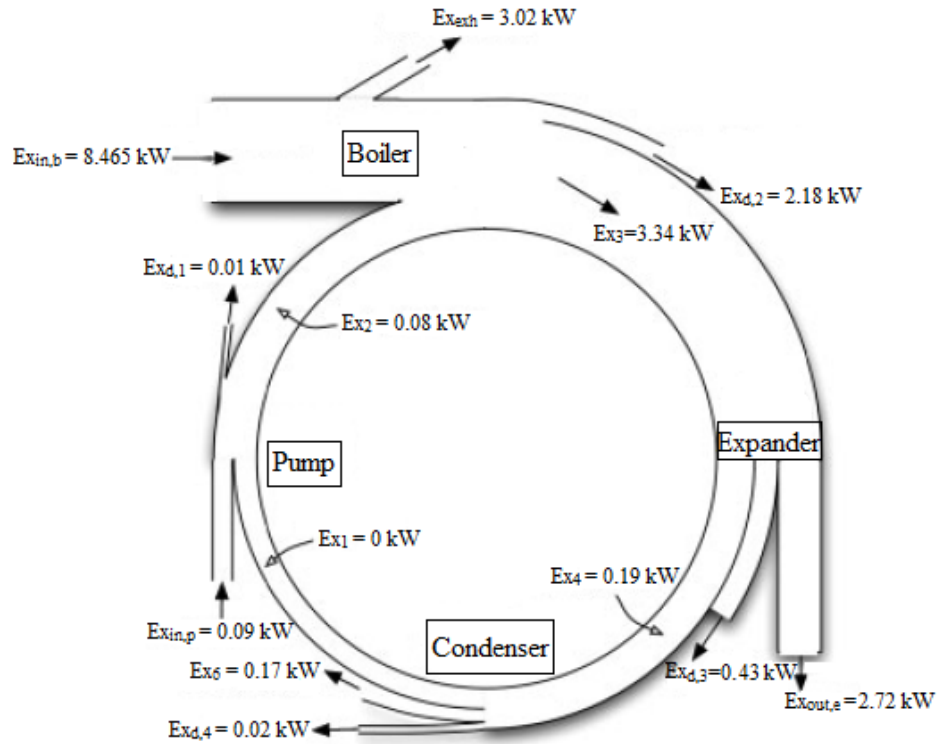


Figure 6.13: Exergy wheel diagram for R404a and $\phi_e = 27^\circ$.

Figure 6.14 shows the exergy wheel graph of ORC for R141b as an organic fluid and expander rolling angle of 69° . It can be observed that boiler and expander have the highest contribution of exergy destructions with 3.02 kW and 0.74 kW, respectively.

Figure 6.15 shows the exergy wheel graph of ORC for R141b as an organic fluid and expander rolling angle of 33° . It can be from the figure that boiler and expander have the highest contribution of exergy destructions with 3.02 kW and 0.62 kW, respectively. It can be observed that exergy destruction in the expander is reduced from 0.74 kW to 0.62 kW by decreasing the rolling angle of expander from 69° to 33° and therefore the exergy output from the expander is increased from 2.41 kW to 2.53 kW.

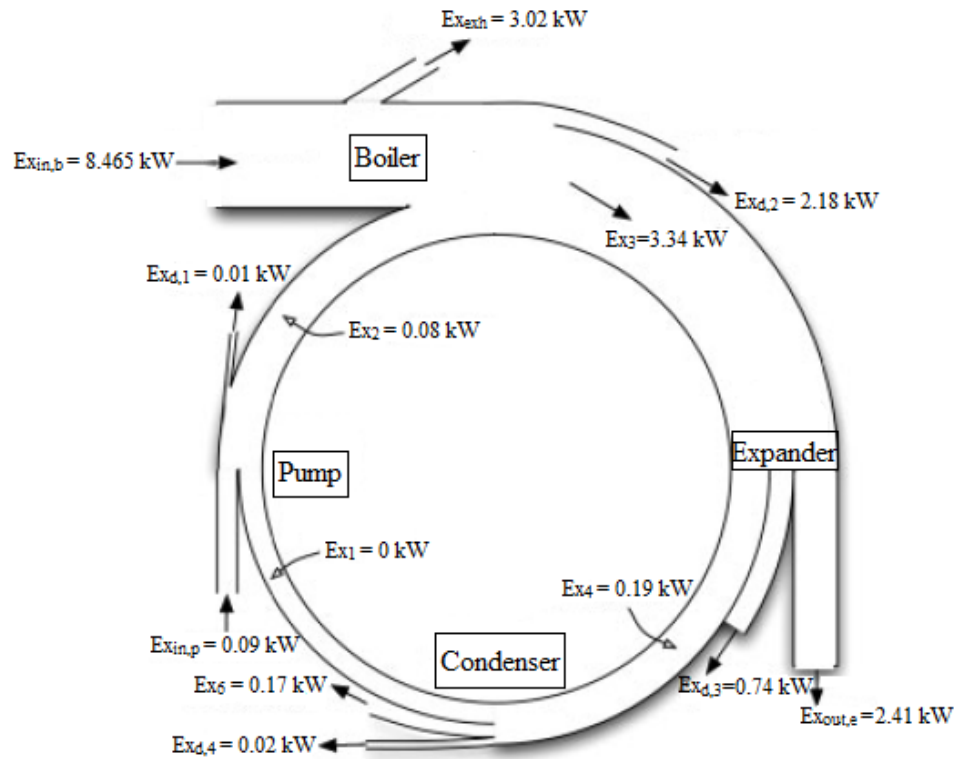


Figure 6.14: Exergy wheel diagram for R141b and $\phi_e = 69^\circ$.

Figure 6.16 shows the exergy wheel graph of ORC for R134a as an organic fluid and expander rolling angle of 57° . It can be observed that boiler and expander have the highest contribution of exergu destructions with 3.02 kW and 1.02 kW, respectively.

Figure 6.17 shows the exergy wheel graph of ORC for R134a as an organic fluid and expander rolling angle of 28° . It can be from the figure that boiler and expander have the highest contribution of exergy destructions with 3.02 kW and 0.88 kW, respectively. It can be observed that exergy destruction in the expander is reduced from 1.02 kW to 0.88 kW by decreasing the rolling angle of expander from 57° to 28° and therefore the exergy output from the expander is increased from 2.13 kW to 2.27 kW.

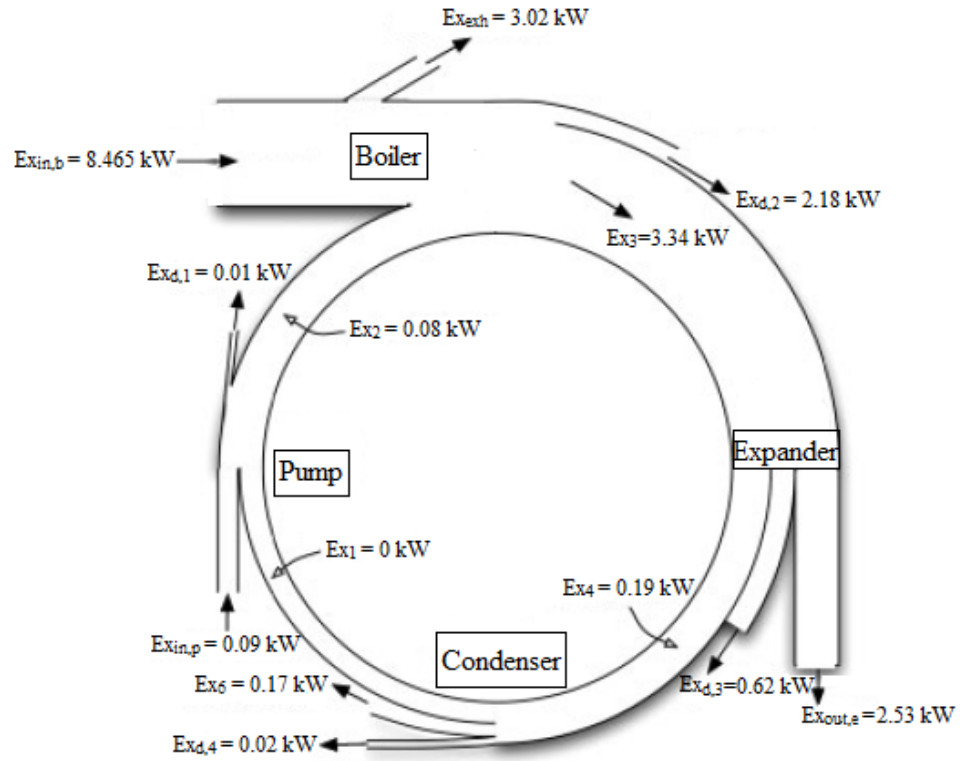


Figure 6.15: Exergy wheel diagram for R141b and $\phi_e = 33^\circ$.

Figure 6.18 shows the exergy wheel graph of ORC for NH_3 as an organic fluid and expander rolling angle of 57° . It can be observed that boiler and expander have the highest contribution of exergu destructions with 3.02 kW and 1.23 kW, respectively.

Figure 6.19 shows the exergy wheel graph of ORC for NH_3 as an organic fluid and expander rolling angle of 29° . It can be from the figure that boiler and expander have the highest contribution of exergy destructions with 3.02 kW and 1.07 kW, respectively. It can be observed that exergy destruction in the expander is reduced from 1.23 kW to 1.07 kW by decreasing the rolling angle of expander from 57° to 29° and therefore the exergy output from the expander is increased from 1.92 kW to 2.08 kW.

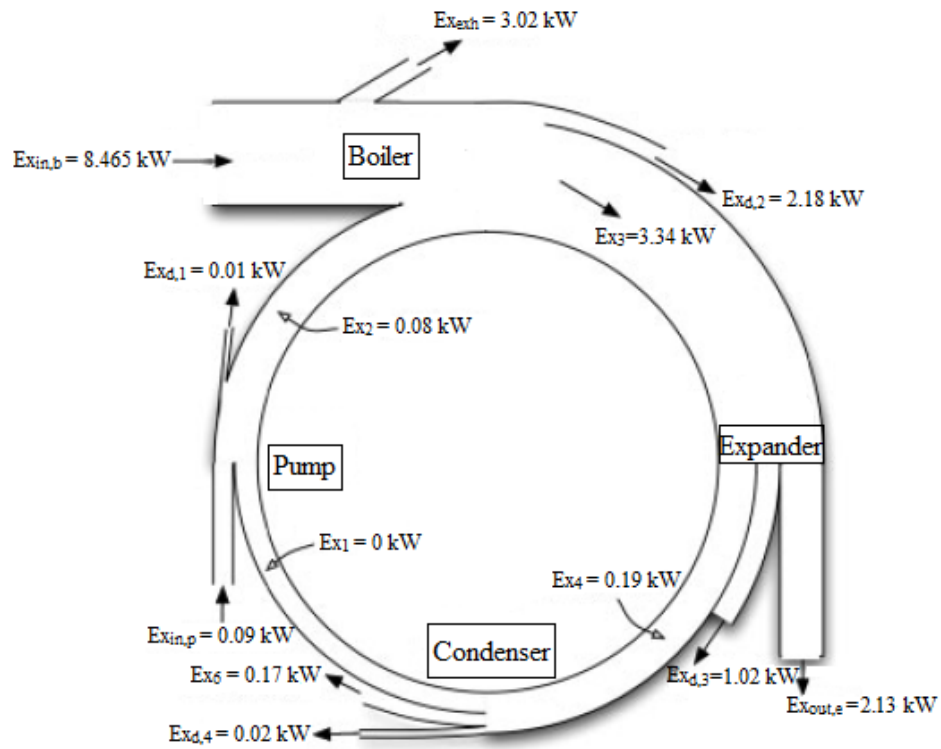


Figure 6.16: Exergy wheel diagram for R134a and $\phi_e = 57^\circ$.

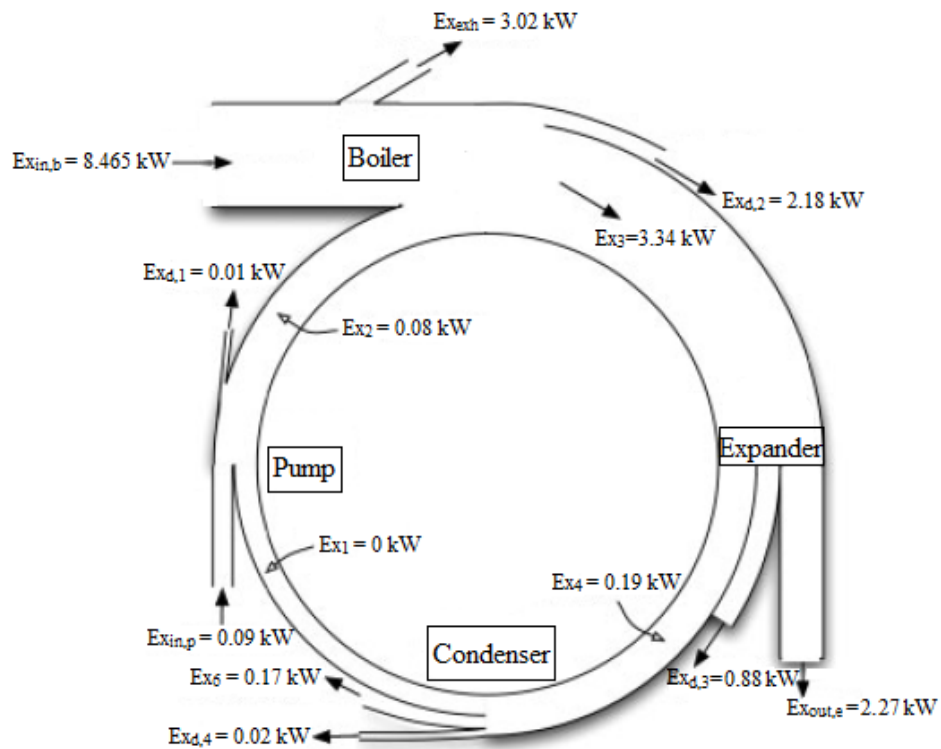


Figure 6.17: Exergy wheel diagram for R134a and $\phi_e = 28^\circ$.

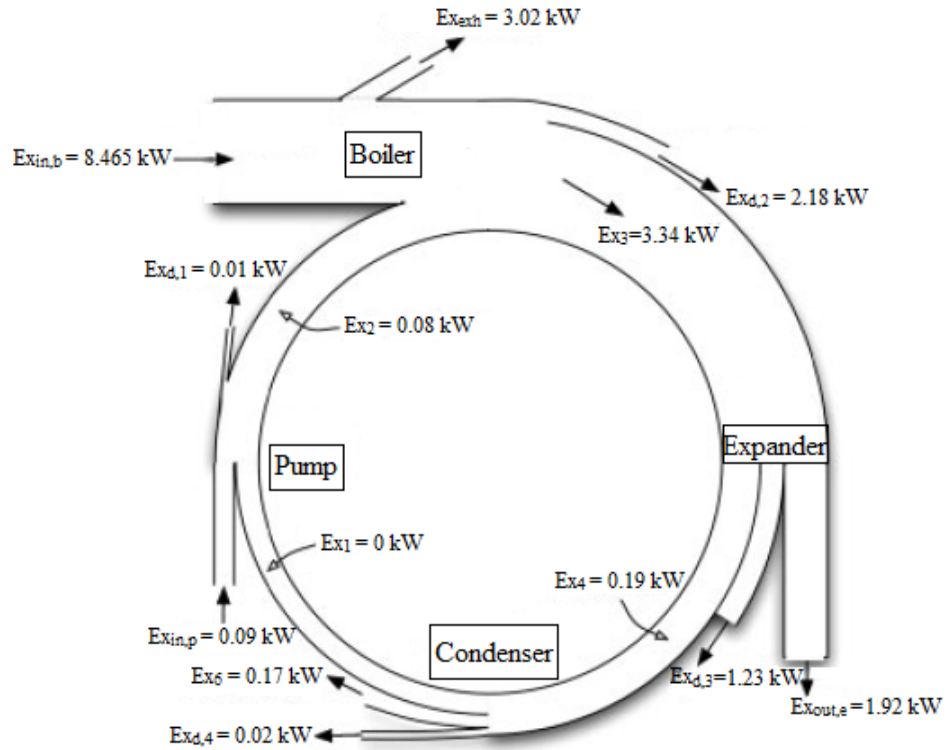


Figure 6.18: Exergy wheel diagram for NH_3 and $\varphi_e = 57^\circ$.

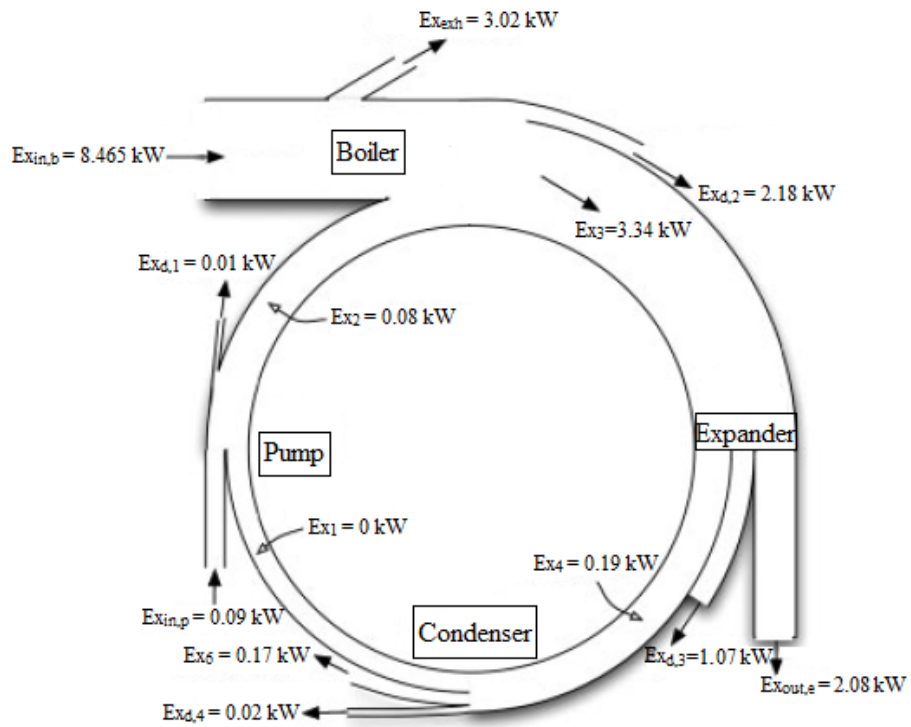


Figure 6.19: Exergy wheel diagram for NH_3 and $\varphi_e = 29^\circ$.

6.3 Parametric Study and Design Optimization

For the purpose of the study, six organic fluids were employed. These organic fluids are R404a, Toluene, R123, R141b, R134a and NH₃. The results for the different working fluids were compared under similar operating conditions.

6.3.1 Influence of the Scroll Geometry

The effect of increased rolling angle on the energy and exergy efficiency of the cycle is given in Figures 6.20 and 6.21. Some fluids were omitted from the figure in order to analyze easily. It can be observed that the first and second-law efficiencies decrease for all the fluids with the increment of the rolling angle. In order to be able to obtain an optimum built-in volume ratio for the scroll machine, rolling angle should be decreased to the value that the rate of increase for the net work output from the scroll expander over the total heat input from the boiler has reached to the maximum value for the supercritical temperature condition at the expander inlet. The number of rotations of the orbiting scroll with respect to the fixed scroll is limited by the rolling angle. The produced shaft power will be lower for reduced rolling angles, however the efficiency will increase until the optimum built-in volume ratio is obtained for the scroll expander through the optimization process.

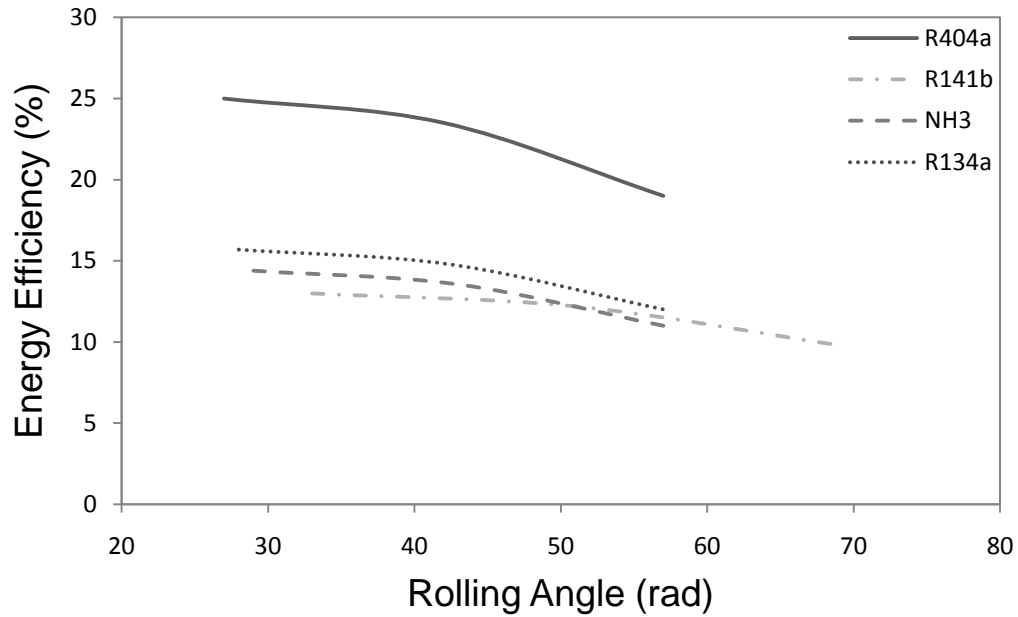


Figure 6.20: Variation of the energy efficiency with the rolling angle of the scroll machine.

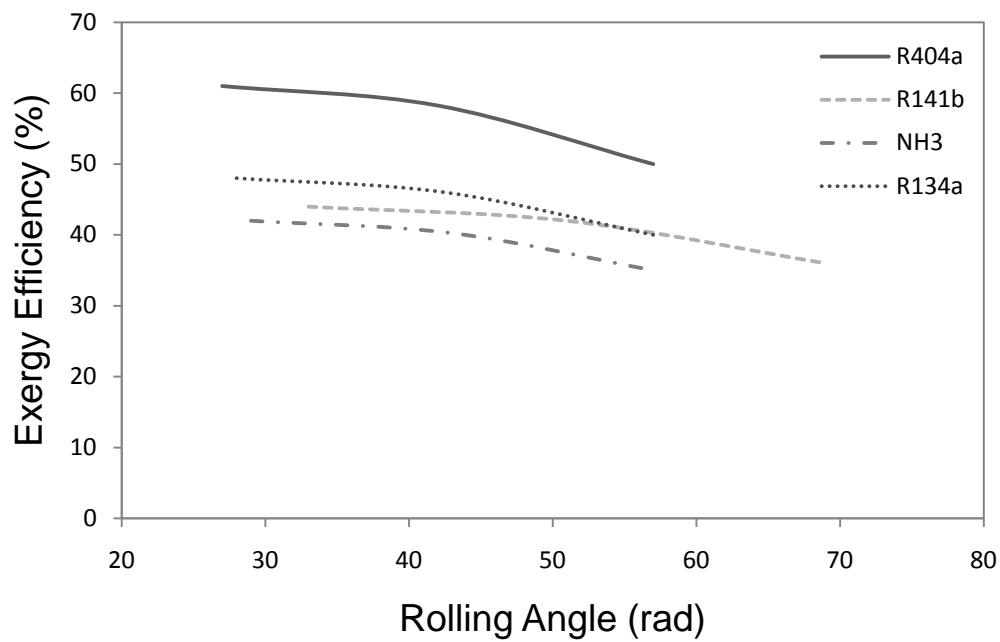


Figure 6.21: Variation of the exergy efficiency with the rolling angle of the scroll machine.

In Figure 6.22, the calculated mass flow rate is shown as a function of the basic circle's radius. It can be seen that the mass flow rate is 1kg/s at 0.5 times the original

radius r_b and reaches to a maximum of 2.4 kg/s at 1.25 times the original radius and then decreases to 1kg/s again when the radius increases to 2 times the original radius for the boiler temperature of 288 K. The scroll height is adjusted to keep the volume constant while varying the radius of the involute's basic circle from 0.5 to 2 times the original design radius r_b . It can be seen from the Figure 6.22 that the mass flow rate decreases with the increment in boiler temperature.

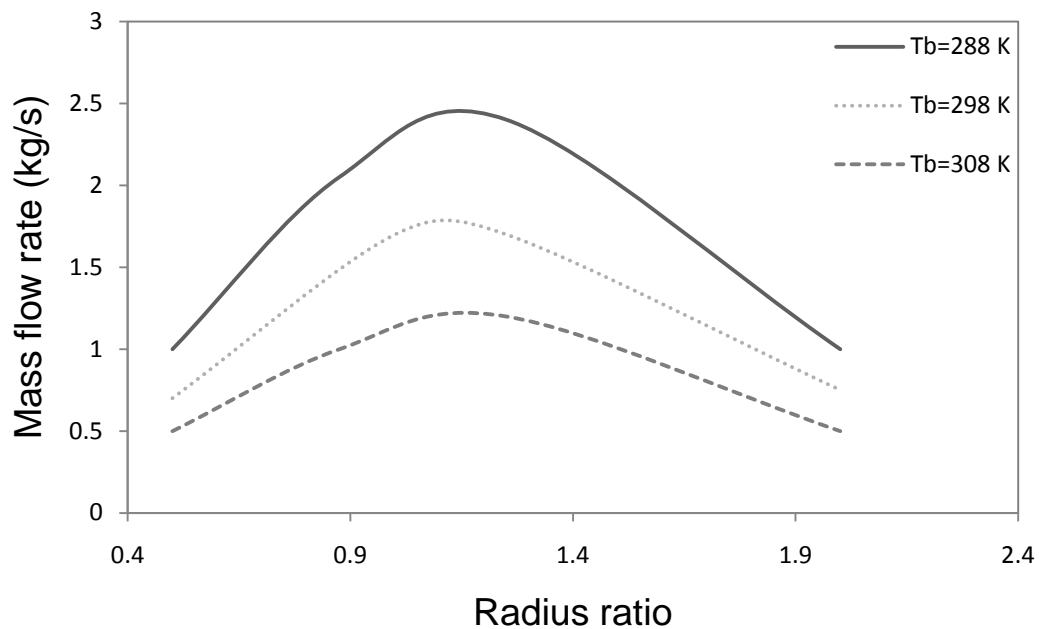


Figure 6.22: The influence of geometry on the mass flow rate.

When the radius of the basic circle decreases by half, the height of the scroll increases by 4 times to keep the expander volume constant. Hence, the area between the scroll and the organic fluid becomes larger, causing more heat transfer from the scroll to working fluid and reduction in the mass flow rate due to increases in heat transfer.

The other relation between the mass flow rate and the basic circle is that when the radius of the basic circle becomes larger the frictional losses increase. The energy

dissipation into frictional loss will also increase the heat transfer from scroll expander elements to the organic fluid causing to a reduction in mass flow rate.

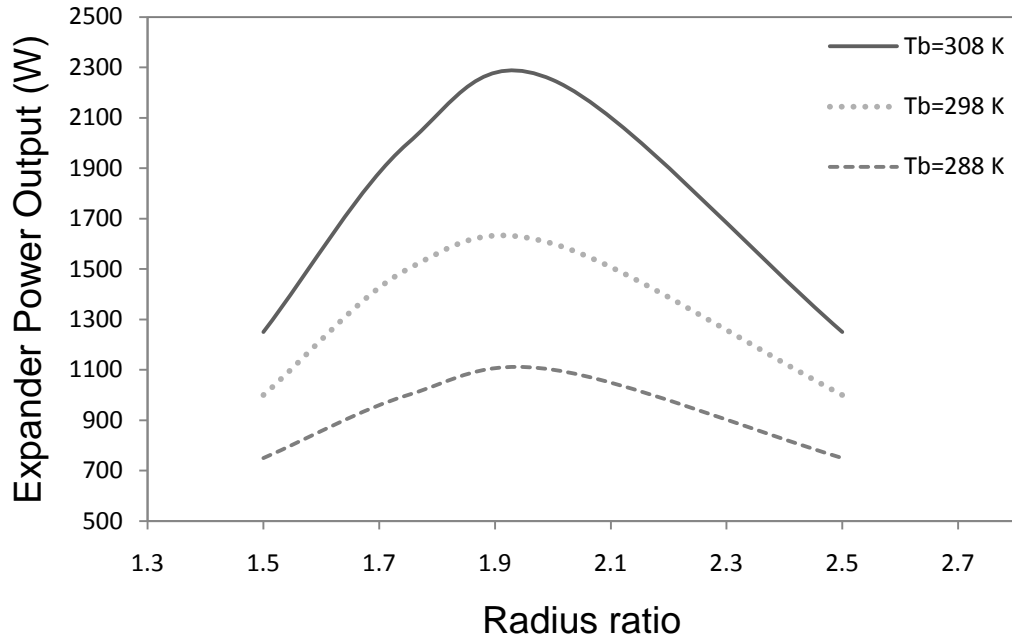


Figure 6.23: The influence of geometry on the expander power output.

In Figure 6.23, the expander power output is plotted as a function of the basic circle's radius. It can be seen that when the radius of the basic circle increases, the power output of the expander also increases. The main factor of this relation is that when the dimension of the basic circle is increased, the dimension of the crankshaft and Oldham ring also needs to be increased in order to keep the scroll machine in balance. As a result the torque of the shaft will be higher. Therefore it can be said that the power output of the scroll machine is strongly depended on the dimension of the scroll. It can be observed from the figure that expander power output increases with the increment in boiler temperature.

Figure 6.24 shows the influence of the radius of the basic circle on the overall expander efficiency. The expander efficiency reaches the highest value of 55% when the radius of the basic circle decreases to 0.75 times the original radius for the boiler temperature of 308 K. It can be observed that the expander performance can be improved by small amount of decrease in the dimension of the scroll and by increasing the boiler temperature.

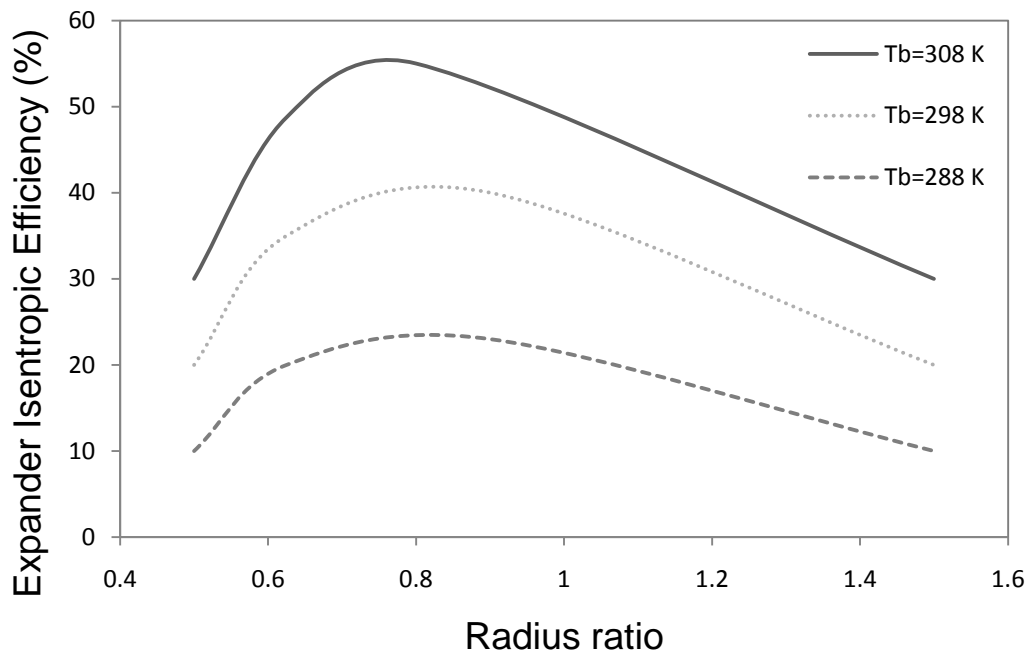


Figure 6.24: The influence of geometry on the overall expander efficiency.

The discharge temperature as a function of the basic circle is shown in Figure 6.25. The power output of the expander increases as the basic circle radius increases, as shown in Figure 6.23. Therefore more work will be dissipated and will heat the working fluid in expander. As a result the discharge temperature of the organic fluid increases when the radius increases. It can be observed that, for the radius of 0.75 times the

original, the overall expander efficiency reaches its maximum value and the discharge temperature drops to its lowest.

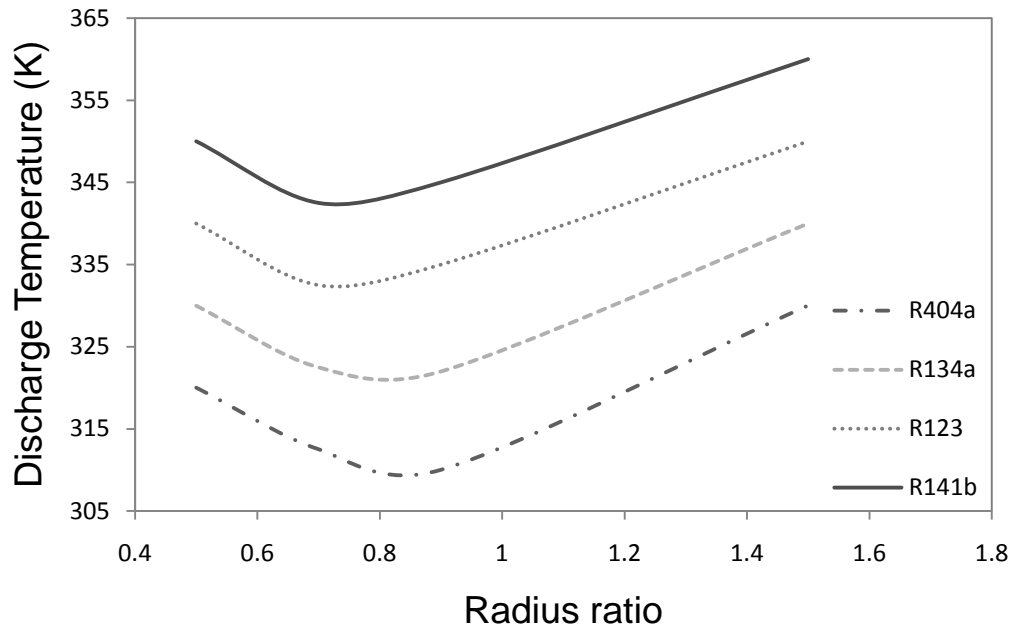


Figure 6.25: The influence of geometry on the expander discharge temperature.

The results show that the mass flow rate can be improved when the radius increases to 1.25 times the original designed radius, but the radius of the basic circle needs to be reduced to 0.75 times the original radius in terms of achieving the best possible efficiency for the scroll expander. Therefore it can be said that the designed radius ($r_b/r_{b,design}=1$) is an optimum value since the mass flow rate and the expander efficiency are both close to their maximum value.

The relationship between the leakage rate and the rotation angle for different inlet pressures and rotating speed of $n = 956$ rpm and $n = 2847$ rpm is shown in Figures 6.26 and 6.27, respectively. From this figure one can see that every curve has a jump at a

rotation angle of 210°. This is due to the expansion pocket opening up to the discharging region and the leakage mode changing at this angle.

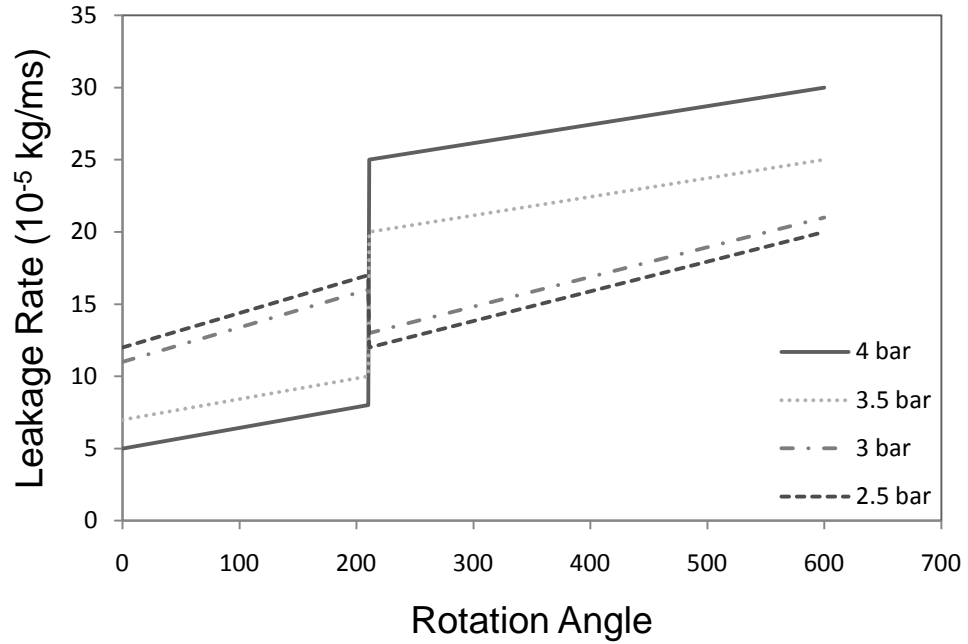


Figure 6.26: Leakage rate for n = 956 rpm.

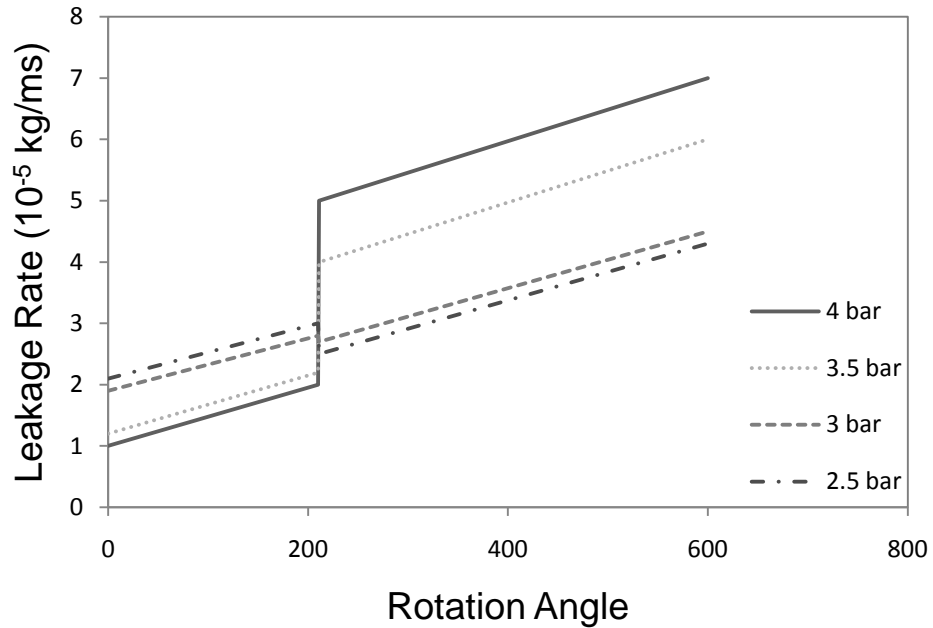


Figure 6.27: Leakage rate for n = 2847 rpm.

6.3.2 Influence of Rotating Speed of Shaft

Figure 6.28 presents the relationship between the expansion ratio and the rotating speed for different inlet pressures. When the inlet pressure is 3, 3.5 or 4 bar, the expansion ratio decreases as the rotating speed increases but is higher than the design ratio of 3.0. The expansion ratios are correlated with inlet pressures at low rotating speed due to the leakage in the process. The lower the inlet pressure is, the lower the ratio becomes. However, when the rotating speed goes up to a certain value all the curves become flat, which means that the ratios become independent of the inlet pressures at high rotating speeds. It can also be seen that the ratio becomes small and below 3.0, when the charging pressure drops to 2 bar, it causes the over-expansion during the process. There is an approximately linear relationship between the mass flow rate and rotating speed (shown in Figure 6.29).

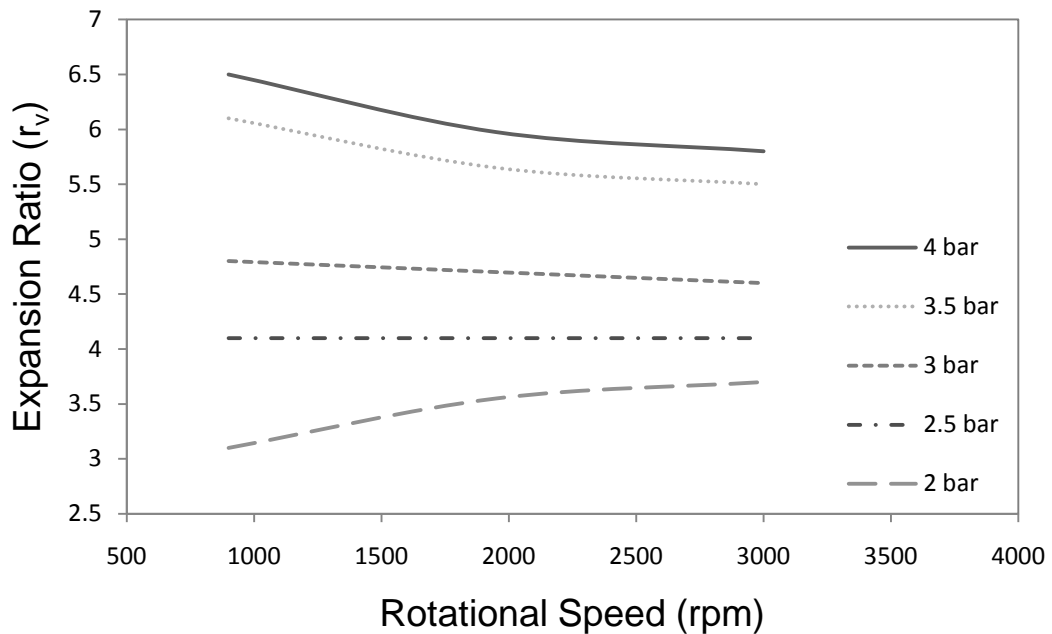


Figure 6.28: Expansion ratio versus rotation speed for various inlet pressures.

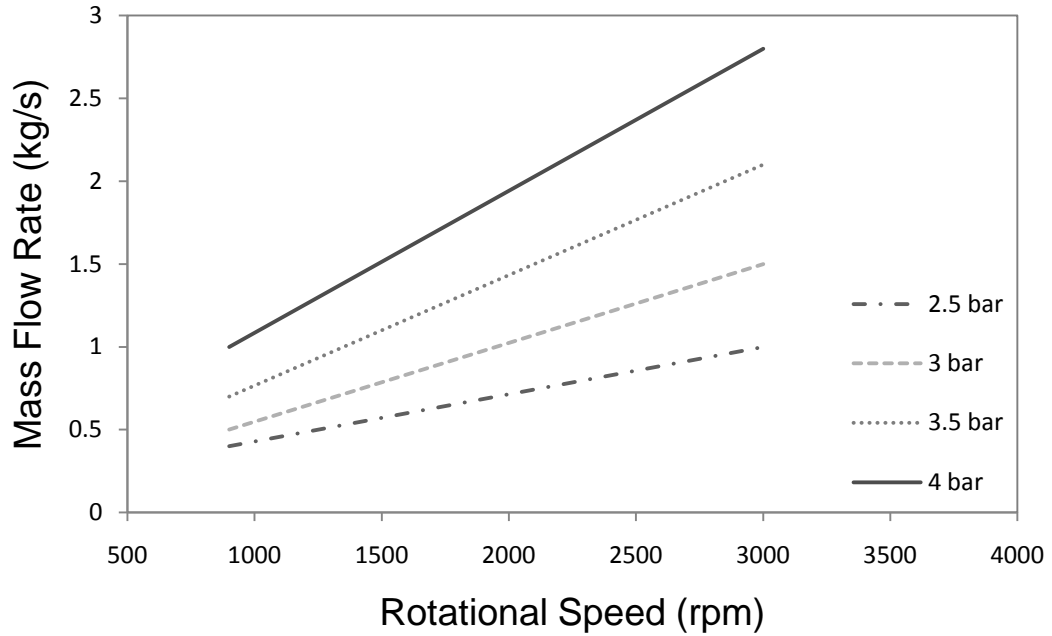


Figure 6.29: Mass flow rate versus rotation speed for various inlet pressures.

It can be seen from Figure 6.30 that the indicated isentropic efficiency becomes relatively larger as the rotating speed increases, but decreases when the charging pressure increases. However, when the inlet pressure is 2.5 bar and an over expansion occurs in the process, the 2.5 bar curve is below the aforementioned value for 3 bar.

It can be seen from Figure 6.31 that the volumetric efficiency increases as the rotating speed increases, changes more quickly at low rotating speeds, and becomes more stable at high rotating speeds. The reason for this may be that the leakage is larger at the low rotating speeds than it is at the higher ones.

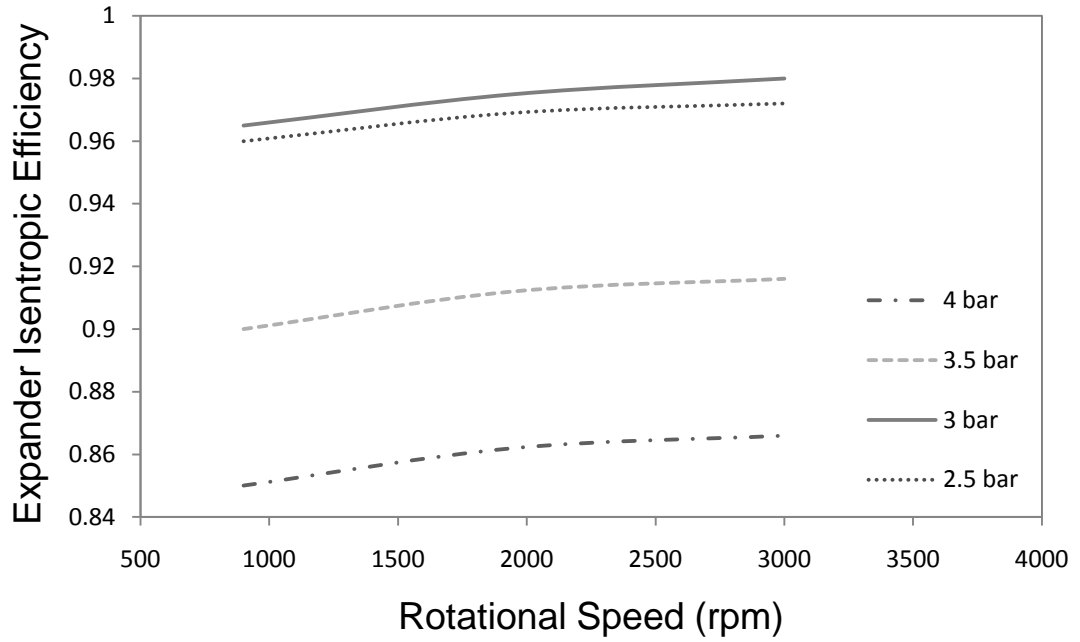


Figure 6.30: Expander isentropic efficiency for various inlet pressures and rotation speeds.

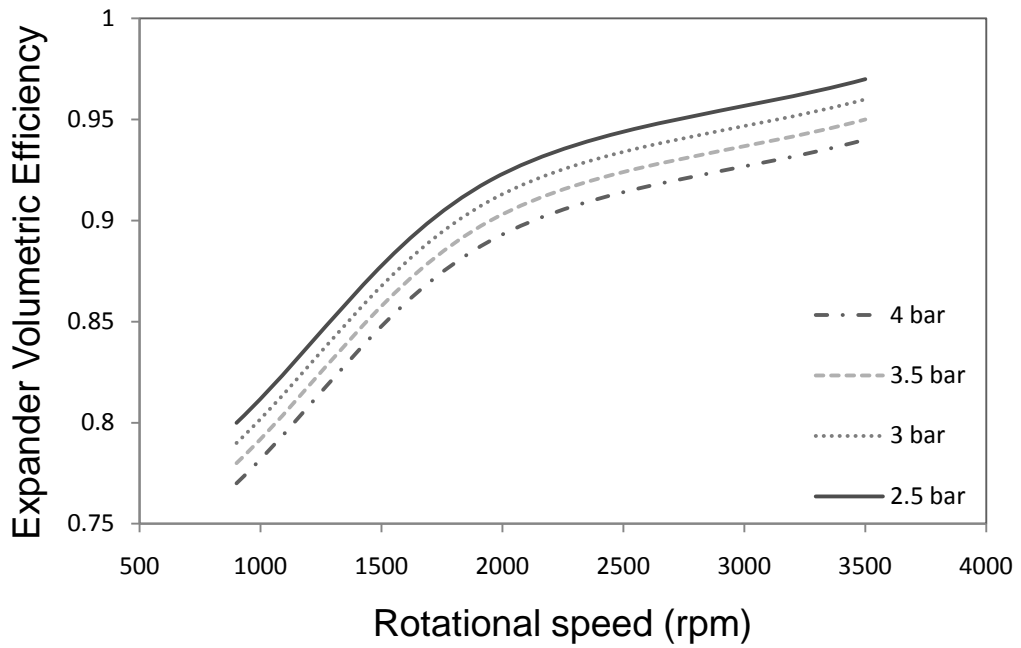


Figure 6.31 Expander volumetric efficiency versus rotation speed for various inlet pressures.

We can see from Figure 6.32 that the theoretical output work of the expander increases as the rotating speed and charging pressure increase. However, in our study, there is an optimum rotating speed, corresponding to each charging pressure, at which the output work is a maximum. The optimum rotating speed falls with a drop in inlet pressure, which can be seen in Figure 6.33. The primary reason is due to the necessity of the increase and other working parameters to match each other.

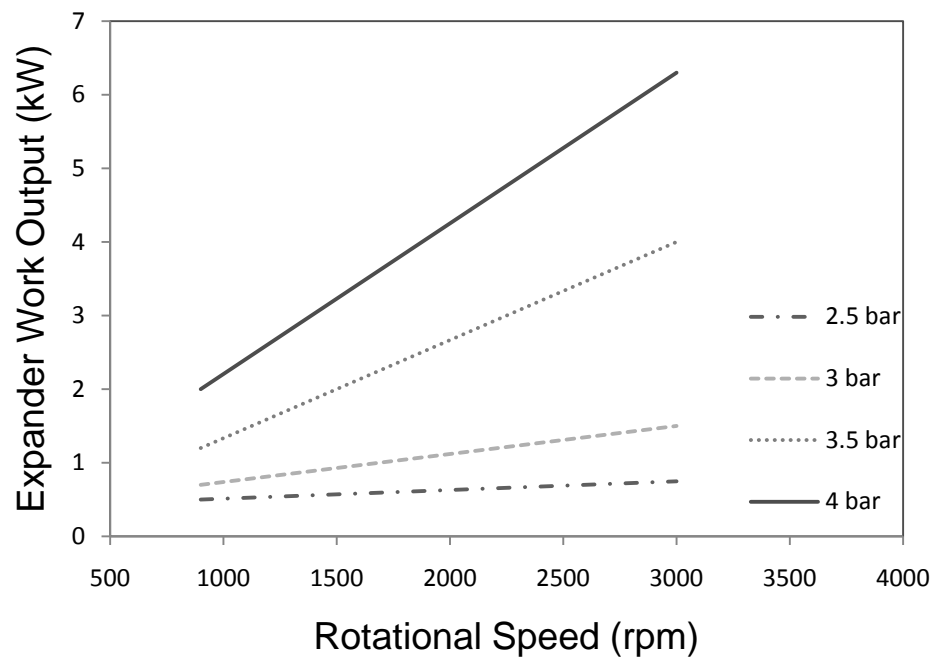


Figure 6.32: Theoretical expander work versus rotating speed for various inlet pressures.

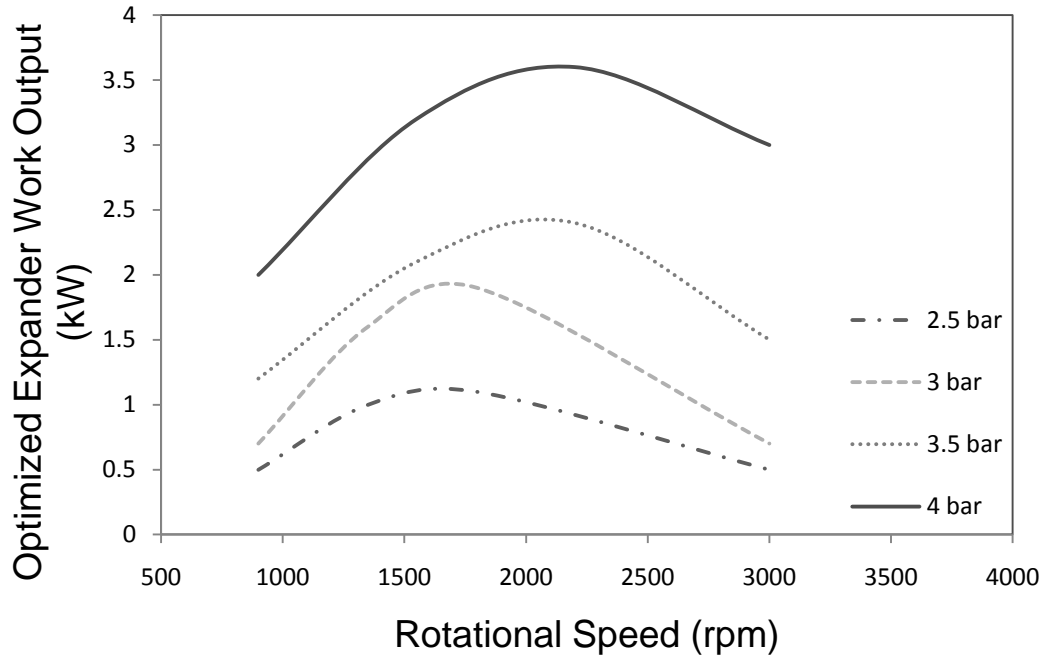


Figure 6.33: Optimum expander work versus rotating speed for various inlet pressures.

6.3.2 Influence of Boiler Outlet Temperature

Figure 6.34 shows the variation of the system energy efficiency with respect to the boiler outlet temperature. The effect of superheating of the working fluid over the energy efficiency of the cycle is shown in the figure for the temperature ranges that vary from the saturation temperature to the critical temperature. The isentropic efficiencies of the expander and pump are taken to be 80%. The condenser temperature and boiler pressure were kept constant at 25°C and 1 MPa, respectively in order to generate the figure. It shows that the efficiency of the cycle for the organic fluids is a weak function of the boiler outlet temperature since it remains approximately constant or slightly increases with the increment of the boiler outlet temperature. It can be concluded that organic fluids do not need to be superheated to increase the energy efficiency of the cycle. It can be observed that R404a shows the best energy efficiency while NH₃ has the lowest

efficiency for the temperature range from 300K to 500K. The figure clearly illustrates that organic fluids can be used to produce power from low-temperature waste heat.

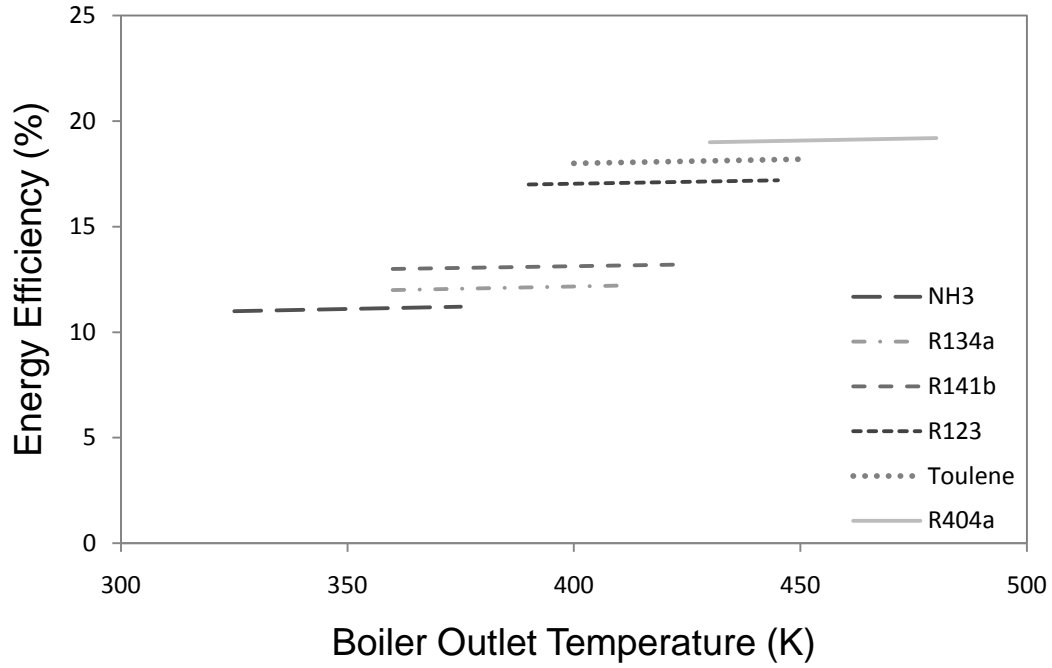


Figure 6.34: Variation of the system thermal efficiency with the expander inlet temperature.

Figure 6.35 shows the variation of the system irreversibility with respect to the boiler outlet temperature for the temperature range changes from saturation temperature to critical temperature for the organic fluids considered. It can be observed that the total system irreversibility increases with the increment of the boiler outlet temperature for all the fluids. The results show the importance of second-law analysis. According to the results in Figure 6.34, the energy efficiency is approximately constant with the boiler outlet temperature. However, combining the first- and second-law analyses shows the best case scenario is obtained when the fluid is operated at saturated conditions before the expander. That means the same energy efficiency with the lower rate of irreversibility can be achieved for the superheated refrigerant if the working fluid is sent to expander at

saturated conditions. Figure 6.35 shows how the system with higher (R404a) and lower (NH_3) energy efficiencies present the lower and higher irreversibilities. Among all the fluids considered in this study, R134a shows the highest irreversibility.

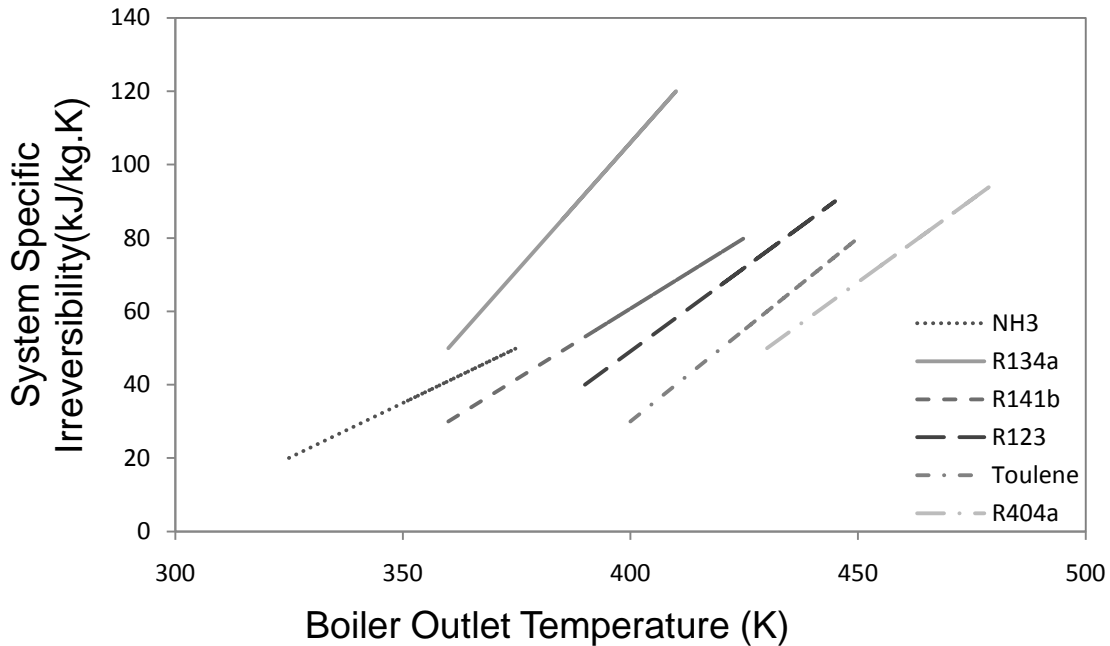


Figure 6.35: Variation of the system irreversibility with the expander inlet temperature.

Figure 6.36 shows the effect of the expander inlet temperature on the system second-law efficiency. It can be concluded for all the fluids that the exergy efficiency decreases with the boiler outlet temperature due to heat transfer at the boiler. It can be observed that exergy efficiency decreases with the increment in the temperature difference between the boiler inlet and outlet. These results agree with the results presented in Figure 6.35, because an increment in the system irreversibility yields a decrease in the system exergy efficiency. Figure 6.36 is plotted by assuming the temperatures of the fluids are constant at their saturation temperature at the boiler inlet. Boiler outlet temperature has been increased to the critical temperature to see the effect of

temperature difference between boiler inlet and outlet on the cycle exergy efficiency. For temperatures between 430 and 525 K, R404a shows the best exergy efficiency; for a range of temperatures 400–430 K, Toluene shows the best efficiency; R123 and R2141b present the best exergy efficiency for temperatures between 380 and 400 K. R134a shows the best efficiencies for a temperature range of 360–380 K and NH₃ for a temperature range of 330–360 K, whereas NH₃ shows the low exergy efficiency among all the evaluated fluids. The effect of the isentropic efficiency of the expander on the second law efficiency was not investigated since it remained constant at 0.8, but it could be predicted that the increase of the expander isentropic efficiency will represent higher exergy efficiencies for the cycle because of the lower irreversibility associated with the expander.

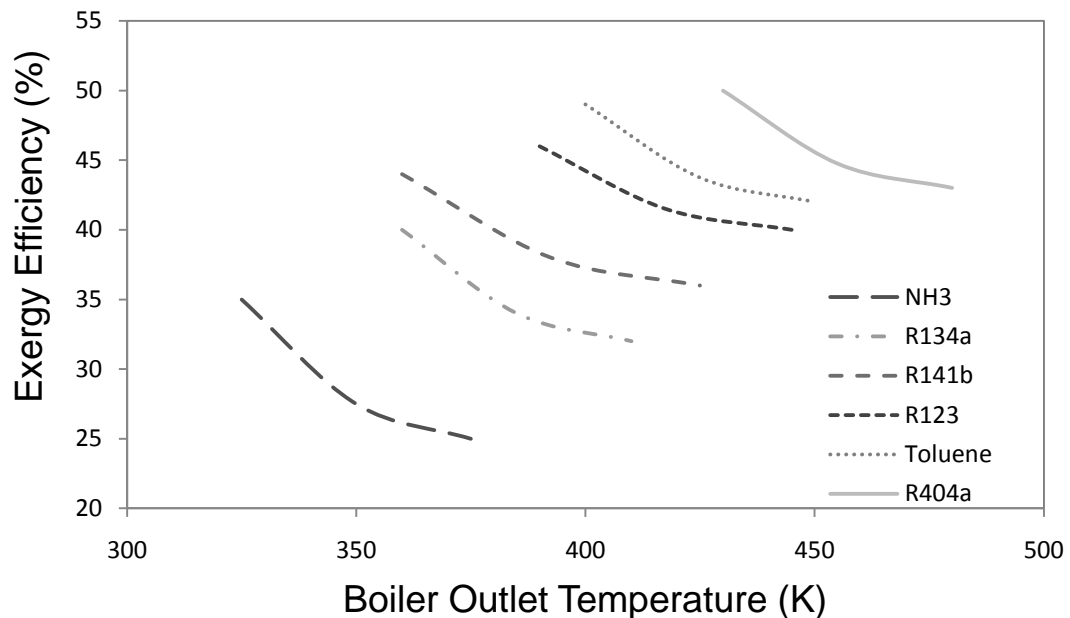


Figure 6.36: Variation of the system second-law efficiency with expander inlet temperature.

6.4.3 Influence of Expander Inlet Pressure

Figure 6.37 shows the variation of the system energy efficiency with the expander inlet pressure. Expander inlet temperature remained at saturated conditions for the constant condenser temperature of 25°C and the maximum pressure used for each fluid was the critical pressure. The isentropic efficiencies of the expander and pump were taken to be 0.80 for the analysis. It can be observed from Figure 6.37 that the system energy efficiency increases with the increment of the expander inlet pressure for all fluids. Both the net work and the boiler heat increase with an increase in the inlet pressure. However the percentage of increase of the net work is higher than that of increase of the boiler heat. Therefore the ratio of the net work to the boiler heat increases with the expander inlet pressure. R404a shows the best energy efficiency for a range of pressure between 0.5 to 4.0 MPa.

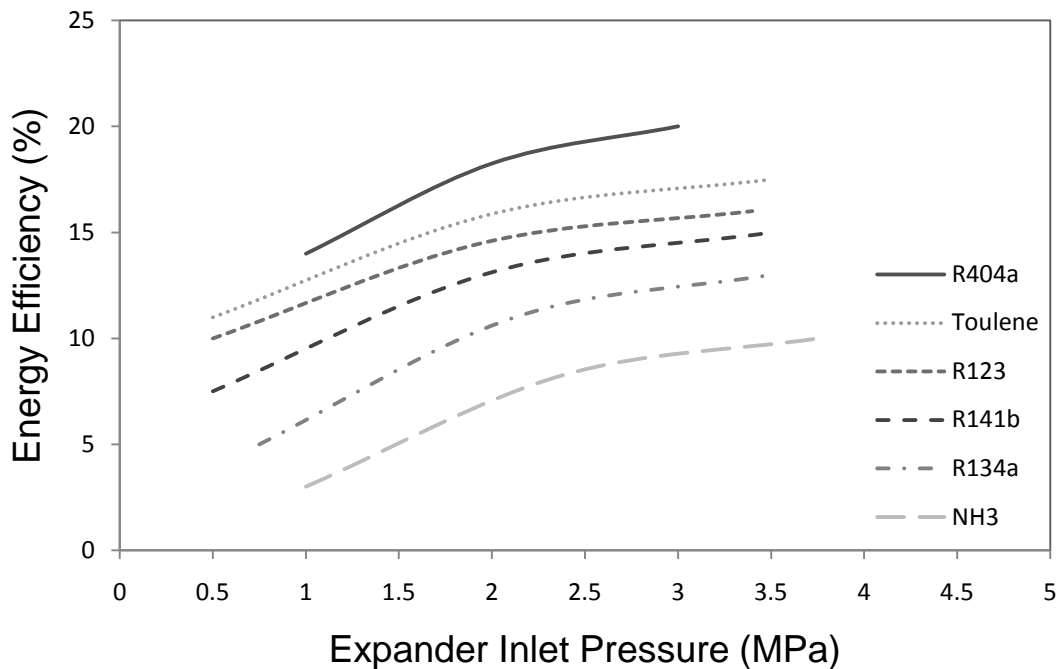


Figure 6.37: Variation of the system energy efficiency with expander inlet pressure.

Figure 6.38 shows the total specific irreversibility versus the expander inlet pressure. It can be observed how the irreversibility increases with the increment of the expander pressure for all the fluids. R404a and Toluene show the highest and lowest irreversibilities respectively.

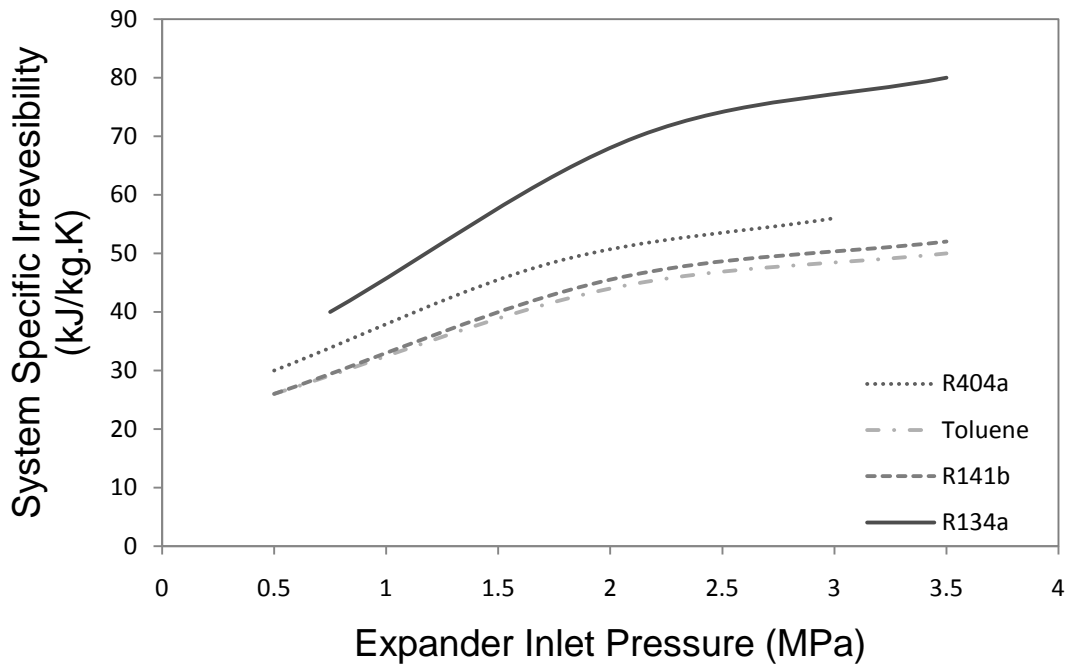


Figure 6.38: Variation of the system irreversibility with the expander inlet pressure.

The variation of the mass flow rate needed to generate the same power output with the expander inlet pressure is shown in Figure 6.39. Using the same conditions given in Figure 6.37 and a fixed power output of 1.7 kW the figure is generated. It can be observed that the mass flow rate needed decreases with the increment of an expander inlet pressure. The reason is due to the increase in the net work output of the cycle with the increment of the expander inlet pressure. These results agree well with the results obtained from Figure 6.37, because an increment of the net work represents an increase in

the cycle efficiency. R141b requires the highest mass flow rate for the pressure range from 0.5 to 4.0MPa and R134a needs the lowest mass flow rate for the expander inlet pressure of 2MPa and above.

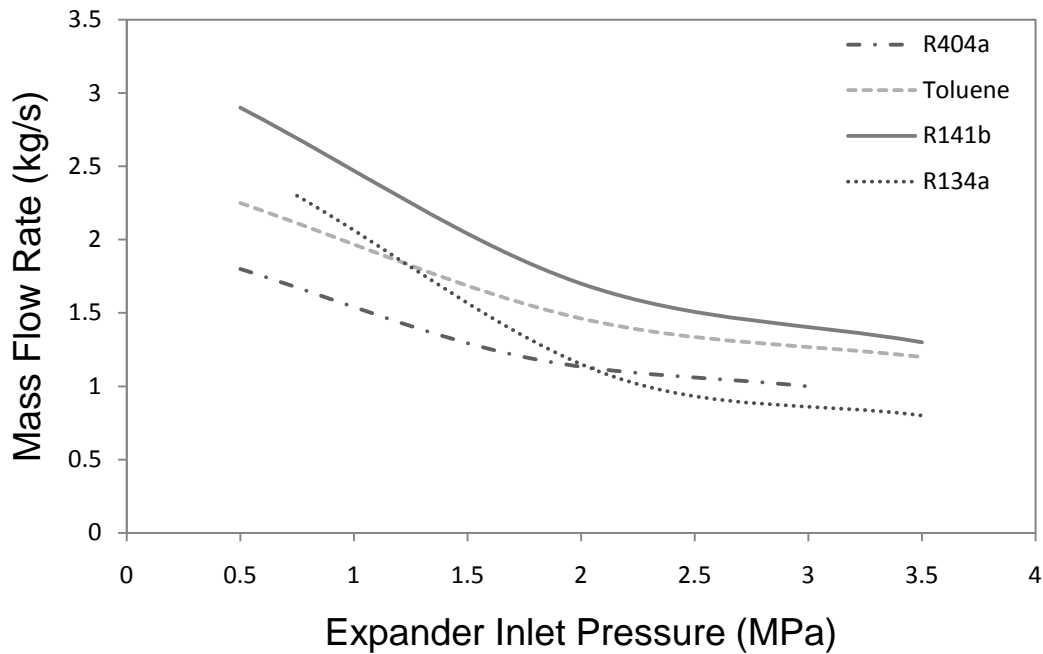


Figure 6.39: Variation of the mass flow rate with the expander inlet pressure.

Figure 6.32 shows the irreversibility rates for each fluid for the case analyzed in Figure 6.39. It can be observed from the figure that the rate of irreversibility is higher for low pressures and decreases with the increment in the expander inlet pressure. Increment in the irreversibility occurs for high expander inlet pressure at 2MPa or above. R404a and R134a show the lowest and the highest irreversibility rates for the expander inlet pressures which ranges from 0.5 to 3.5MPa among other organic working fluids.

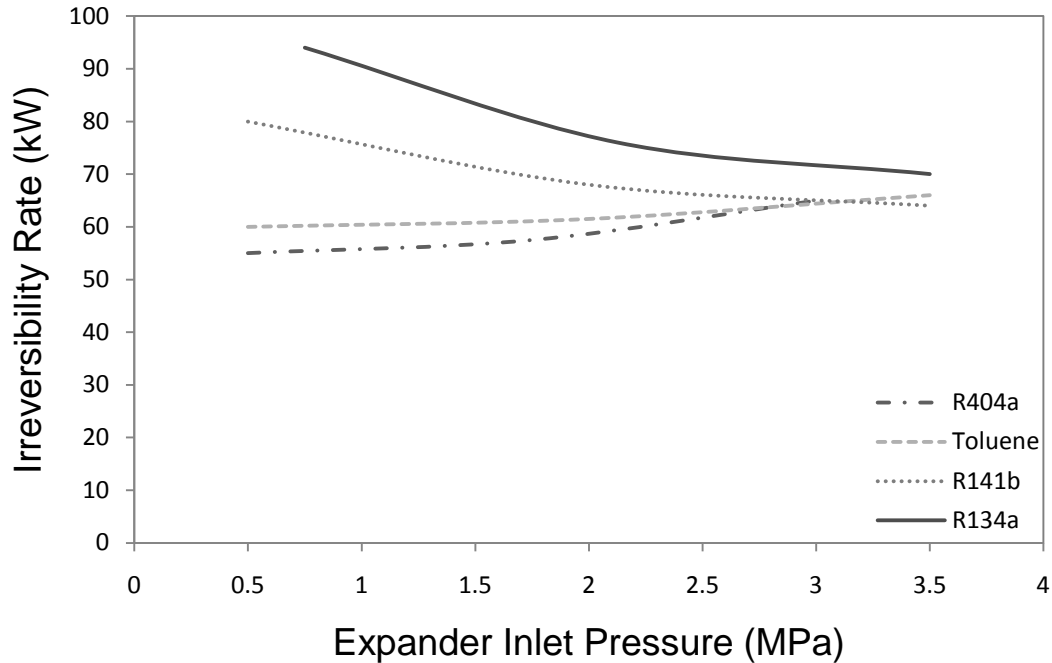


Figure 6.40: Variation of the irreversibility rate with the expander inlet pressure.

6.4.4 Influence of Condenser Outlet Temperature

Figure 6.41 shows the variation of energy efficiency with the condenser outlet temperature for the constant boiler pressure at 2.5MPa. It can be observed from the figure that the system energy efficiency decreases linearly with the increase in the condenser outlet temperature. The isentropic efficiencies of the expander and pump were 0.85. The results obtained from Figure 6.41 agree well with the results shown in Figures 6.37 and 6.34 where R404a and NH₃ shows the best and worst energy efficiencies among the evaluated working fluids.

Figure 6.42 illustrates the exergy efficiency of the system with the condenser outlet temperature for R404a, R134a and NH₃. It can be observed that the exergy efficiency decreases with the increment of the condenser outlet temperature for all fluids. It can be indicated from Figures 6.41 and 6.42 that ORC will be more suitable in places

with low ambient temperature in terms of heat transfer in order to obtain higher energy and exergy efficiencies.

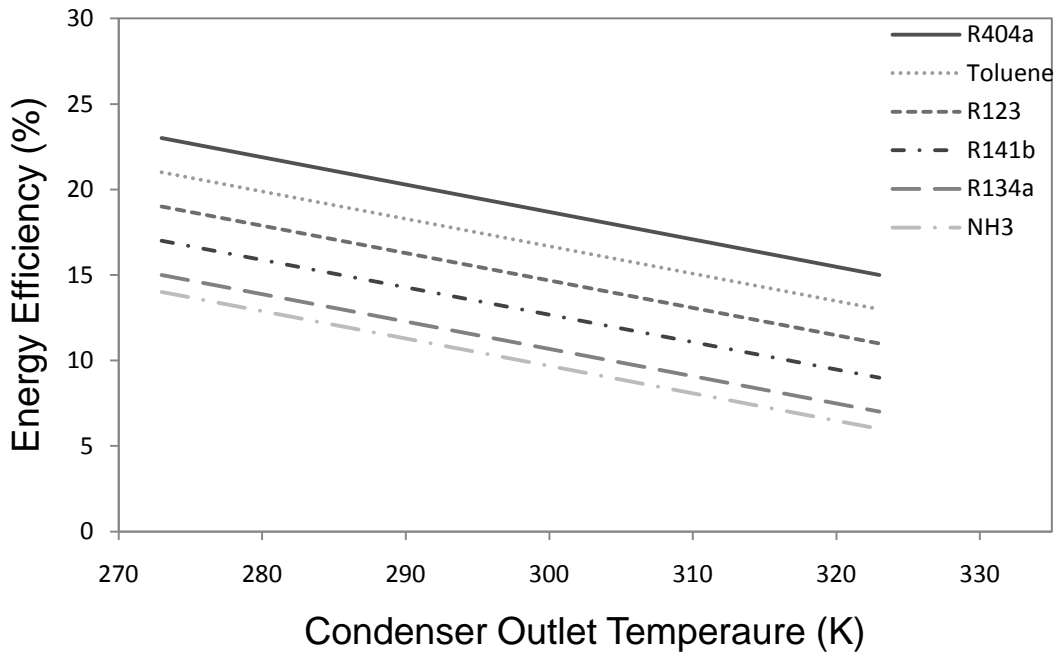


Figure 6.41: Variation of the energy efficiency with the condenser outlet temperature.

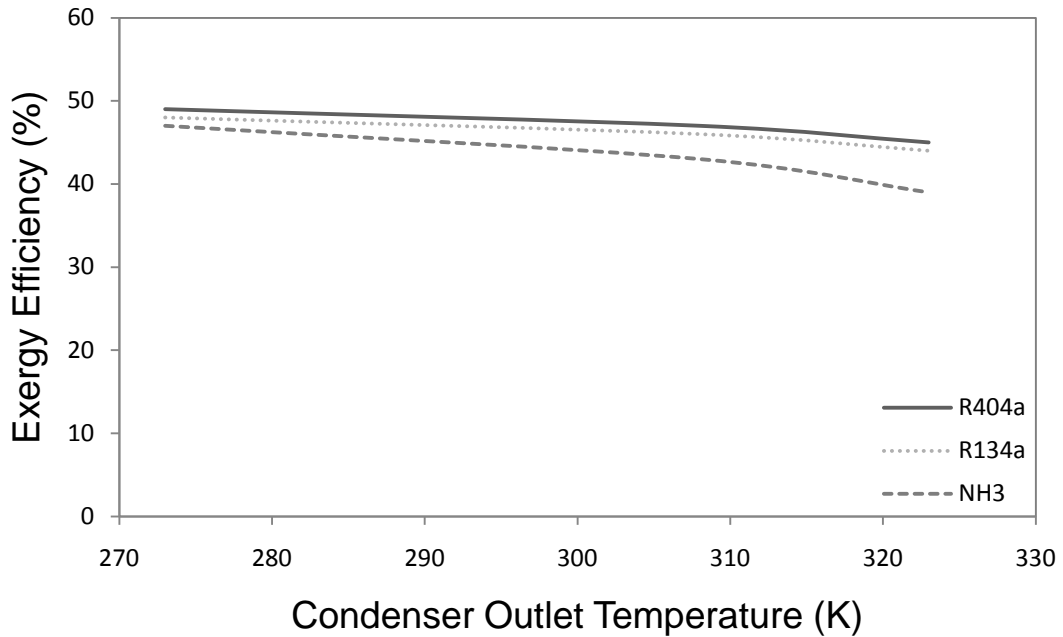


Figure 6.42: Variation of the exergy efficiency with the condenser outlet temperature.

6.4 Model Verification

6.4.1 Validation of mass flow rate and suction temperature

Figures 6.43 and 6.44 show the validations of the mass flow rate and suction temperature of the expander considered in this study. From the comparison of the measured and calculated data, it can be seen that the expander model accurately predicts the mass flow rate and suction temperature. The relative error in mass flow rate and suction temperature is calculated using the absolute difference between the measured data and modeled prediction divided by the measured data. The validation is performed by using the measured data which is used by Lemort (2008) and the values compared to the predicted data that is obtained by calculations through modeling. For the operating points, the maximum error was 4.92% for the prediction of the mass flow rate and 3.36% for the prediction of the suction temperature.

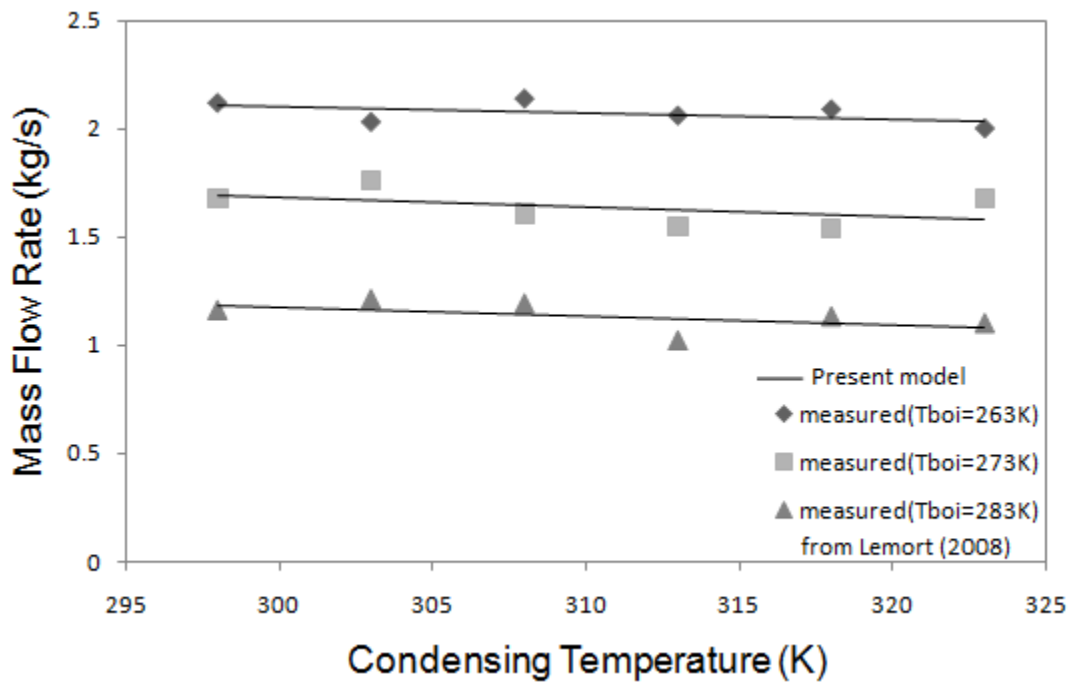


Figure 6.43: Validation of the mass flow rate.

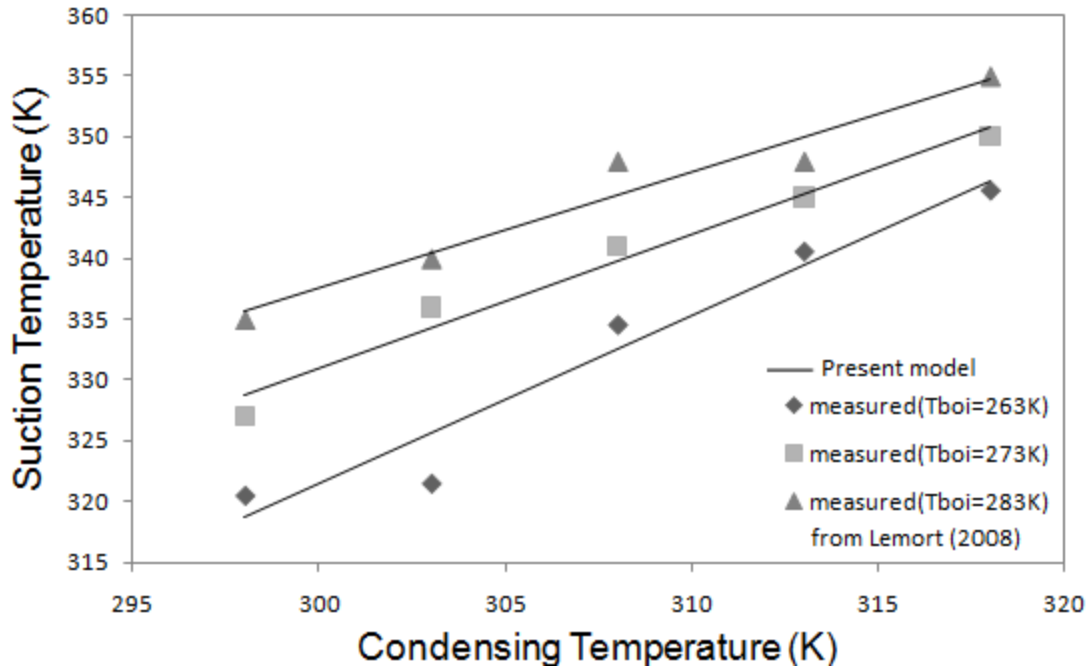


Figure 6.44: Validation of the suction temperature.

6.4.2 Validation of the power output

Figure 6.45 shows the validation of the expander power output. It can be seen from the experimental data, which is given by Lemort (2008), that the power values for the boiler temperature of 268K and 278K cross at a condensing temperature between 310K and 315K. Therefore the power output decreases with increasing boiler temperature when the condenser temperature is lower than 310 K and increases with increasing boiler temperature when the condenser temperature is higher than 315K. The reason is that power output is mass flow rate times the expander work per unit mass flow rate. When the boiler temperature increases, the mass flow rate increases (see Figure 6.43) while the expander work per unit mass flow rate decreases. Therefore the variation of power output with the boiler temperature depends on which factor dominates. Figure 6.45 shows that the curves of the predicted power for the boiler temperatures of 263K and 273K cross at

condensing temperature of 310K. That concludes, starting from 310K, the effect of boiler temperature on mass flow rate is more dominant than the effect of boiler temperature on the expander work output per mass flow rate. It can be evaluated from the figure that the maximum relative error is 5.83% for the prediction of power output for three different boiler temperatures.

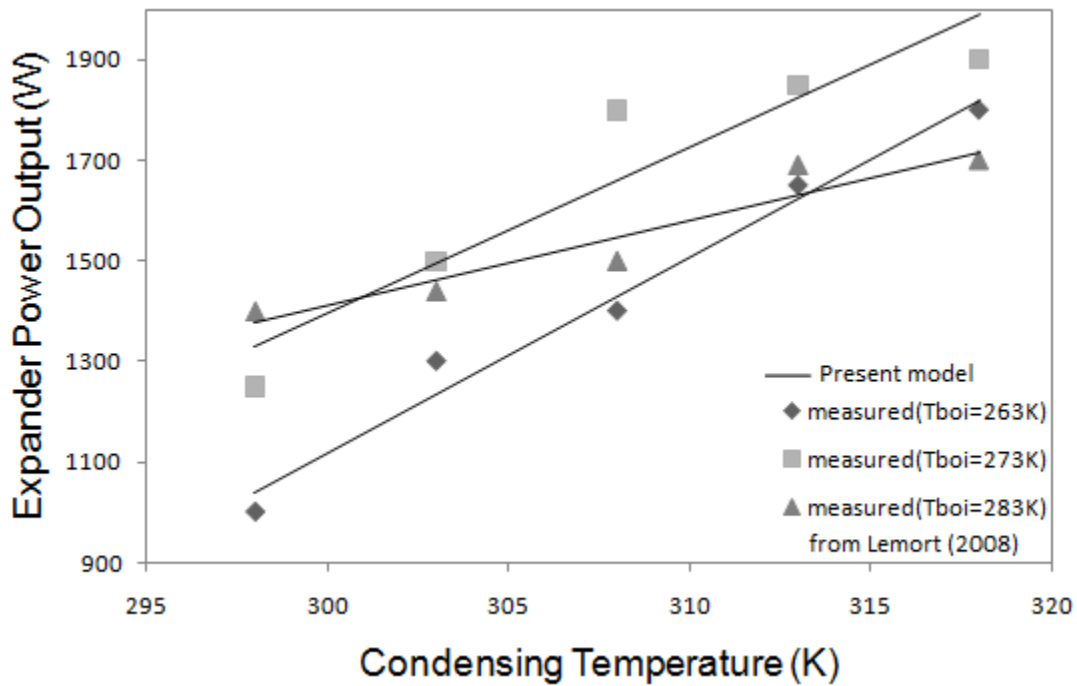


Figure 6.45: Validation of the power output.

6.5 Thermoeconomic Optimization

The procedure generated by Garceau (1983) used to optimize the Rankine cycle operating in one of two modes. When a particular set of decision variables is far from the optimal set, there will be a large difference in the total operating cost between two successive iterations. This difference can be used as a measure of the distance from the optimum. When the difference is large, the entire set of decision variables is changed based on the input set of marginal prices. When the difference is smaller than some pre-determined

value, only one decision variable is changed and a new set of state variables, shadow prices, and marginal prices are evaluated. Using this new set of marginal prices, another decision variable is changed and a new set of marginal prices is computed. This is automatically repeated until all the decision variables have been changed. Each time a complete set of new decision variables is generated, the program displays the parameters necessary to evaluate the system design. This procedure can be used to generate a variety of data. It is possible to parametrically vary any or all of the fixed decision variables. The parameters that were varied (Table 6.4) included fuel cost, exergy efficiency, and boiler temperature. The stratagem was to monitor the change in the optimal design by changing fuel cost and work output for several hot water requirements.

Table 6.4: Parametrically varied fixed system parameters of the Rankine cycle.

Parameter Varied	Range Varied	Increment
Specific fuel cost	2-4 \$/MJ	1 \$/MJ
Exergy efficiency (%)	0.4-0.6	0.1 %
Boiler temperature	380-421 K	14 K

The trends in stream and performance variables associated with increasing fuel costs are that of increasing the system's performance. As the cost of fuel increases, the boiler efficiency, pump isentropic efficiency, as well as the expander isentropic efficiency also increases. The condenser's thermodynamic performance increases because the steam's condensing temperature (or pressure as can be seen in Figure 6.48) decreases, approaching to the required hot water temperature. This general increase in performance allows the steam mass flow rate, boiler pressure, and expander work to decrease. As an example of this increase in the system's performance, Figures 6.46 and 6.47 clearly show

the increase in boiler efficiency and expander isentropic efficiency associated with the increasing fuel costs for different values of the work/heat ratio. Figure 6.49 shows the cost per unit electricity produced by the Rankine cycle as a function of exergy efficiency for various fluids.

Figures 6.50-6.52 illustrate net revenue curves as a function of the exergy efficiency for a required hot fluid temperature of 250°F and for various market conditions. Examination of these curves shows an increase in the optimal amount of electricity as the market price of electricity increases. Also, as fuel costs rise, the optimal amount of electricity production decreases.

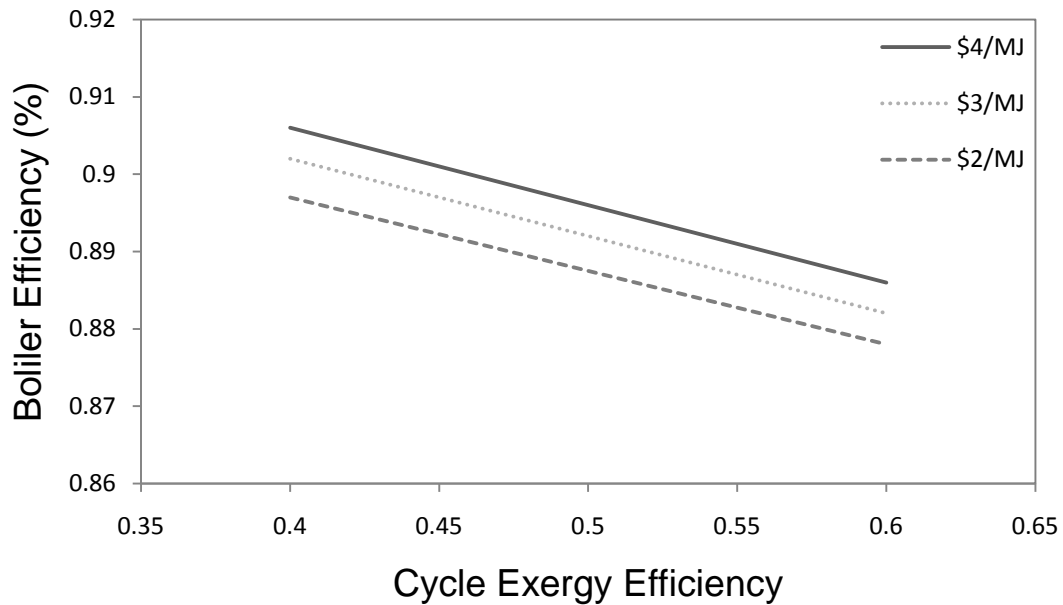


Figure 6.46: Optimum boiler efficiency as a function of exergy efficiency for various fuel prices.

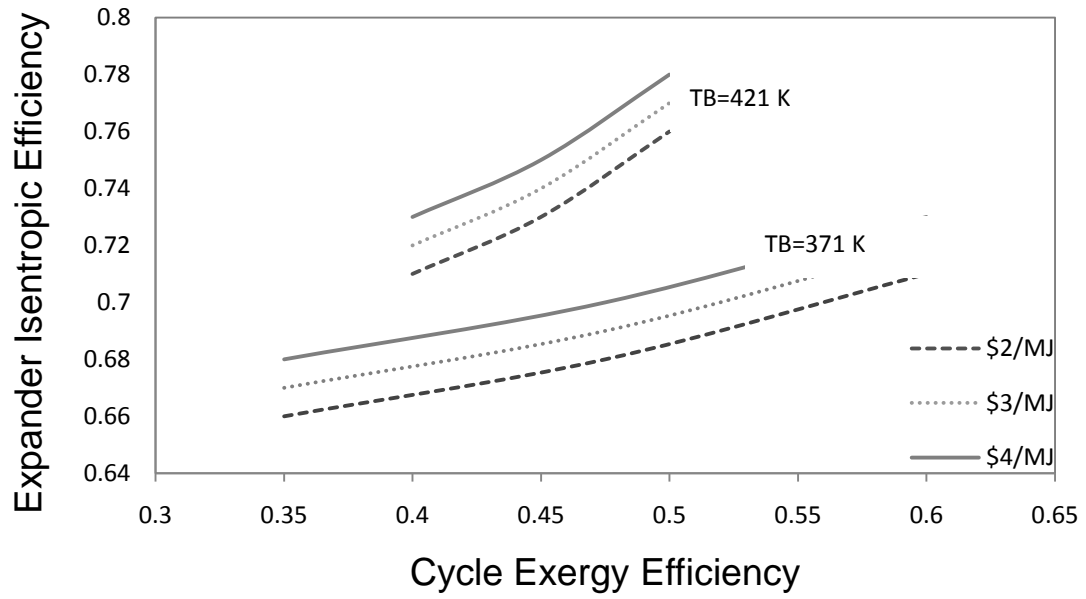


Figure 6.47: Optimum expander efficiency as a function of exergy efficiency for various fuel prices and boiler temperatures.

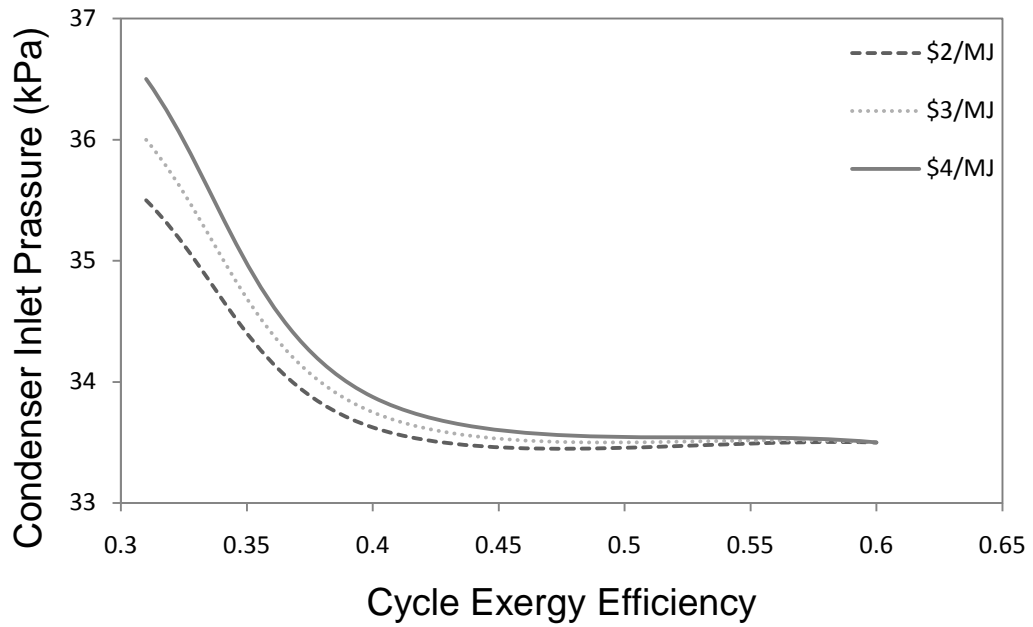


Figure 6.48: Optimum condenser inlet pressure as a function of exergy efficiency for various fuel prices.

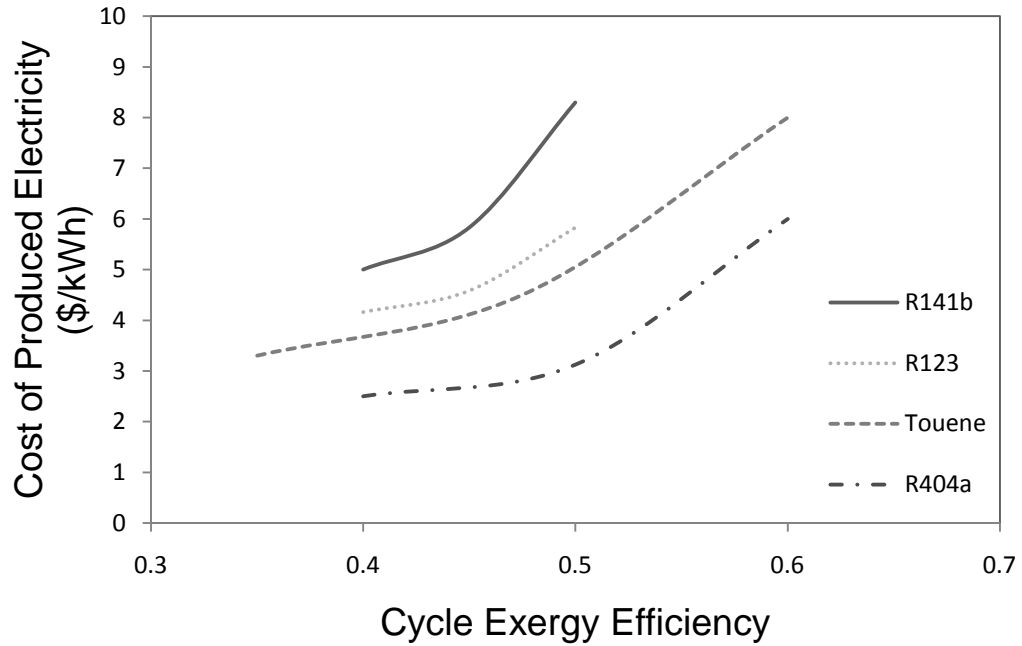


Figure 6.49: Cost of produced electricity as a function of exergy efficiency for various working fluids.

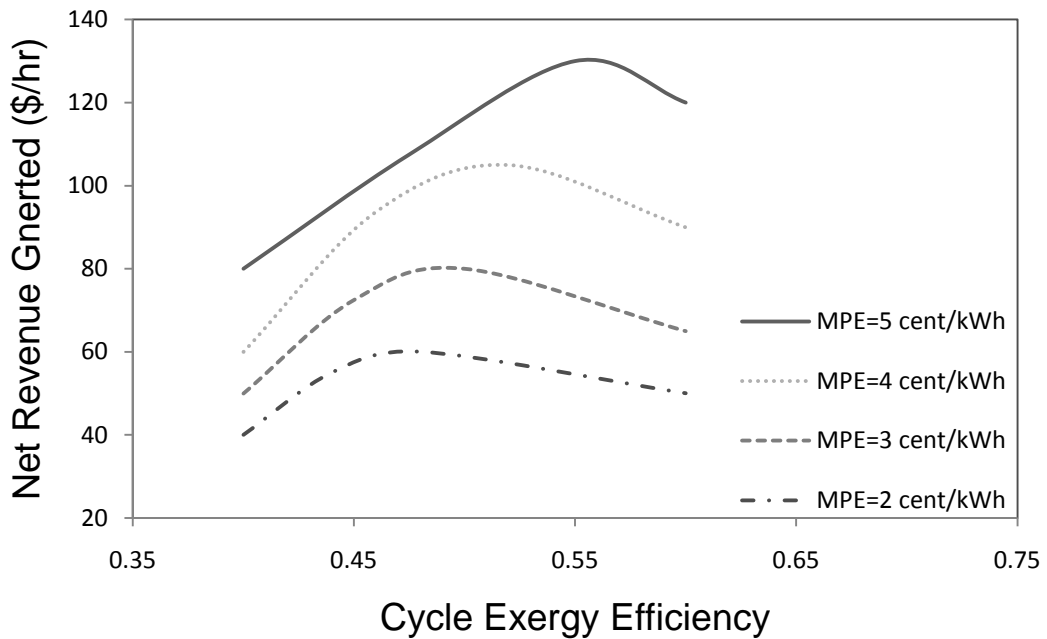


Figure 6.50: Net revenue generated as a function of exergy efficiency for various market prices of electricity and a fuel cost of \$2 per/MJ.

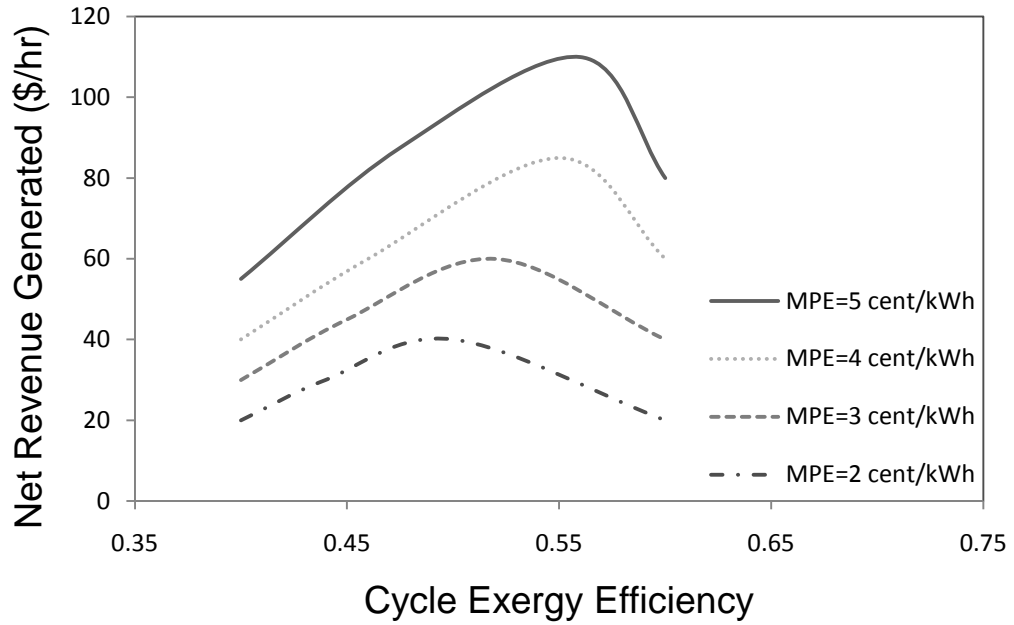


Figure 6.51: Net revenue generated as a function of exergy efficiency for various market prices of electricity and a fuel cost of \$3 per/MJ.

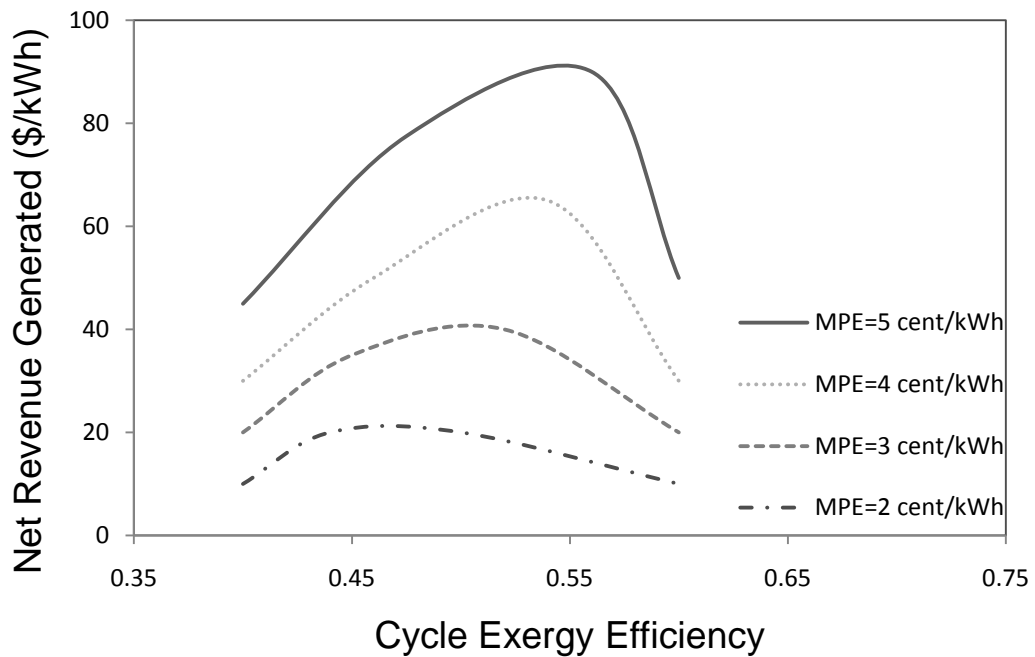


Figure 6.52: Net revenue generated as a function of exergy efficiency for various market prices of electricity and a fuel cost of \$4 per/MJ.

7 CONCLUSIONS AND RECOMMENDATIONS

7.1 Conclusions

In this thesis the possibility of converting scroll compressor into expander is investigated. Refrigeration equipment manufacturers produce scroll compressors massively for refrigeration and air conditioning applications. It is shown here that, through appropriate modeling, catalog data of scroll compressors can be used to predict the operation in reverse, as expanders. The modification of the geometry with respect to rolling angle and involute angles are necessary to use scroll compressor as expanders in heat engines. If no modifications are made to the scroll compressor, the efficiency of the Rankine cycle will result low because the built-in volume ratio is not adapted to the cycle configuration for the same pressure and temperature levels in the expanders.

A low capacity scroll compressor is selected from a refrigeration equipment manufacturer and using the equations for modeling of positive displacement compressors and the compressor manufacturer data for nominal operation, isentropic efficiency, built-in volume ratio and the flow coefficient of the scroll machine have been determined. After these determinations, the expander model has been used to predict the operation of the same scroll machine in reverse as it without and modification of the geometry. The resulting Rankine cycle is non-realizable with a low efficiency of 14% since the sink temperature for the cycle is far below the normal environmental temperature. In order to run a feasible Rankine cycle with the selected expander, without changing the scroll geometry and the working fluid, the upper pressure and temperature must be increased. It is found that by increasing the pressure and temperature at the expander intake to

supercritical value, that is 68 bar and 264 °C, the cycle becomes realizable and achieves an efficiency of 18%.

In the second phase of the study, modification of the scroll geometry is applied for different organic fluids to obtain a better design. The parameters defining the scroll geometry are adapted and the volumes of the different chambers are calculated by the geometric equations and plotted as a function of the orbiting angle (θ) for the suction, compression/expansion and discharge processes in order to calculate the built-in volume ratio of a scroll machine.

Several working fluids for Rankine cycle are investigated for the modified scroll geometry. The results showed that the rolling angle of the scroll machine should be modified in order to obtain an appropriate built-in volume ratio. First and second-law analysis showed that energy and exergy efficiency of the Rankine cycle is strongly depended on the geometry of the scroll expander. Built-in volume ratio of the scroll expander is modified with respect to rolling angle and influence of the modified geometry on the efficiency is evaluated for different working fluids. The results show that it is possible to improve the efficiency of the cycle by adjusting the scroll geometry for all fluids. R404a clearly gives the best results for the modified geometry and the energy efficiency is increased to 25% from 19% while the exergy efficiency is increased to 61% from 50%. It can be said that the rolling angle should be reduced to have an optimum built-in volume ratio for the cycle in terms of appropriate temperature and pressure range that will ensure higher energy and exergy efficiency.

Percentage of the exergy destroyed in each component with respect to the total system exergy destruction is calculated for different scroll geometries and organic fluids.

R404a with rolling angle of 33° gave the best results for the ORC that the evaporator is the component with the highest exergy destruction contribution (75.3%) followed by the expander with 23.2% for the ORC with expander rolling angle of 69° . For the ORC with modified expander, the evaporator is still the highest contributor to the total exergy destruction of the system contributing 78.7% of the total destruction. However, the exergy destruction in the expander reduced from 23.2 to 19.8% in comparison by using expander with the rolling angle of 33° . This exergy reduction is mainly due to decreased leakage loss which is implied by geometric modification in rolling angle that accounts for 3.4% of exergy destruction.

A Parametric study is performed in order to evaluate the influence of the geometric and thermodynamic parameters on the cycle performance. It can be concluded that organic fluids need to be superheated as the cycle thermal efficiency remains approximately constant when the inlet temperature of the expander is increased. However using the second-law analysis it can be said that superheating organic fluids increase the irreversibility. Therefore organic fluids must be operated at saturated conditions to reduce the total irreversibility of the system. It can be also concluded that the thermal efficiency of ORC increases when the condenser temperature is decreased. Therefore using ORC in locations with low ambient temperature will be more effective.

Design optimization of the geometry showed that the mass flow rate can be improved when the radius increases to 1.25 time the original designed radius but the radius of the basic circle needs to be reduced to 0.75 times the original radius in terms of achieving the best possible efficiency for the scroll expander. Therefore it can be said that the designed radius ($r_b/r_{b,design}=1$) is an optimum value since the mass flow rate and the

expander efficiency are both close to their maximum value. The relationship between the leakage rate and the rotation angle for different inlet pressures and rotating speed of $n = 956$ rpm and $n = 2847$ rpm compared through the analysis and From the leakage-rotating speed graphics one can see that every curve has a jump at a rotation angle of 210° . The reason is that the expansion pocket opens up to the discharging region and the leakage mode changes at this angle.

The expander model is validated with the experimental results which are taken from the literature study. The results show that the expander model predicts the mass flow rate, discharge temperature and power output very well since the calculated values in the expander model agree with the experimental data within the range of error between 3.36% and 5.83%.

Thermoeconomic optimization method is applied for the rankine cycle system to evaluate the cost of the system and net generated revenue as a function of exergy efficiency to be able to produce most economic system to generate electricity depending on market conditions and fuel prices. It is found that best possible solutions can be obtained for the exergy efficiency of approximately 55% in terms of cost of the system and net revenue.

The procedure can be applied for the conversion of scroll compressors use in reverse, as expanders for Rankine cycles applications. Through an appropriate modeling, scroll compressors can be used to predict the operation in reverse, as expanders. If no modifications are made to the scroll compressor, the efficiency of the Rankine cycle will result low because the built-in volume ratio is not adapted to the cycle configuration for the same pressure and temperature levels in the expanders.

7.2 Recommendations

The expander model developed in this thesis is comprehensive and accurate to predict the behavior of the scroll compressor as an expander for the power generation through the organic Rankine cycle. However there is still need to develop models to investigate how the geometry is affecting scroll expander performance in order to reduce leakages and friction losses. Some recommendations can be given for the future studies as follows

- A computational fluid model could be developed for the inlet and outlet port of the expander to optimize the geometry to minimize pressure drop.
- The new geometry of the scroll expander needs to be studied. Modifications need to be made regarding the modelling leakage flow between scroll chambers and heat transfer between the working fluid and scrolls based on the new geometry.
- There are more than 15 geometric parameters affecting the scroll geometry. The following parameters, namely rolling angle, inner involute starting angle, outer involute starting angle, inner involute initial angle and outer involute initial angle are evaluated. Therefore, the number of geometric parameters affecting the scroll geometry and expansion process can be increased for the new model and optimization method can be applied for the extended thermoeconomic analysis obtaining exergy efficiency as a function of all the geometric variables which needs to be used as a objective function for the multi-objective optimization process.
- Since the efficiency of the expander is strongly depended on leakages between the gaps of the scroll expander, a comprehensive leakage and friction flow analysis should be performed to reduce flank and radial leakage losses.

References

- Badr, O., “Multi-vane expanders as prime movers for low-grade energy organic Rankine-cycle engines,” *Applied Energy*, vol. 16, no. 2, pp. 129-146, 1984.
- Badr, O., Ocallaghan, P., Probert, S., “Performances of Rankine-cycle engines as functions of their expanders' efficiencies,” *Applied Energy*, vol. 18, no. 1, pp. 15-27, 1984.
- Baek, J., Groll, E., Lawless, P., “Piston-cylinder work producing expansion device in a transcritical carbon dioxide cycle. Part I: experimental investigation,” *International Journal of Refrigeration*, vol. 28, no. 2, pp. 141-151, 2005.
- Bell, I., Lemort, V., Braun, J., Groll, E., “Development of liquid-flooded scroll compressor and expander models”, *International Compressor Engineering Conference at Purdue*, paper 1283, July 14-17, 2008.
- Birol, F., “Key World Energy Statistics”, International Energy Agency (EIA). Website: <http://www.iea.org/textbase/nppdf/free/2006/key2006.pdf>. Accessed on February 23, 2010
- Blunier, B., Pucci, M., Cirrincione, G., Cirrincione, M., Miraoui, A., “A Scroll Compressor With a High-Performance Sensorless Induction Motor Drive for the Air Management of a PEMFC System for Automotive Applications”, *IEEE Transactions on Vehicular Technology*, Vol. 57, pp. 3413-3427, 2008.
- Bombarda, P., Invernizzi, C.M., Pietra, C., “Heat recovery from Diesel engines: A thermodynamic comparison between Kalina and ORC cycles,” *Applied Thermal Engineering*, vol. 30, no. 2, pp. 212-219, 2010.
- Borsukiewiczgozdur, A., Nowak, W., “Comparative analysis of natural and synthetic refrigerants in application to low temperature Clausius–Rankine cycle,” *Energy*, vol. 32, no. 4, pp. 344-352, 2007.
- Brasz, J.J., Biederman, B.P., Holdman, G., “Power production from a moderate-temperature geothermal source”, *GRC Annual Meeting*, Reno NV, September 25-28, 2005.
- Bush, J.W., Beagle, W.B., “Derivation of general relationship governing the conjugacy of scroll profiles”, *Proceedings of International Compressor Engineering Conference at Purdue*, pp. 1079-1088, 1992.
- Bush, J.W., Elson, J.P., “Scroll compressor design criteria for residential air conditioning and heat pump applications, Part II: Design criteria”, *Proceedings of the International Compressor Engineering at Purdue*, pp. 93-97, 1988.

Caillat, J.L., Ni, S., Daniels, M., "A computer model for scroll compressors", *Proceedings of the International Compressor Engineering at Purdue*, pp. 47-55, 1988.

Chen, Y., Halm, N.P., Groll, E.A., Braun, J.E., "Mathematical modeling of scroll compressors-part I: compression process modeling", *International Journal of Refrigeration*, Vol.25, pp. 731-750, 2002.

Chen, Y., Lundqvist, P., Johansson, A., Platell, P., "A comparative study of the carbon dioxide transcritical power cycle compared with an organic rankine cycle with R123 as working fluid in waste heat recovery," *Applied Thermal Engineering*, vol. 26, no. 17, pp. 2142-2147, 2006.

Colonna, P., Guardone, A., Nannan, N.R., Zamfirescu, C., "Design of the dense gas flexible asymmetric shock tube", *Journal of fluids engineering, Transactions of ASME*, Vol. 130, pp. 11-16, 2008.

Creux, L., Rotary Engine, U.S. Patent no. 801182, 1905.

DeBlois, R.L., Stoeffler, R.C., "Instrumentation and data analysis techniques for scroll compressor", *Proceedings of the International Compressor Engineering Conference at Purdue*, pp. 182-188, 1988.

Drost, R.T., Quesada, J.F., "Analytical and experimental investigation of a scroll compressor lubrication system", *Proceedings of the International Compressor Engineering at Purdue*, pp. 551-560, 1992.

Ennis, C., *Scientific assessment of ozone depletion 2006 : pursuant to article 6 of Montreal protocol on substances that deplete the ozon layer*. Geneva: WMO, 2007.

Etemad, S., Nieter, J., "Design optimization of the scroll compressor", 1988.

Fraas, A., *Engineering evaluation of energy systems*. New York: McGraw-Hill, 1982.

Gravesen, J., Henriksen, C., "The Geometry of the Scroll Compressor", *SIAM Review*, Vol. 43, pp. 113-126, 2001.

Guangbin, L., Yuanyang, Z., Liansheng, L., Pengcheng, S., "Simulation and experiment research on wide ranging working process of scroll expander driven by compressed air", *Applied Thermal Engineering*, Vol. 30, pp. 2073-2079, 2010.

Hagiwara, S., "Development of scroll compressor of improved high-pressure-housing", *Proceedings of the International Compressor Engineering at Purdue*, pp. 495-500, 1998.

Haiqing, G., Yitai, M., Minxia, L., "Some design features of CO swing piston expander," *Applied Thermal Engineering*, vol. 26, no. 2, pp. 237-243, 2006.

Halm, N.P., "Mathematical Modeling of Scroll Compressors", *Master Thesis*, Purdue University, 1997

Harada, J., "Development of a Small Scale Scroll Expander", Master Thesis, Oregon State Uni, 2010

Hase, S., Sano, K., Yamamoto, S., Hirano, H., Kohayakawa, T., Ishii, N., "Development of the high efficiency horizontal type scroll compressor", *Proceedings of the International Compressor Engineering at Purdue*, pp. 447-456, 1994.

Hayano, M., Sakata, H., Nagatomo, S., Nurasaki, H., "An analysis of losses in scroll compressors", *Proceedings of International Compressor Engineering Conference at Purdue*, pp. 189-197, 1988.

Hettiarachchi, H.D., Golubovic, M., Worek, W.M., Ikegami, Y., "The Performance of the Kalina Cycle System 11(KCS-11) With Low-Temperature Heat Sources," *Journal of Energy Resources Technology*, vol. 129, no. 3, p. 243, 2007.

Hirano, T., Matsumura, N., Takeda, K., "Development of high efficiency scroll compressors for air conditioners", *Proceedings of International Compressor Engineering Conference at Purdue*, pp. 65-74, 1988.

Houghton, J.T., Ding, Y., Griggs, D.J., Noguer, M., Linden, P.J., Dai, X., Maskell, K., Johnson, C.A., "Climate Change 2001", *IPCC Third Assessment Report*, Cambridge University Press, 2001

Hung, T., "A review of organic rankine cycles (ORCs) for the recovery of low-grade waste heat," *Energy*, vol. 22, no. 7, pp. 661-667, 1997.

Hung, T., "Waste heat recovery of organic Rankine cycle using dry fluids," *Energy Conversion and Management*, vol. 42, no. 5, pp. 539-553, 2001

Ingley, H.A., Reed, R., Goswami, D.Y., "Optimization of a scroll expander applied to an ammonia/water combined cycle system for hydrogen production", *Proceedings of the Solar World Congress*, Orlando, Florida, paper 1545, August 2-12, 2005.

Ishii, N., Fukushima, M., Sano, K., Sawai, K., "A study on dynamic behavior of a scroll compressor", *Proceedings of International Compressor Engineering Conference at Purdue*, pp. 901-916, 1986.

Ishii, N., Yamamura, M., Muramatsu, S., Sawai, K., "Mechanical efficiency of a variable speed scroll compressor", *Proceedings of the International Compressor Engineering at Purdue*, pp. 192-199, 1990.

- Ishii, N., Yamamura, M., Muramatsu, S., Yamada, S., Takahashi M., “A study on high mechanical efficiency of a scroll compressor with fixed cylinder diameter”, *Proceedings of the International Compressor Engineering at Purdue*, pp. 677-686, 1994.
- Ishii, N., Yamaoto, S., Muramatsu, S., Yamamura, M., Masatoshi, T., “Optimum combination of parameters for high mechanical efficiency of a scroll compressor”, *Proceedings of the International Compressor Engineering at Purdue*, pp. 181a1-181a8, 1992.
- Itoh, T., Fujitoni, M., Takeda, K., “Investigation of discharge flow pulsation in scroll compressors”, *Proceedings of the International Compressor Engineering at Purdue*, pp. 683-692, 1994.
- Jang, K., Jeong, S., “Temperature and heat flux measurement inside variable speed scroll compressor”, *20th International Congress of Refrigeration, IIR/IIF, Sydney*, pp. 293-302, 1999.
- Jianguo, Q., “Study on basic parameters of scroll fluid machine based on general profile”, *Mechanism and Machine Theory*, 2009.
- Johnston, J.R., Cao, J., Priedeman, D.K., Christensen, R.N., “Experimental Testing of Gerotor and Scroll Expanders Used in, and Energetic and Exergetic Modeling of, and Organic Rankine Cycle”, *Journal of Energy Resources Technology*, Vol. 131, pp. 1-9, 2009.
- Kane, M., Larrain, D., Favrat, D., Allani, Y., “Small hybrid solar power system”, *Energy*, Vol. 28, pp. 1427-1443, 2003.
- Kawabe, I., Ichikawa, T., Hibi, M., Nakamura, M., “Development in 2in1 type scroll compressor”, *Proceedings of the International Compressor Engineering at Purdue*, pp. 593 601, 1992.
- Kim, H.J., Ahn, J.M., Cho, S.O., Cho, K.R., “Numerical simulation on scroll expander-compressor unit for CO₂ trans-critical cycles”, *Applied Thermal Engineering*, Vol. 28, pp. 1654-1661, 2008.
- Kim, H.J., Ahn, J.M., Park, I., Rha, P.C., “Scroll expander for power generation from a low-grade steam source,” *Proceedings of the Institution of Mechanical Engineers, Part A: Journal of Power and Energy*, vol. 221, no. 5, pp. 705-711, 2007.
- Kim, H.J., Ahn, J.M., Park, I., Rha, P.C., “Scroll expander for power generation from a low-grade steam source”, *Proc. IMechE*, Vol. 221, pp. 705-712, 2007.
- Kim, Y., “Modeling on the performance of an inverter driven scroll compressor”, *Proceedings of the International Compressor Engineering Conference at Purdue*, pp. 755-760, 1998.

Klein, S.A., *Engineering Equation Solver (EES)*. fchart.com: F-Chart Software, 2009.

Larjola, J., "Electricity from industrial waste heat using high-speed organic Rankine cycle (ORC)," *International Journal of Production Economics*, vol. 41, no. 1, pp. 227-235, 1995.

Lee, G.H., "Performance simulation of scroll compressors". *Proceedings of the Institution of Mechanical Engineers, Part A: Journal of Power and Energy*, Vol. 216, pp. 169-179, 2002.

Lemort, V., Quoilin, S., Cuevas, C., Lebrun, J., "Testing and modeling a scroll expander integrated into an Organic Rankine Cycle", *Applied Thermal Engineering*, Vol. 29, pp. 3094-3102, 2009.

Lemort, V., Quoilin, S., Cuevas, C., Lebrun, J., "Testing and modeling a scroll expander integrated into an Organic Rankine Cycle," *Applied Thermal Engineering*, vol. 29, no. 14, pp. 3094-3102, 2009.

Lemort, V., Quoilin, S., Lebrun, J., "Numerical simulation of a scroll expander for use in Rankine cycle", *International Compressor Engineering Conference at Purdue*, paper 1324, July 14-17, 2008.

Li, H., Wang, D., Wang, H., Chan, P., "Research of oil-injected scroll compressors working process", *Proceedings of the International Compressor Engineering Conference at Purdue*, pp. 118b1-118b14, 1992.

Mago, P., Chamra, L., Srinivasan, K., Somayaji, C., "An examination of regenerative organic Rankine cycles using dry fluids," *Applied Thermal Engineering*, vol. 28, no. 8, pp. 998-1007, 2008.

Mago, P.J., Chamra, L.M., Somayaji, C., "Performance analysis of different working fluids for use in organic Rankine cycles," *Proceedings of the Institution of Mechanical Engineers, Part A: Journal of Power and Energy*, vol. 221, no. 3, pp. 255-263, 2007.

Manolakos, D., Kosmadakis, G., Kyritsis, S., Pa, G., "Identification of behaviour and evaluation of performance of small scale, low-temperature Organic Rankine Cycle system coupled with a RO desalination unit," *Energy*, vol. 34, no. 6, pp. 767-774, Jun. 2009.

Manolakos, D., Papadakis, G., Kyritsis, S., Bouzianas, K., "Experimental evaluation of an autonomous low-temperature solar Rankine cycle system for reverse osmosis desalination," *Desalination*, vol. 203, no. 1, pp. 366-374, 2007.

Marchese, A.J., "Dynamics of an orbiting scroll with axial compliance- Part II: Experimental techniques", *Proceedings of the International Compressor Engineering at Purdue*, pp. 871-881, 1992.

Mathias, J.A., Johnston, J.R., Cao, J., Priedeman, D.K., Christensen, R.N., “Experimental Testing of Gerotor and Scroll Expanders Used in, and Energetic and Exergetic Modeling of, an Organic Rankine Cycle,” *Journal of Energy Resources Technology*, vol. 131, no. 1, p. 012201, 2009.

Mcdonald, C., Rodgers, C., “Small recuperated ceramic microturbine demonstrator concept,” *Applied Thermal Engineering*, vol. 28, no. 1, pp. 60-74, 2008.

Miller, E.W., Hendricks, T.J., Peterson, R.B., “Modeling Energy Recovery Using Thermoelectric Conversion Integrated with an Organic Rankine Bottoming Cycle,” *Journal of Electronic Materials*, vol. 38, no. 7, pp. 1206-1213, 2009.

Morishita, E., Inaba, T., Nakamura, T., Works, W., “ Scroll compressor analytical model”, *Proceedings of the International Compressor Engineering Conference at Purdue*, pp. 486-495, 1984.

Nieter, J., “Dynamic of scroll suction process”, *Proceedings of the International Compressor Engineering Conference at Purdue*, pp. 165-174, 1988.

Peterson, R.B., Wang, H., Herron, T., “Performance of a small-scale regenerative Rankine power cycle employing a scroll expander,” *Proceedings of the Institution of Mechanical Engineers, Part A: Journal of Power and Energy*, vol. 222, no. 3, pp. 271-282, 2008.

Pichanusakorn P., Bandaru, P., “Nanostructured thermoelectrics,” *Materials Science and Engineering: R: Reports*, vol. 67, no. 2, pp. 19-63, 2010.

Puff, R., Krueger, M., “Influence of the main constructive parameters of a scroll compressor on its efficiency”, *Proceedings of the International Compressor Engineering at Purdue*, pp. 107-118, 1992.

Quoilin, S., “Experimental study and modeling of a low temperature Rankine cycle for small scale cogeneration”, *Master Thesis*, University of Liege, Belgium, 2007.

Quoilin, S., Lemort, V., Lebrun, J., “Experiment study and modeling of an Organic Rankine Cycle using scroll expander”, *Applied Energy*, Vol. 87, pp. 1260-1268, 2010.

Richardson, H., Gatecliff, G., “Comparison of the high side vs. low side scroll compressor design”, *Proceedings of the International Compressor Engineering at Purdue*, pp. 603-610, 1992.

Rodgers, R.J., Wagner, T.C., “Scroll compressor flow modeling: Experimental and computational investigation”, *Proceedings of the International Compressor Engineering at Purdue*, pp. 206-215, 1990.

- Roy, P., Desilets, M., Galanis, N., Nesreddine, H., Cayer, E., “Thermodynamic analysis of a power cycle using a low-temperature source and a binary NH₃-H₂O mixture as working fluid”, *International Journal of Thermal Sciences*, pp. 1-11, 2009.
- Saitoh, T., Yamada, N., Wakashima, S., “Solar Rankine Cycle System Using Scroll Expander”, *Journal of Environment and Engineering*, Vol.2, pp. 708-719, 2007.
- Saitoh, T., Yamada, N., Wakashima, S., “Solar Rankine Cycle System Using Scroll Expander,” *Journal of Environment and Engineering*, vol. 2, no. 4, pp. 708-719, 2007.
- Saleh, B., Koglbauer, G., Wendland, M., Fischer, J., “Working fluids for low-temperature organic Rankine cycles,” *Energy*, vol. 32, no. 7, pp. 1210-1221, 2007.
- Sato, H., Itoh, T., Matsuda, S., Fujitani, M., Kobayashi, H., Mizuno, H., “High Efficiency and Large Capacity 3D Scroll Compressor GU Series”, *Technical Review*, Vol.43, 2006.
- Sawai, K., Yamamura, M., Kojima, Y., Yamamoto, S., Kawahara, S., Sakai, M., Tsubokawa, M., Ishii, N., “A compact horizontal type scroll compressor for room air conditioners”, *Proceedings of the International Compressor Engineering at Purdue*, pp. 569-575, 1992.
- Schuster, A., Karellas, S., Aumann, R., “Efficiency optimization potential in supercritical Organic Rankine Cycles,” *Energy*, vol. 35, no. 2, pp. 1033-1039, 2010.
- Schuster, A., Karellas, S., Kakaras, E., Spliethoff, H., “Energetic and economic investigation of Organic Rankine Cycle applications,” *Applied Thermal Engineering*, vol. 29, no. 8, pp. 1809-1817, 2009.
- Schuster, A., Karellas, S., Kakaras, E., Spliethoff, H., “Energetic and economic investigation of Organic Rankine Cycle applications”, *Applied Thermal Engineering*, Vol. 29, pp. 1809-1817, 2009.
- Schuster, A., Karl, J., “Simulation of an Innovative Stand-Alone Solar Desalination System Using an Organic Rankine Cycle”, *International Journal of Thermodynamics*, Vol. 10, pp. 155-163, 2007.
- Scumann, S.P., “Measurement of orbiting scroll motion”, *Proceedings of the International Compressor Engineering at Purdue*, pp. 453-462, 1994.
- Shu, H.T., Peraccho, A.A., “Dynamics of an orbiting scroll with axial compliance- Part I: Simulation of orbiter axial motion”, *Proceedings of the International Compressor Engineering at Purdue*, pp. 861-870, 1992.
- Stirling, R., “Stirling air engine and the heat regenerator,” U.S. Patent 4081.

Stošić, N., “Screw Compressors in Refrigeration and Air Conditioning”. *HVAC&R Research*, Vol. 10, pp. 3, 2004.

Subiantoro, A., Ooi, K., “Design analysis of the novel Revolving Vane expander in a transcritical carbon dioxide refrigeration system,” *International Journal of Refrigeration*, vol. 33, no. 4, pp. 675-685, 2010.

Suefuji, K., Shiibayashi, M., Tojo, K., “Performance analysis of hermetic scroll compressor”, *Proceedings of the International Compressor Engineering at Purdue*, pp. 75-84, 1992.

Tahir, M.M., Yamada, N., Hoshino, T., “Efficiency of Compact Organic Rankine Cycle System with Rotary-Vane-Type Expander for Low-Temperature Waste Heat Recovery,” *International Journal of Environmental Science And Engineering*, vol. 2, no. 1, pp. 11-16, 2010.

Thombare, D., Verma, S., “Technological development in the Stirling cycle engines,” *Renewable and Sustainable Energy Reviews*, vol. 12, no. 1, pp. 1-38, 2008.

Tojo, K., Igekawa, M., Maeda, N., Machiela, S., Shiibayashi, M., Uchikiawa, N., “Computer modeling of scroll compressor with self-adjusting back-pressure mechanism”, *Proceedings of the International Compressor Engineering at Purdue*, pp. 872-886, 1986.

Tseng, C., Chang, Y., “Family design of scroll compressors with optimization”, *Applied Thermal Engineering*, Vol. 26, pp. 1074-1086, 2006.

Wagner, T.C., Marchese, A.J., “Characterization of thermal pressures in scroll compressors”, *Proceedings of the International Compressor Engineering at Purdue*, pp. 97-106, 1992.

Wang, B., Li, X., Shi, W., “A general geometrical model of scroll compressors based on discretional initial angles of involute”, *International Journal of Refrigeration*, Vol. 28, pp. 958-966, 2005.

Wang, H., Peterson, R.B., Herron, T., “Experimental performance of a compliant scroll expander for an organic Rankine cycle,” *Proceedings of the Institution of Mechanical Engineers, Part A: Journal of Power and Energy*, vol. 223, no. 7, pp. 863-872, 2009.

Wang, X., Zhao, L., Wang, J., Zhang, W., Zhao, X., Wu, W., “Performance evaluation of a low-temperature solar Rankine cycle system utilizing R245fa,” *Solar Energy*, vol. 84, no. 3, pp. 353-364, 2010.

Winandy, E, Saavedra, C.O., Lebrun, J., “Experimental analysis and simplified modelling of a hermetic scroll refrigeration compressor”, *Applied Thermal Engineering*, Vol. 22, pp. 107-120, 2002.

Xiaojun, G., Liansheng, L., Yuanyang, Z., Pengcheng, S., "Research on a Scroll Expander Used for Recovering Work in a Fuel Cell," *International Journal Of Thermodynamics*, vol. 7, no. 1, pp. 1-8, Mar. 2004.

Xiaojun, G., Liansheng, L., Yuanyang, Z., Pengcheng, S., "Research on a Scroll Expander Used for Recovering work in a Fuel Cell", *International Journal of Thermodynamics*, Vol. 7, pp. 1-8, 2004.

Yagoub, W., Doherty, P., Riffat, S., "Solar energy-gas driven micro-CHP system for an office building," *Applied Thermal Engineering*, vol. 26, no. 14, pp. 1604-1610, 2006.

Yamamoto, T., "Design and testing of the Organic Rankine Cycle," *Energy*, vol. 26, no. 3, pp. 239-251, 2001.

Yanagisawa, T., Fukuta, M., Ogi, Y., Hikichi, T., "Performance of an oil-free scroll type air expander", *Proc. Of the ImechE Conf. Trans. On compressors and their systems*, pp. 167-174, 2001.

Yanagisawa, T., Shimizu, T., Fukuta, M., Handa, T., "Study on fundamental performance of scroll expander". *Transactions of the Japan Society of Mechanical Engineers*, Vol. 54, pp. 2798-2803, 1988.

Yang, B., Peng, X., He, Z., Guo, B., Xing, Z., "Experimental investigation on the internal working process of a CO₂ rotary vane expander," *Applied Thermal Engineering*, vol. 29, no. 11, pp. 2289-2296, 2009.

Yong, H., "Leakage calculation through clearances", *Proceedings of the International Compressor Engineering at Purdue*, pp. 93-97, 1994.

Yuanyang, Z., Liansheng, L., Jiang, S., Wei, Z., Pengcheng, S., "Research on oil-free air scroll compressor with high speed in 30 kW fuel cell", *Applied Thermal Engineering*, Vol. 23, pp. 593-603, 2003.

Yuanyang, Z., Liansheng, L., Pengcheng, S., "Thermodynamic simulation of scroll compressor/expander module in automotive fuel cell engine", *Proc. IMechE 220 Part D: J.Automobile Engineering*, Vol. 220, pp. 571-577, 2006.

Zamfirescu, C., Dincer I., "Thermodynamic analysis of a novel ammonia-water trilateral Rankine cycle", *Thermochimica Acta*, Vol. 477, pp. 7-15, 2008.

Zhang, B., Peng, X., He, Z., Xing, Z., Shu, P., "Development of a double acting free piston expander for power recovery in transcritical CO₂ cycle," *Applied Thermal Engineering*, vol. 27, no. 8, pp. 1629-1636, 2007.

Zhu, J., Wang, D., "Research on the discharge port of scroll oil pump", *Proceedings of the International Compressor Engineering at Purdue*, pp. 611-621, 1992.